AFSWC-TR-61-38

SWC
TR
61-38

HEADQUARTERS

AIR FORCE SPECIAL WEAPONS CENTER

AIR FORCE SYSTEMS COMMAND

KIRTLAND AIR FORCE BASE, NEW MEXICO

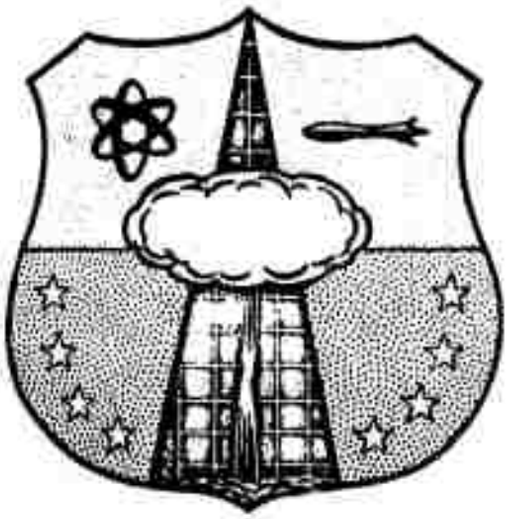

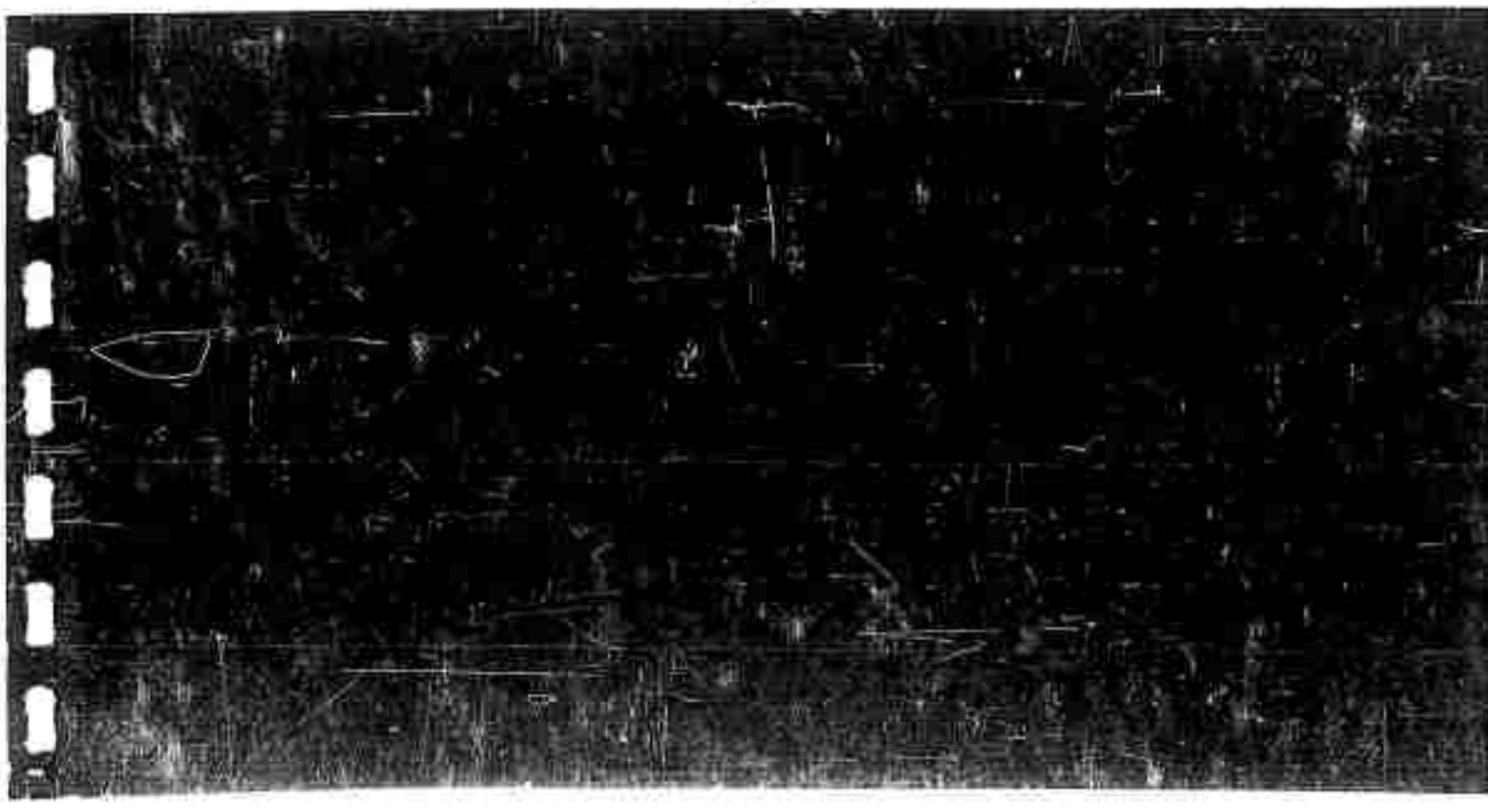

ARPA Order No. 6-61, Task 5
ARPA Code - 7200
PROJECT 4988
TASK 48005

ARTIFICIAL INJECTION OF ELECTRONS INTO THE GEOMAGNETIC FIELD

David D. Elliott

LOCKHEED MISSILES AND SPACE DIVISION
Sunnyvale, Calif.

Contract No. AF 29(601)-2453

MAY 1961

ARTIFICIAL INJECTION OF ELECTRONS INTO THE GEOMAGNETIC FIELD

by

David D. Elliott

Lockheed Missiles and Space Division
Sunnyvale, California

May 1961

Research Directorate
AIR FORCE SPECIAL WEAPONS CENTER
Air Force Systems Command
Kirtland Air Force Base, New Mexico

Approved:

LEONARD A. EDDY
Colonel USAF
Director, Research Directorate

Project No. 4988
Task No. 48005

Contract No. AF 29(601)-2453

HEADQUARTERS
AIR FORCE SPECIAL WEAPONS CENTER
Air Force Systems Command
Kirtland Air Force Base, New Mexico

Major General Charles M. McCorkle
Commander

Colonel Carey L. O'Bryan, Jr.
Deputy Commander

Colonel Leonard A. Eddy
Director, Research Directorate

ABSTRACT

This study is concerned with the question of: (1) The feasibility of injecting 1-Mev electrons into the geomagnetic field from a satellite-borne electron accelerator, (2) the types of geomagnetic experiments which can be performed with the injected electron beam, and (3) the import of the experiments.

In summary, the results of the study are as follows: (1) A satellite will require a payload capability of about 1,000 pounds in order to carry an electron accelerator with the desired characteristics. (2) Two different types of accelerators are required, each for specific experiments. There are commercial accelerators which would be suitable for the injection experiments. One is a 1-Mev pulsed accelerator, 100 amps for 4×10^{-6} sec with a repetition rate of about one per second. The other is a 1-Mev d-c accelerator with an output current of 10^{-3} amps. (3) The electron injection and trapping will not be seriously affected by either satellite charging or the diamagnetic field of the injected electrons. (4) At altitudes greater than about four earth radii, magnetic shells can be filled with trapped electrons, and their trapping lifetime can be subsequently measured. (5) The bounce time of trapped electrons can be measured to an accuracy of better than 1 percent. (6) The geographic position of magnetic conjugate points can be measured, but the accuracy of the measurements is dependent on the type of radar system employed in the experiment. With either aircraft-borne radar or a complex ground radar system, it should be possible to measure the position to conjugate point to within 10 km.

PUBLICATION REVIEW

This report has been reviewed and is approved.

Felix W. Jones Jr. Col USAF

for WILLIAM N. D'ETTORE
Colonel USAF
Deputy Chief of Staff for Operations

CONTENTS

Section		Page
	ABSTRACT	ii
	CONTENTS	iii
	LIST OF ILLUSTRATIONS	v
	LIST OF TABLES	vii
	EXPLANATION OF UNITS	viii
1.	INTRODUCTION	1-1
2.	THE EARTH'S MAGNETIC FIELD	2-1
3.	CHARGED PARTICLES IN THE GEOMAGNETIC FIELD	3-1
	3.1 Motion of a Charged Particle Trapped in the Geomagnetic Field	3-1
	3.2 The Van Allen Belt	3-11
4.	TECHNIQUES FOR ELECTRON INJECTION	4-1
	4.1 Injection From the Earth's Surface	4-1
	4.2 Explosive Injection From a Ballistic Rocket	4-1
	4.3 Injection From a Satellite	4-2
5.	DESCRIPTION OF THE EXPERIMENTS TO BE PERFORMED WITH ARTIFICIALLY INJECTED ELECTRONS	5-1
	5.1 Introduction	5-1
	5.2 Filled Shell Experiments	5-1
	5.3 Bounce-Time Measurement	5-3
	5.4 Conjugate-Point Measurement	5-3
6.	THE FILLING OF MAGNETIC SHELLS	6-1
	6.1 Introduction	6-1
	6.2 Equatorial Orbit Injection	6-4
	6.3 Polar Orbit Injection	6-7
	6.4 Summary of the Values of $\Delta\Phi$	6-11

Section		Page
	6.5 Injection Time	6-12
	6.6 Influence of Accelerator Beam Fluctuations	6-14
	6.7 Magnitude of Injected Flux	6-15
7.	BOUNCE-TIME MEASUREMENT	7-1
	7.1 Introduction	7-1
	7.2 Satellite and Electron Motion	7-1
	7.3 Synchrotron Radiation From Electrons	7-3
	7.4 Synchrotron Radiation Signal Duration	7-9
	7.5 Background Noise Sources	7-11
	7.6 Signal-to-Noise Ratio	7-15
	7.7 Bounce-time Experiment	7-15
8.	CONJUGATE-POINT MEASUREMENT	8-1
	8.1 Introduction	8-1
	8.2 The Shape of the Electron Beam at the Conjugate to the Injection Point	8-2
	8.3 Beam Spread Due to Multiple Scattering in the Atmosphere	8-9
	8.4 Radar Reflection From an Extended Region of Ionization	8-16
	8.5 Conjugate-point Measurement	8-17
9.	SATELLITE CHARGING	9-1
	9.1 Introduction	9-1
	9.2 Neutralization by a Thermal Plasma	9-5
	9.3 The Effect of a Plasma on a Charged Satellite	9-6
10.	DIAMAGNETIC EFFECT OF THE INJECTED ELECTRONS	10-1
	10.1 Introduction	10-1
	10.2 Pulsed Injection	10-1
	10.3 DC Injection	10-6
11.	CONCLUSIONS AND RECOMMENDATIONS	11-1
	11.1 Conclusions	11-1
	11.2 Recommendations	11-2
12.	REFERENCES	12-1

LIST OF ILLUSTRATIONS

Figure		Page
2-1	Definition of the Coordinates of a Typical Field Line of a Magnetic Dipole	2-1
2-2	The Total Intensity of the Geomagnetic Field at the Surface of the Earth (in Gauss)	2-4
2-3	Approximate Intersections of Lines of Force of the Geomagnetic Field With the Earth's Surface in the Northern and Southern Hemisphere	2-5
2-4	Sketch Showing the Probable Distortion of the Geomagnetic Field by the Solar Wind on a Magnetically Disturbed Day	2-8
3-1	Locus of the Mirror Points of Particles Trapped in the Geomagnetic Field	3-4
3-2	$S(\alpha_e)$ as a Function of the Sine of the Equatorial Pitch Angle	3-7
3-3	The Quiet-Day Flux Contours of Electrons and Protons	3-12
3-4	The Integral Invariant Equator (B = 0.22 Gauss)	3-13
3-5	The Integral Invariant Equator (B = 0.20 Gauss)	3-14
3-6	The Energy Spectrum of Protons Above 75 Mev in the Lower Van Allen Radiation Belt at an Altitude of 1200 km	3-15
3-7	The Differential Energy Spectrum of Electrons at the Foot of the Outer Belt	3-17
6-1	Definition of the Magnetic Shell	6-1
6-2	Geographic and Geomagnetic Coordinate Systems	6-3
6-3	Two-Dimensional Coordinate System for Equatorial Orbit Calculations	6-5
6-4	Intersections of a Polar Orbit Satellite and an Equatorial Orbit Satellite With a Magnetic Shell	6-8
6-5	Variation With Altitude of the Ratio of Injection Time to Electron Longitudinal Drift Time	6-13
7-1	Relative Position of the Satellite and the Electrons After One Bounce	7-2

Figure		Page
7-2	The Line Spectrum of Synchrotron Radiation From an Electron Circulating With a Frequency of 440 Kc/sec	7-6
7-3	The Continuous Approximation of the Spectrum of Synchrotron Radiation From an Electron Circulating With a Frequency of 440 Kc/sec	7-7
7-4	Angular Coordinate for Synchrotron Radiation	7-8
7-5	Relative Position of the Satellite and Electron (Bounce-Time Measurement)	7-10
8-1	Separation and Neutralization of Two Beam Electrons by Polarized, Fully Ionized Plasma	8-7
8-2	Projection of Scattering Angles on the Plane of Electron Motion	8-11
8-3	Definition of Scattering Angles	8-12
8-4	The Mean Spread Due to Multiple Scattering of a Narrow Beam of 1-Mev Electrons Striking the Top of the Atmosphere	8-15
8-5	Relative Position of Radar Station and the Region of Ionization (Conjugate Point Measurement)	8-16
9-1	The Logarithm of the Concentration of the Various Atmospheric Constituents at Two Extremes of the Solar Cycle	9-2
9-2	A Normal, Daytime, Free-Electron Distribution During Sunspot Maximum	9-3
9-3	Vertical Temperature Distribution at the Two Extremes of the Solar Cycle	9-4
9-4	Atmospheric D. C. Conductivity in the Absence of a Magnetic Field	9-9
9-5	Satellite Potential During the Electron Injection Pulse	9-13
10-1	Coordinate System of a Current Loop	10-2
10-2	Cross Section of a Current Loop	10-7

LIST OF TABLES

Table		Page
4-1	Characteristics of Two Electron Accelerators	4-3
6-1	Satellite Injection Angular Intervals and Angular Velocities	6-11
6-2	Ratio of the Injection Time to the Drift Time	6-12
6-3	Values of $\left(\frac{\Delta r}{2a_e} - 1\right)$	6-15
6-4	Altitude Dependence of Injected Flux and Estimated Values of Van Allen Electrons Between 0.9 and 1.1 Mev	6-16
7-1	A Comparison of the Bounce Times Predicted by Two Different Geomagnetic Models	7-16
8-1	A Comparison of Geographic Positions of Conjugate Points Predicted by Two Different Geomagnetic Models	8-19
9-1	Values of $\ell n\ \Lambda$ and γ_E	9-9

EXPLANATION OF UNITS

Throughout this report, the mks system of units has been used. In a few cases, for the purpose of conventionality, numerical values of quantities are listed in cgs units. When these quantities appear in equations, however, the mks values are to be used.

A possible source of confusion is the assignment of two magnetic moments. One, designated as m, is the moment of a permanent-magnet dipole and has units of webers-meter. The other, designated as M, is the moment of a current loop and has units of ampere-meter^2. The two moments are related by the equation

$$m = \mu_o M \tag{1}$$

where μ_o is the vacuum permeability.

Section 1
INTRODUCTION

The purpose of this study is to examine the feasibility of introducing a measurable number of high energy electrons (the order of 1 Mev) into the region of the earth's magnetic field above the significant atmosphere, and to determine the types of experiments which can be performed using these electrons as a research tool. The Argus experiment has demonstrated that it is possible to inject artificially electrons into the earth's field. This study, however, is concerned with injection mechanisms other than nuclear explosions and has been directed toward more precise experiments in which the position of injection, the electron energy, the number of electrons, and the injection pitch-angle can be controlled.

The work is divided into four parts. First, for the purpose of definition, a general description will be given of the facts known about the earth's magnetic field, the solar interaction with the field, charged particle motion in the field, and the Van Allen belt. Second, a compilation of techniques for injecting the electrons into the field is given with particular attention being given to a satellite-borne electron accelerator. Third, an investigation of the experiments which can be performed with the injected electron beam is reported relating the results of the experiments to the problems of current interest in the fields of geomagnetism and the magnetic trapping of charged particles. Finally, an examination is made of those problems which might limit the feasibility of electron injection involving the areas of satellite charging and the effect of the diamagnetic field associated with the injected current. In each of the sections, the work is not intended to be exhaustive, but rather a thorough study of the obvious problems and experiments. As the program reaches fruition, a more intensive analysis will undoubtedly turn up other useful experiments and perhaps unforeseen problems.

Section 2
THE EARTH'S MAGNETIC FIELD*

The gross features of the geomagnetic field are similar to those of a uniformly magnetized sphere; this dipole approximation to the field is sufficiently accurate for most of the work in this study. If the earth's field is treated as that from a dipole situated at the earth's center, the dipole has a moment

$$1.13 \times 10^{17} \text{ weber-meter}$$

From Smythe (Ref. 1), a magnetic dipole with moment m has the field components given below (see Fig. 2-1 for definition of coordinates).

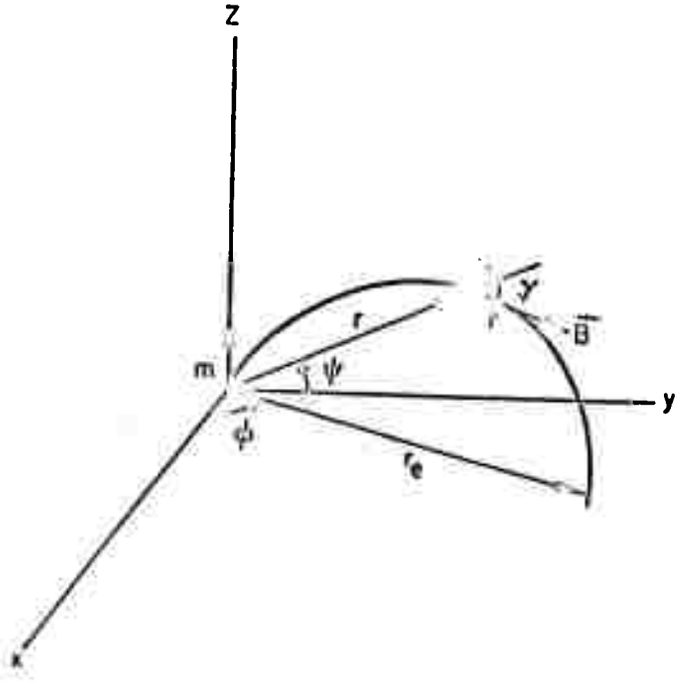

Fig. 2-1 Definition of the Coordinates of a Typical Field Line of a Magnetic Dipole

*The material in this section and the following section is taken in part from Satellite Environment Handbook (Ref. 3)

$$B_r = \frac{m}{2\pi} \frac{\sin \psi}{r^3} \tag{2.1a}$$

$$B_\psi = \frac{-m}{4\pi} \frac{\cos \psi}{r^3} \tag{2.1b}$$

$$B_\phi = 0 \tag{2.1c}$$

The magnitude of the field is

$$B = \left(B_r^2 + B_\psi^2 + B_\phi^2\right)^{1/2} = \frac{m}{4\pi} \frac{1}{r^3} \left(1 + 3 \sin^2 \psi\right)^{1/2} \tag{2.2}$$

A magnetic line of force has the equation

$$r = r_e \cos^2 \psi \tag{2.3a}$$

$$\phi = \text{constant} \tag{2.3b}$$

when r_e is the distance from the dipole to the point where the field line intersects the equatorial plane ($\psi = 0$). The total strength of the field along a given line of force is, therefore,

$$B = \frac{m}{4\pi} \frac{1}{r_e^3} \frac{\left(1 + 3 \sin^2 \psi\right)^{1/2}}{\cos^6 \psi} \tag{2.4}$$

The angle γ between a line of force and the radius vector is given by

$$\tan \gamma = \frac{1}{2} \cot \psi \tag{2.5}$$

The inclination of the field is $\frac{\pi}{2} - \gamma$

In the next section, it will be necessary to have the expression for the radius of curvature of a field line

$$r_c = \frac{\left[\left(\frac{dr}{d\psi}\right)^2 + r^2\right]^{3/2}}{r^2 + 2\left(\frac{dr}{d\psi}\right)^2 - r\frac{d^2r}{d\psi^2}} \tag{2.6a}$$

$$r_c = \frac{r_e}{3}\cos\psi\,\frac{\left(1 + 3\sin^2\psi\right)^{3/2}}{\left(1 + \sin^2\psi\right)} \tag{2.6b}$$

A better approximation to the geomagnetic field is obtained if the condition is dropped that the dipole is situated at the earth's center. The best agreement (Ref. 2) with the real field is obtained if the dipole is shifted 436 km from the center towards the point 15.6°N. lat., 150.9°E. long.; the dipole is then tilted so that its axis intersects the earth's surface at the two points, 75.0° S. lat., 120.4° E. long., and 81.0° N. lat., 84.7° W. long. With an eccentric, tilted dipole, it is sometimes necessary to differentiate between a geographic coordinate system and a magnetic coordinate system. The following notation will be used:

Geographic coordinate system (spherical coordinate system with the origin at the earth's center and the Z-axis collinear with earth's spin axis).

Ψ = latitude, measured from the geographic equator

Θ = colatitude, measured from the earth's spin axis

Φ = longitude, measured from Greenwich

R = radial distance, measured from the earth's center

R_E = radius of the earth, 6.37×10^6 m

$\overline{R}$ = radial distance in units of earth radii, measured from the earth's center

magnetic coordinate system (spherical coordinate system with the origin at the earth's magnetic dipole and the Z-axis colinear with the dipole axis).

ψ = latitude, measured from the magnetic equator
θ = colatitude, measured from the magnetic dipole axis
φ = longitude, usually measured from approximately 70°W. geographic longitude; can be arbitrary, however
r = radial distance, measured from the dipole center
$\bar{r}$ = radial distance in units of earth radii

The conjugate points of a given field line in the simple case of a centered dipole are defined as the two points which satisfy $\psi = -\psi$. In the displaced and tilted system, the conjugate points are defined as the two points of intersection of a field line with the surface of the earth.

If the parameters of the geomagnetic field, such as the conjugate points, must be known with precision,the dipole model is inadequate. A survey of the field over the earth's surface shows many irregularities, and, in places, these local anomalies may constitute an important fraction of the total field (Fig. 2-2). Several workers (Ref. 3) have made spherical harmonic analyses of the earth's field using a large but finite number of terms to match the field at the surface of the earth. As is to be expected, this analysis shows that the effects of the local anomalies fall off rapidly with increasing altitude; far above the earth's surface, the dipole approximation is valid. Vestine and Siblev (Ref. 4) have calculated the conjugate points for a number of lines using a 48-term harmonic analysis. Their results are shown in Fig. 2-3. Conjugate points are indicated by pairs of dots; solid lines are the loci of the conjugate points.

Thus far, we have considered a static geomagnetic field. In reality, however, the direction and magnitude of the field are constantly fluctuating. The transient variations in the geomagnetic field arise mainly from interaction between the geomagnetic field and the ionized gas moving out from the sun. This gas which flows radially outward is referred

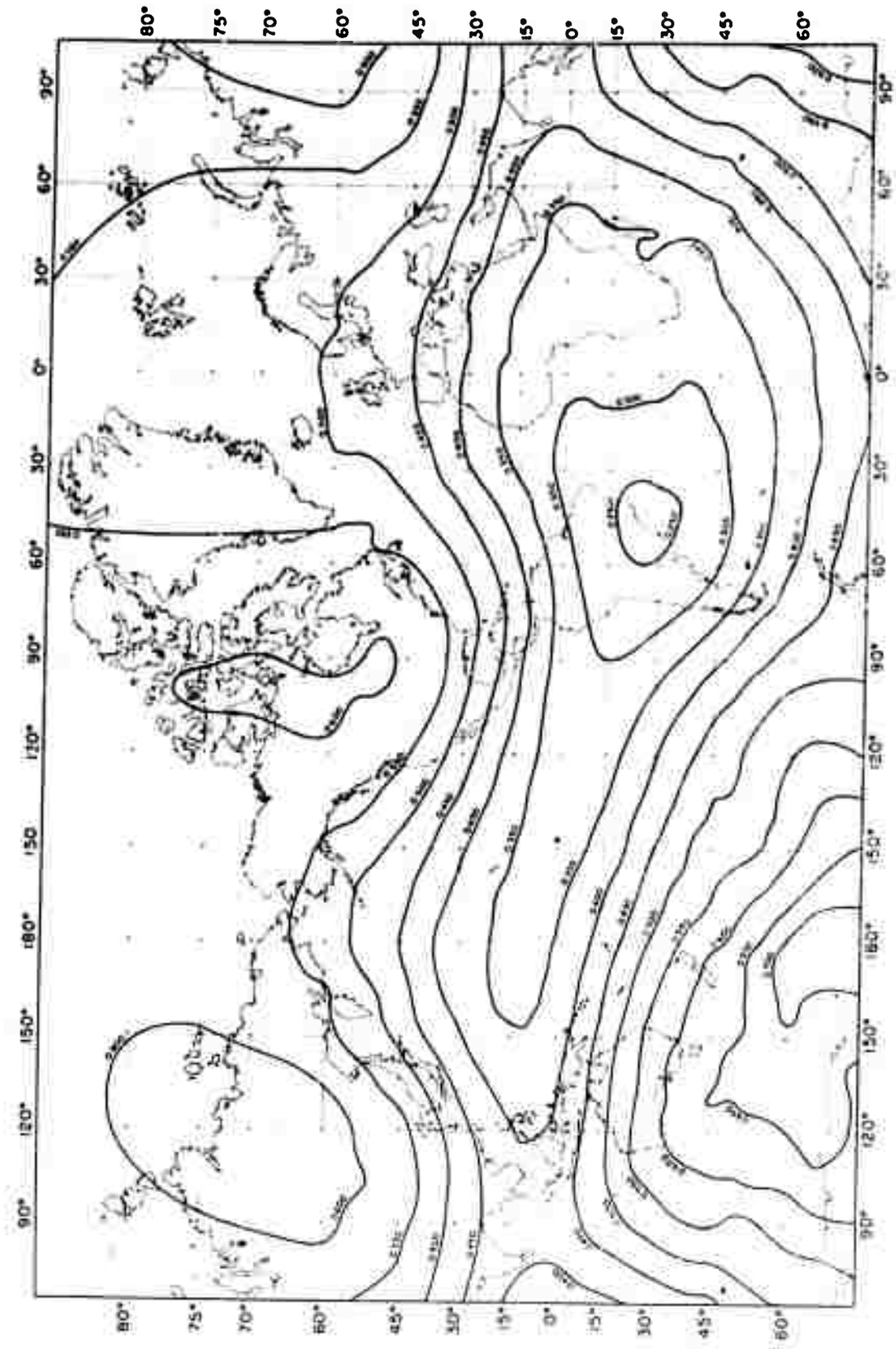

Fig. 2-2 The Total Intensity of the Geomagnetic Field at the Surface of the Earth (In Gauss).

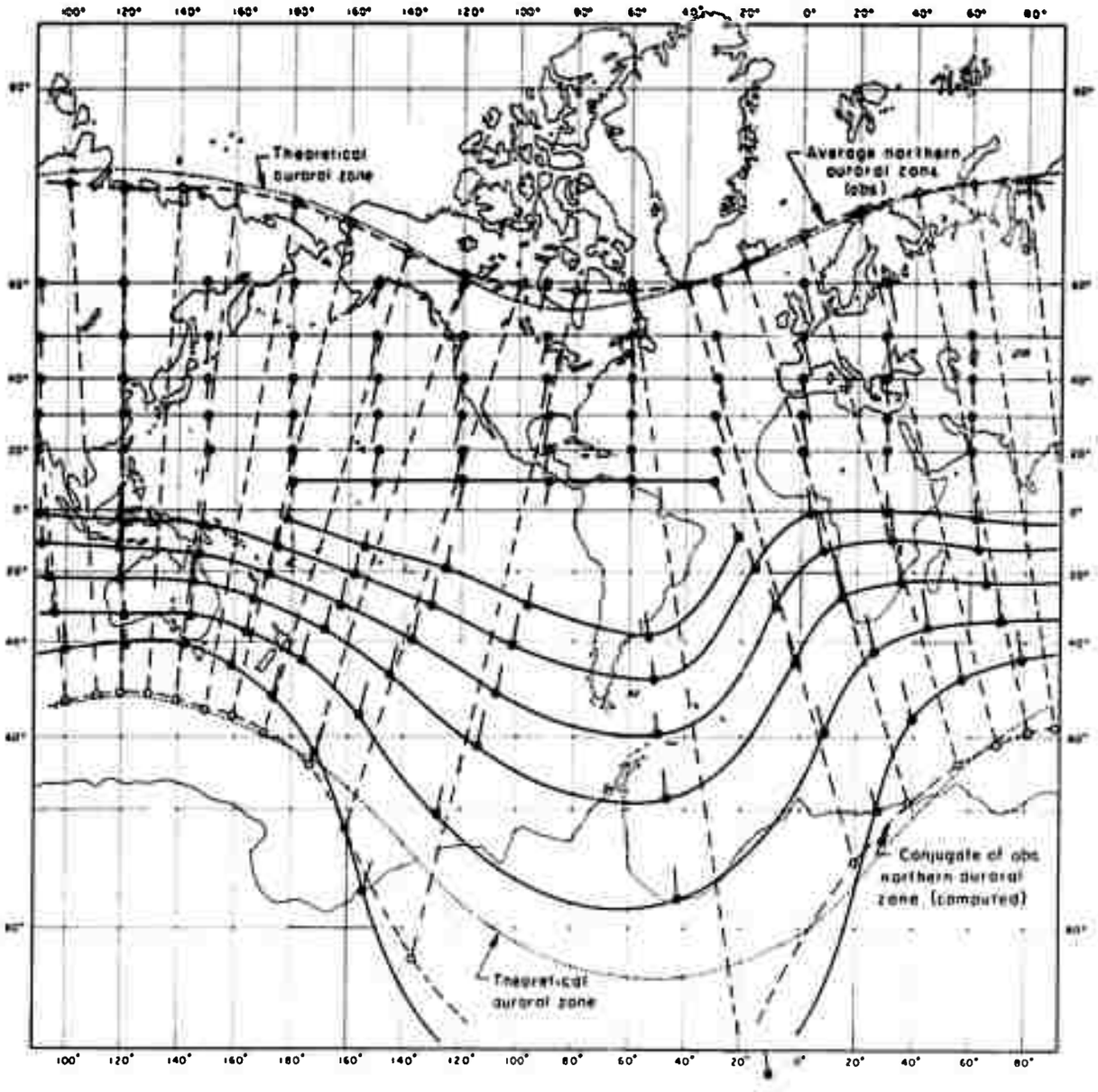

Fig. 2-3 Approximate Intersections of Lines of Force of the Geomagnetic Field With the Earth's Surface in the Northern and Southern Hemisphere. Conjugate points are indicated by dots.

to as the solar wind (Ref. 5). The best direct evidence for the existence of a continuous solar wind comes from the comet-tail observations of Biermann (Ref. 6). The solar wind will push into the geomagnetic field roughly to the point where the kinetic energy density of the solar wind is equal to the magnetic-field energy density. By equating these two energy densities and assuming that the magnetic field strength is given by

$$B = B_o\left(\frac{R_E}{r}\right)^3 \tag{2.7}$$

where

B_o = the field strength at the earth's surface
R_E = the radius of the earth
r = the radial distance to the point where the field strength is B

we obtain

$$r = R_E\left(\frac{B_o^2}{\mu_o\, n\, mv^2}\right)^{1/6} \tag{2.8}$$

where n is the density of solar wind particles, m is their average mass, and v the solar wind velocity. Taking $B_o = 0.35$ gauss (3.5×10^{-5} webers/m^2), $n = 3 \times 10^7$ protons (and electrons) per m^3, and $v = 3 \times 10^5$ m/sec for quiet solar conditions, we find that the solar wind will penetrate to $r = 7.7\ R_E$. During periods of solar activity, appropriate values for the solar wind may be as high as $n = 10^{10}\ m^{-3}$ and $v = 1.5 \times 10^6$ m/sec, leading to a value $r = 1.7\ R_E$. The solar wind blowing against the geomagnetic field will probably distort the field into the shape shown in Fig. 2-4 (Ref. 7). The front surface is determined by the impact pressure of the solar wind while the long "tail" is closed by the pressure of the transverse thermal motion

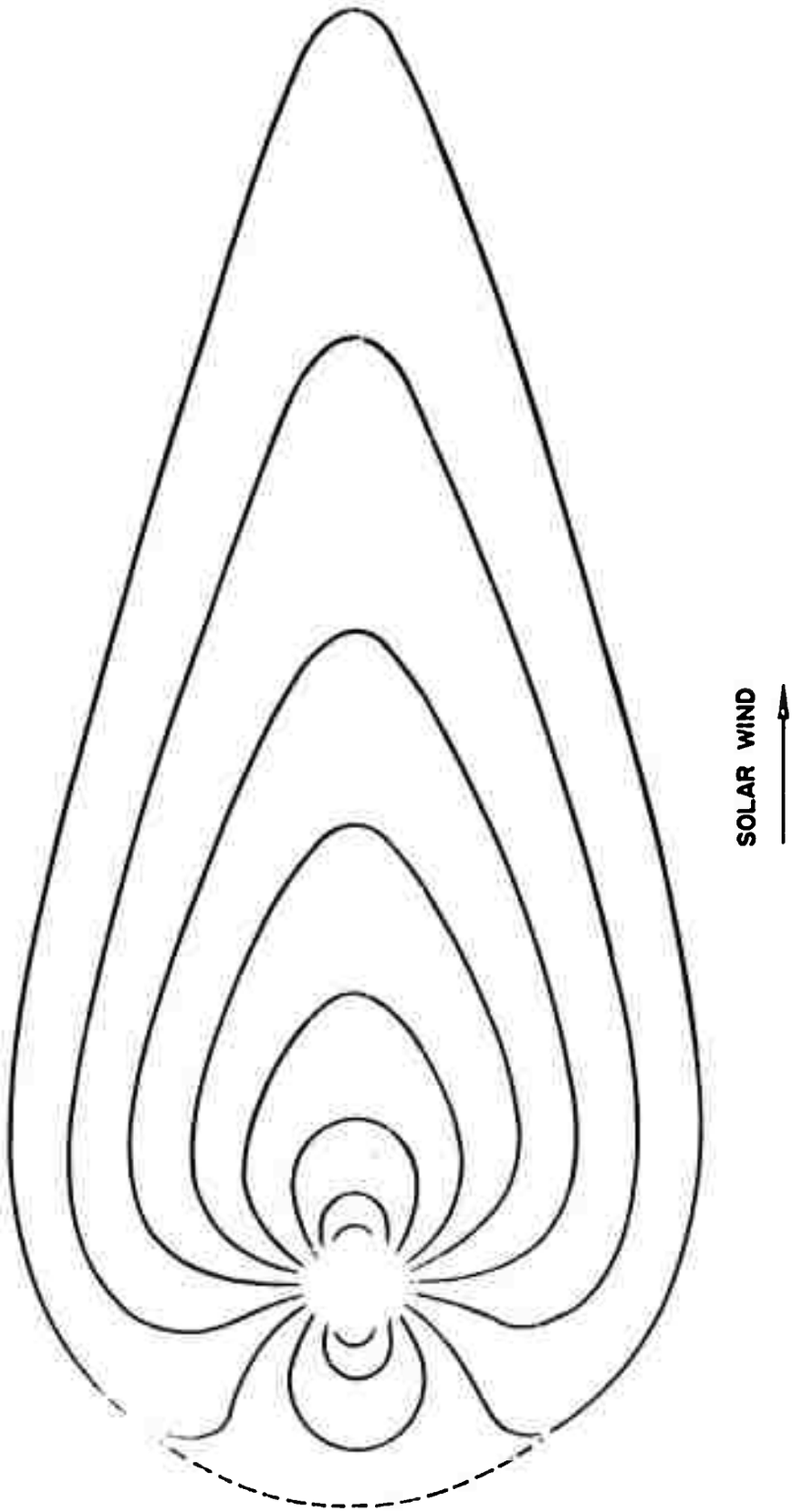

Fig. 2-4 Sketch Showing the Probable Distortion of the Geomagnetic Field by the Solar Wind on a Magnetically Disturbed Day

of the solar wind particles. In all cases, the plasma pressure is equal to $\frac{B^2}{2\mu_o}$ at the interface. Clearly, in the region of high-altitude satellite orbits, such a distorted field will lead to large diurnal effects.

Sudden increases in the solar wind pressure lead to the phenomenon of magnetic storms. The impact of the strengthened solar wind increases the distortion of the geomagnetic field, generates hydromagnetic waves which propagate to the lower ionosphere, and injects charged particles into regions where they become magnetically trapped. It is these two major magnetic transients, the diurnal effect and the magnetic storm, which can be studied with artificially injected electron currents.

Section 3
CHARGED PARTICLES IN THE GEOMAGNETIC FIELD

3.1 MOTION OF A CHARGED PARTICLE TRAPPED IN THE GEOMAGNETIC FIELD

Because of interest in the effect of the geomagnetic field on primary cosmic rays approaching the earth, the problem of charged-particle motion in a magnetic dipole field has been studied quite thoroughly by Störmer (Ref. 8) and Alfvén (Ref. 9). In solving for the particle orbits, a class of solutions was found in which the particles are magnetically "trapped." These solutions were considered to be of academic interest only because no external source, such as cosmic rays, can inject particles into trapped orbits. The discovery of the Van Allen belt made up of trapped electrons and protons has brought renewed interest to the analysis of trapped, charged-particle dynamics in the earth's field. A complete description of trapped particle motion would entail numerical solutions of the equations of motion. However, a good approximation to the exact motion can be obtained by making use of quantities which are nearly con served—the adiabatic invariants of motion.

A particle trapped in a dipole field executes three principal motions:

(1) A particle moves in a circle of radius $a_c = p_\perp/(ZeB)$ with an angular frequency $\omega_c = \dfrac{Ze\ Bc^2}{(T + mc^2)}$,

where

m = the mass of the particle

T = its kinetic energy

$p_\perp$ = its component of momentum perpendicular to the local magnetic field direction

c = the velocity of light
Ze = the particle charge
B = the magnitude of the local magnetic field

For Van Allen radiation particles, $a_e << r$, where r is the distance to the center of the earth from the magnetic field line about which the particle is spiraling. This circular motion is properly called cyclotron motion; a_e is the cyclotron radius and ω_e is the cyclotron frequency. The center of the circle is called the particle's guiding center.

(2) The guiding center of a particle whose velocity vector makes an angle α (the pitch angle) with the magnetic field direction at a position where the field strength is B moves nearly along the field line to a position where the field strength is $B_m = B/\sin^2 \alpha$. The position at which $B = B_m$ is called the mirror point, and a particle reaching this point will be reflected back along the field line. Thus, a particle which is trapped in the geomagnetic field, besides executing small scale cyclotron motion, moves very nearly along a field line and bounces back and forth between northern and southern hemisphere mirror points.

(3) As a trapped particle bounces back and forth between mirror points, its guiding center slowly drifts in longitude, positively charged particles drift westward, and negatively charged particles drift eastward.

There are three invariants which describe the motion of a charged particle trapped in a static magnetic field. Each of the invariants will be described briefly as they relate to the Van Allen radiation belt. For a more detailed discussion with many references to previous work on this subject, see Northrup and Teller (Ref. 10). The three invariants are as follows:

(1) The first invariant is the magnetic moment invariant. The magnetic moment of a charged particle in a magnetic field is given by

$M = 1/2\left[c^2 p_\perp^2/B(T + mc^2)\right]$. As long as the particle motion and field configuration are such that the magnetic field strength changes only very slightly over the distance the particle moves in one cyclotron period, the magnetic moment will remain constant, i.e., $p_\perp^2/B$ is a constant of the motion. (T remains constant in a static magnetic field.)

(2) The second invariant is the integral or longitudinal invariant. The integral invariant is given by $J = \oint v_{||} dl$, where $v_{||}$ is the component of the particle velocity parallel to the local magnetic field, dl is the element of length along the line of force, and the integral is evaluated between mirror points. This invariant of the motion places an additional constraint on the motion of a trapped particle. If a trapped particle drifts in the geomagnetic field so that M and J are constant, the particle must drift in such a way that it eventually returns to the same field line from which it started. The constancy of M only requires that B_m be constant; the additional constancy of J requies that the particle drift along a well defined integral invariant surface. One of the useful and instructive results of the integral invariant calculations is shown in Fig. 3-1. In this figure, the integral invariant calculations of Jensen et al., (Ref. 11) are used to indicate some paths or traces described by the mirror points of particles trapped in the geomagnetic field.

(3) The third invariant is the flux invariant. The flux invariant is simply the conservation of magnetic flux inside the integral invariant surface defined in the paragraph above.

$$\Phi = \int_s \vec{B} \cdot \vec{ds}$$

where $\vec{ds}$ is an element of area. The integral is evaluated over any surface joining the magnetic equator of the earth to the integral invariant surface. The

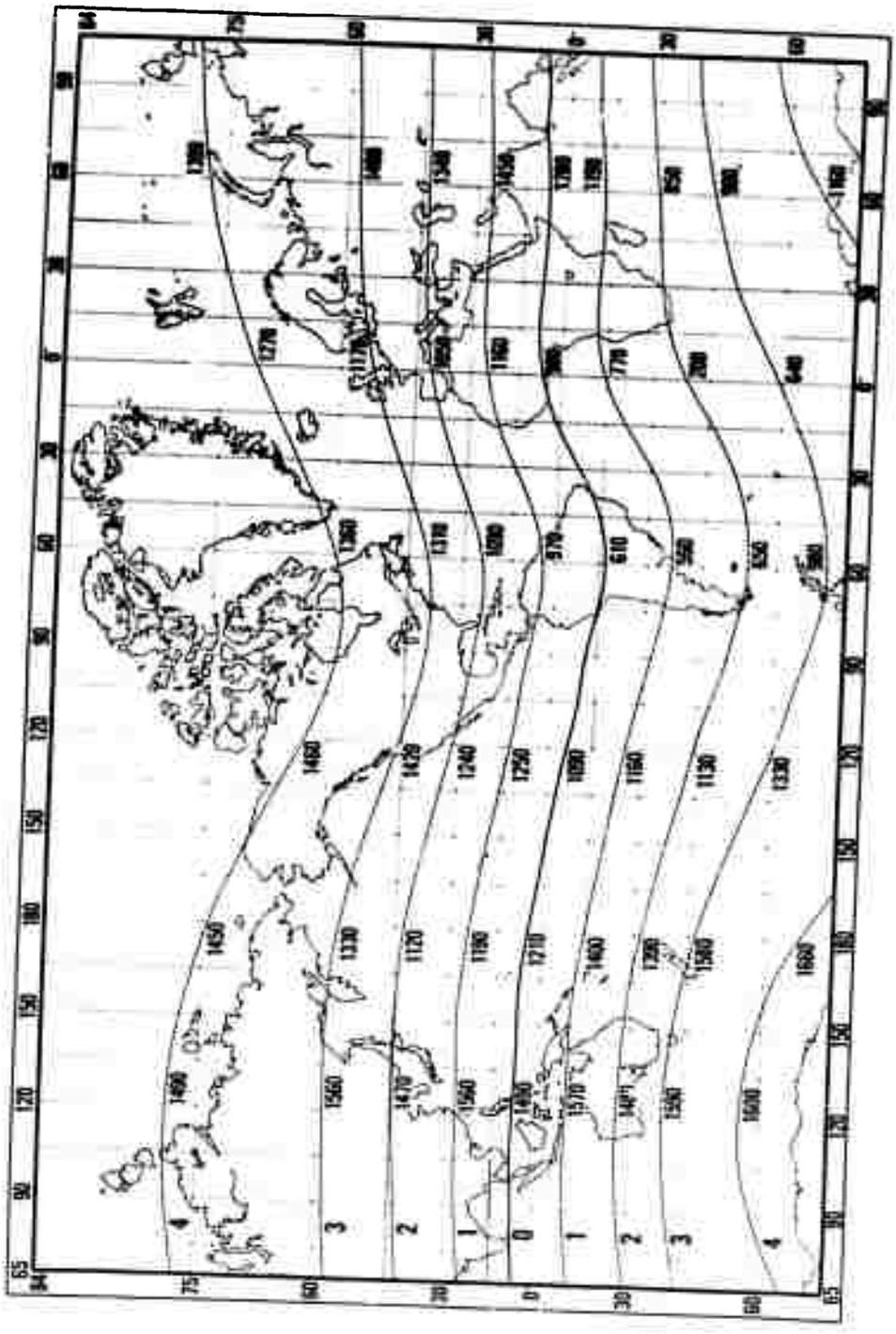

Fig. 3-1 Locus of the Mirror Points of Particles Trapped in the Geomagnetic Field. The trace marked 0 is the integral invariant equator; the pairs of traces labeled 1, 2, 3, or 4 are conjugate traces. Mirror altitudes, in kilometers, are given at 60° intervals along each trace. (The magnetic fields were arbitrarily chosen as follows: Trace 0, B = 0.20 Gauss; Trace 1, B = 0.22 Gauss; Trace 2, B = 0.28 Gauss; Trace 3, B = 0.30 Gauss; and Trace 4, B = 0.32 Gauss.)

constancy of Φ requires that, if the geomagnetic field were slowly to contract or expand (as happens during some phases of geomagnetic storms), the integral invariant surface must change its size accordingly so that Φ is conserved. During this process, M and J also remain constant. An alternate way of stating the flux invariant is to say that the drifting particle follows slow movements of the magnetic field.

Experiments described in later sections are designed to measure some of the parameters associated with trapped electron motion. With this in mind, we will examine in more detail some of the features of the trapped particle motion described above.

3.1.1 Bounce Time

The time for a particle to move from one mirror point to the conjugate mirror point, and then return, is called the bounce time.

$$T_B = 4 \int_0^L \frac{dl}{v_{||}} \tag{3.1}$$

In this integral, dl is measured along a field line, L is the distance from the magnetic equator to the mirror point, and $v_{||}$ is the component of the particle's velocity parallel to the local magnetic field.

$$v_{||} = v \cos \alpha \tag{3.2}$$

From the conservation of the magnetic moment,

$$v_{||} = v \left(1 - B/B_m\right)^{1/2} \tag{3.3}$$

If $\frac{\partial B}{\partial t} = 0$, then v is constant and the bounce time in a pure dipole field is given by

$$T_B = \frac{4\, r_e}{v} \int_0^{\psi_m} d\psi \, \frac{\cos\psi \, (1 + 3\sin^2\psi)^{1/2}}{(1 - B/B_m)^{1/2}} \tag{3.4}$$

$$B/B_m = \frac{(1 + 3\sin^2\psi)^{1/2}}{\cos^6\psi} \, \frac{\cos^6\psi_m}{(1 + 3\sin^2\psi_m)^{1/2}} \tag{3.5}$$

where ψ_m is the latitude of the mirror point (magnetic coordinates are used throughout), and r_e identifies the particular line of force being considered. The integrand in Eq. (3.4) is singular at $\psi = \psi_m$; however, the singularity is integrable. The integration has been performed numerically over most of the range of ψ, and in the vicinity of ψ_m an approximate expression has been integrated analytically.

$$T_B = \frac{4\, r_e}{v} \, S(\psi_m) \tag{3.6}$$

ψ_m ean be related to the pitch angle at the equator α_e by

$$\sin^2\alpha_e = \frac{\cos^6\psi_m}{(1 + 3\sin^2\psi_m)^{1/2}} \tag{3.7}$$

Figure 3-2 shows $S(\alpha_e)$ as a funetion of $\sin\alpha_e$. The striking feature is the eonstancy of S. For rough ealculations, thc bounce time ean be approximated by

$$T_B \approx \frac{4\, r_e}{v} \tag{3.8}$$

Putting r_e into units of earth radii, and taking v equal to the veloeity of light, the bounee for a high energy electron is

$$T_B \approx (8.5 \times 10^{-2})\, \bar{r}_c \text{ see} \tag{3.9}$$

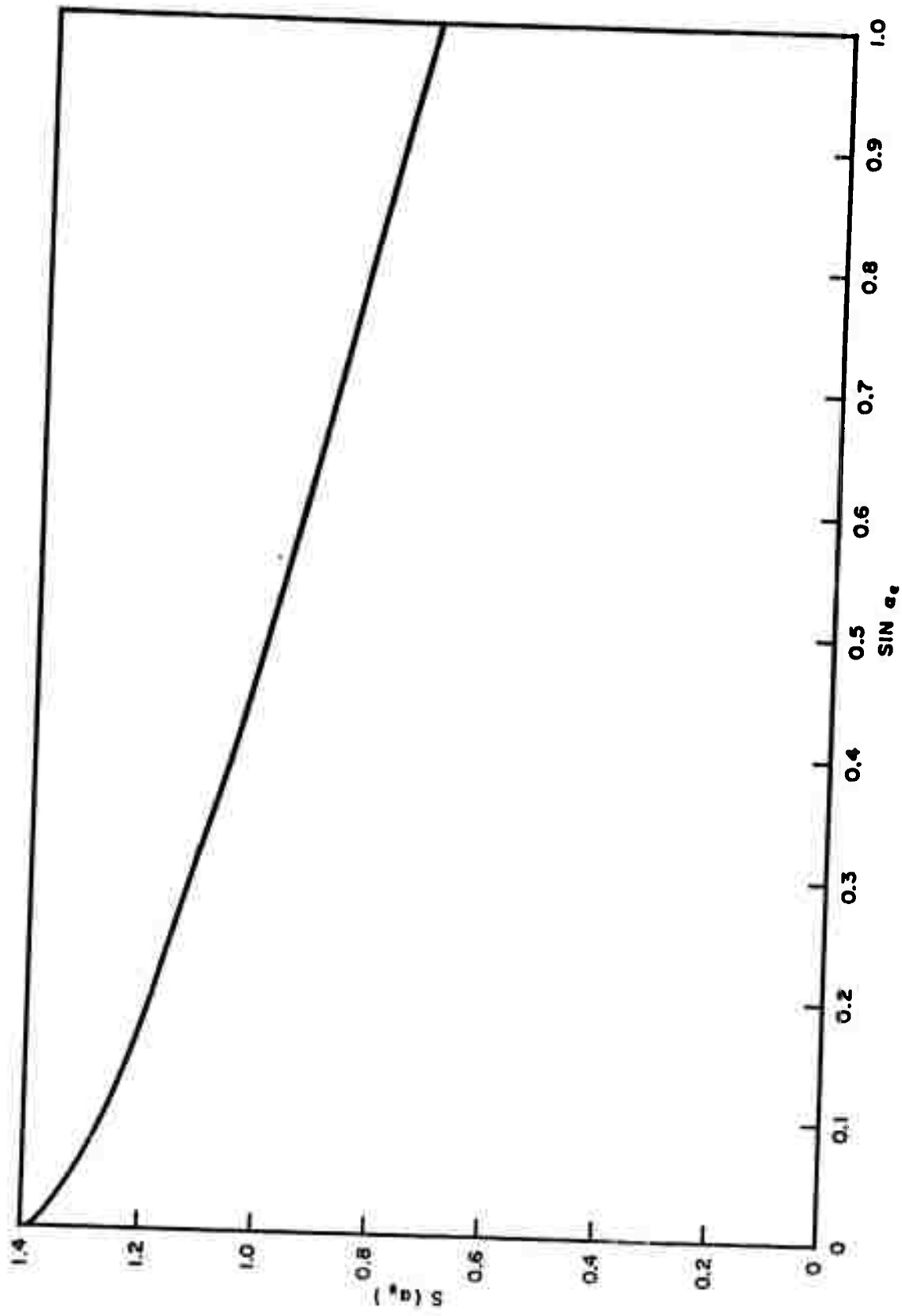

Fig. 3-2 $S(\alpha_e)$ as a Function of the Sine of the Equatorial Pitch Angle. $S(\alpha_e)$ is related to the bounce time by: $S(\alpha_e) = \frac{V}{4 r_e} T_B(\alpha_e)$

Therefore, trapped electron bounce times have order of magnitude values from 0.1 sec to 1.0 sec.

3.1.2 Longitudinal Drift Time

The time for a particle to drift longitudinally once around the earth is called the longitudinal drift time. Spitzer (Ref. 12) gives an expression for the instantaneous longitudinal drift velocity, which is perpendicular to both $\vec{r}$ and $\vec{B}$.

$$V_D = \frac{1}{\omega_c r_c}\left(\frac{1}{2} v_\perp^2 + v_{||}^2\right) \tag{3.10}$$

ω_c is the particle's cyclotron angular frequency, and r_c is the radius of curvature of the field line. The rate of change of the particle's longitudinal angle is then

$$\frac{d\varphi}{dt} = \frac{V_D}{r \cos\psi} \tag{3.11}$$

The average value of $\frac{d\varphi}{dt}$ over one bounce time is

$$\overline{\frac{d\varphi}{dt}} = \frac{4}{T_B}\int_0^{\psi_m} d\psi \frac{V_D}{V_{||}} \frac{(1 + 3\sin^2\psi)^{1/2}}{\cos^2\psi} \tag{3.12a}$$

$$\overline{\frac{d\varphi}{dt}} = \frac{6p}{T_B e r_e B_e}\int_0^{\psi_m} d\psi \frac{(1 + \sin^2\psi)(2 - B/B_m)\cos^3\psi}{(1 - B/B_m)^{1/2}(1 + 3\sin^2\psi)^{3/2}} \tag{3.12b}$$

where p is the electron's momentum and B_e is the magnitude of the magnetic field on the equator at the point $r = r_e$. The drift time is

$$T_D = \frac{2\pi}{\overline{\frac{d\varphi}{dt}}} \tag{3.13a}$$

$$T_D = \frac{4\pi}{3} \frac{e\, r_e^2\, B_e}{pv} \frac{\displaystyle\int_0^{\psi_m} d\psi \; \frac{\cos\psi\,(1 + 3\sin^2\psi)^{1/2}}{(1 - B/B_m)^{1/2}}}{\displaystyle\int_0^{\psi_m} d\psi \; \frac{(1 + \sin^2\psi)\,(2 - B/B_m)\cos^3\psi}{(1 - B/B_m)^{1/2}\,(1 + 3\sin^2\psi)^{3/2}}} \tag{3.13b}$$

Welch and Whitaker (Ref. 13) and Watson, et al. (Ref. 29) indicates that the ratio of the two integrals in Eq. (3.13b) is unity to about 30 percent over the range of ψ_m from 0 to 60°. For high energy electrons, the drift time may, therefore, be approximated by

$$T_D = \frac{4\pi}{3} \frac{e\, r_e^2\, B_e}{pc} \tag{3.14}$$

On the equator, the magnetic field is

$$B_e = (9 \times 10^{15})\, r_e^{-3} \text{ webers/m}^2 \tag{3.15}$$

For a one-Mev electron, the drift time is then

$$T_D = \frac{4.2 \times 10^3}{\bar{r}_e} \text{ sec} \tag{3.16}$$

where $\bar{r}_e$ is in units of earth radii. The drift times have order of magnitude values from 1,000 sec to 100 sec.

3.1.3 Lifetime

The description of trapped, charged-particle motion, thus far, has not included any loss mechanisms, and the particles would be trapped indefinitely. If radiative energy loss is negligible, which is the case except for very high energy electrons, the dominant loss mechanisms are scattering and ionization in the upper atmosphere. Since the atmospheric density falls off nearly exponentially with increasing altitude, most of the energy loss

occurs when the particle is nearest the earth, namely, at the mirror points. A detailed description of the analysis of this energy degradation and eventual loss of the particle from a stable, trapped orbit is beyond the scope of the present study. The analysis has been made, however, by Walt and MacDonald (Ref. 14). The general features of trapped particle loss are:

(1) The particle loses energy by excitation of the atmospheric atoms in the vicinity of the mirror points. The rate of energy loss increases as the particle's energy decreases.

(2) The position of the mirror points gradually decreases in altitude, and hence, goes into a region of greater atmospheric density and consequently greater energy loss. This lowering of the mirror points is caused by atmospheric Coulomb multiple-scattering over the particle's entire orbit.

(3) There is cataclysmic particle loss in the vicinity of the geomagnetic anomalies, such as the Cape Town anomaly. Here, the geomagnetic field is so much weaker than at the conjugate mirror point that those particles normally mirroring at relatively low altitudes are dumped into the atmosphere and lost.

(4) To demonstrate the conservation of the particle's magnetic moment, it had to be assumed that the geomagnetic field changed negligibly over an area defined by one cyclotron revolution of the particle. This assumption breaks down at high altitudes where the field is weak and the cyclotron radius is large. If the magnetic moment is not constant, the mirror point position is not stable and the particles would be only quasi-trapped and eventually would be lost into the atmosphere. It has been suggested that the outer altitude limit of the Van Allen electron belt is defined by this magnetic moment non-conservation.

(5) During magnetic storms, the earth's field is compressed, hydromagnetic waves propagate along field lines, diamagnetic ring currents are generated, and the upper atmosphere is heated and expands, thereby increasing the atmospheric density in the region of the mirror points. Each of these effects

can temporarily increase the loss of trapped particles. In particular, recent work (Ref. 15) has shown that the hydromagnetic waves can cause the breakdown of the magnetic moment invariance for Van Allen protons, and, thereby, set the outer altitude limit on the proton belt.

3.2 THE VAN ALLEN BELT

The Van Allen radiation belt has been shown to consist of two components: (1) a hard proton component (the proton belt) centered at about 10×10^3 km from the earth's magnetic axis; and (2) an electron component (the electron belt) centered at about 22×10^3 km from the earth's magnetic axis.

3.2.1 Protons

Contours of constant proton flux are shown in Fig. 3-3. These contours are symmetrical about the integral invariant equator. Since the geomagnetic field is not centered about the earth's spin axis, the height of the contours above the earth's surface is a function of longitude. The location of the integral invariant equator relative to geographic coordinates is shown in Figs. 3-4 and 3-5. Altitudes corresponding to constant proton flux at various positions around the integral invariant equator are expressed in kilometers by the numbers at the arrows. The location of the integral invariant equator and the altitudes were obtained from the high-order, spherical-harmonic analysis of the geomagnetic field carried out by Jensen et al. (Ref. 11). Figure 3-4 indicates the altitude at the bottom of the radiation belt where the counting rate is just above cosmic ray background. The field strength here is $B = 0.22$ gauss. Similarly, Fig. 3-5 indicates the altitudes along the integral invariant equator where the flux of protons with energies greater than 40 Mev is 100 protons cm^{-2} sec^{-1} (about 50 times cosmic ray background).

The proton spectrum has been measured by Freden and White (Ref. 16) near the bottom of the belt. Their results are shown in Fig. 3-6. It is expected that the proton

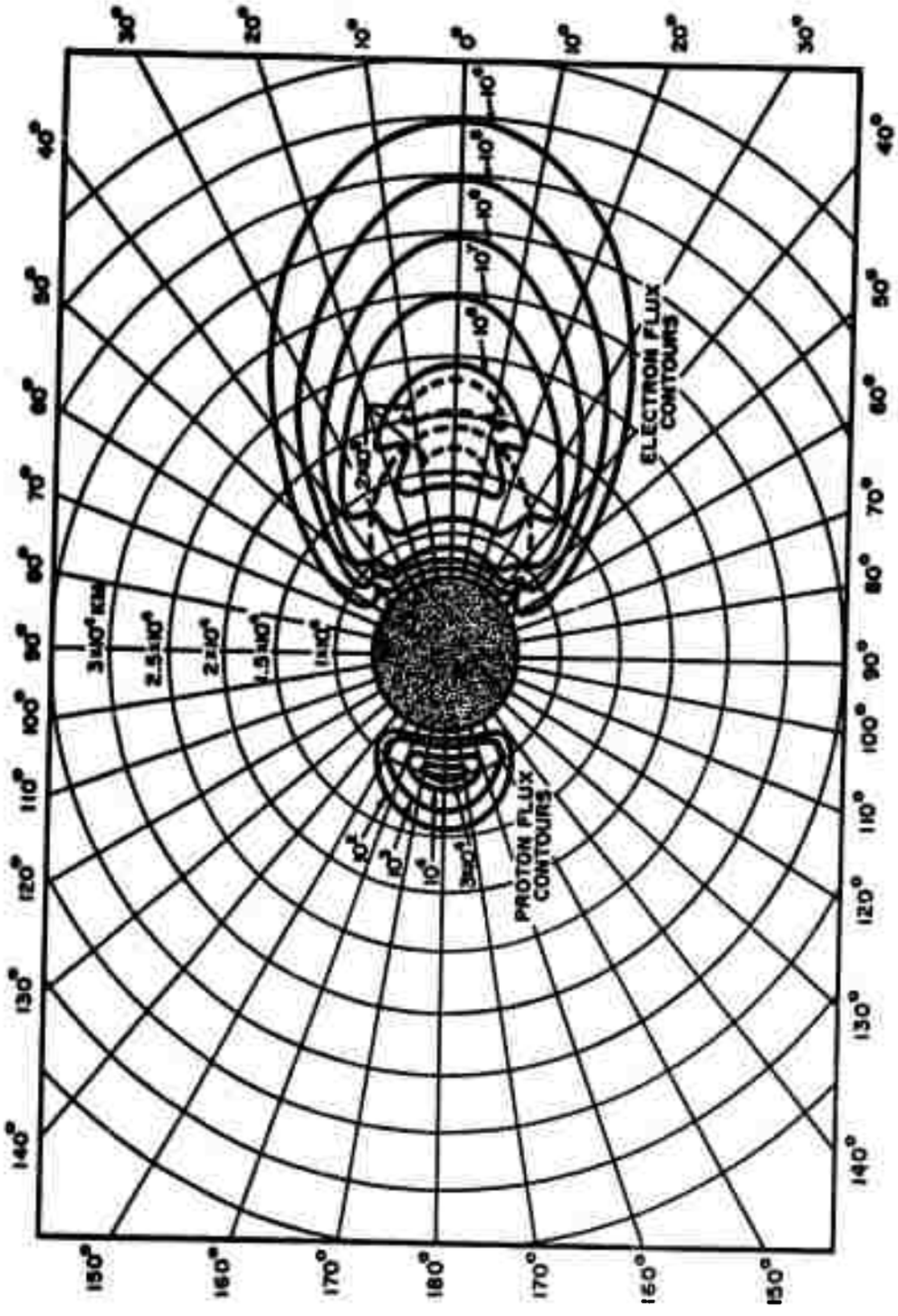

Fig. 3-3 The Quiet-Day Flux Contours of Electrons With Energies Greater Than 20 Kev (Electrons cm^{-2} sec^{-1}) and Protons With Energies Greater Than 40 Mev (Protons cm^{-2} sec^{-1}). The electron contours are not well known and may be in error by several orders of magnitude. For a conservative upper limit, the given electron flux values could be multiplied by 10^3 for the outer zone and 10^4 for the inner zone. The radiation is symmetrical about the integral invariant equator.

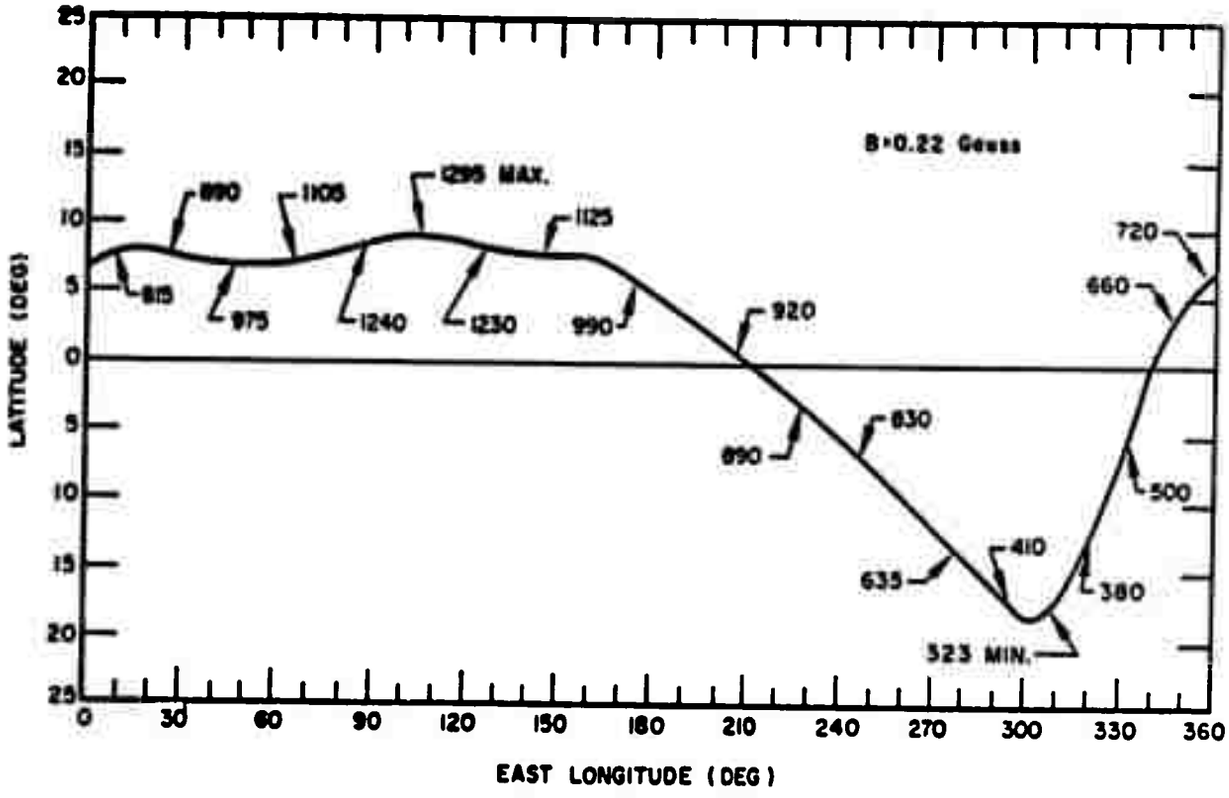

Fig. 3-4 The Integral Invariant Equator (B = 0.22 Gauss). In this figure is shown the path which a particle trapped in the geomagnetic field with 90° pitch angle will follow. The latitude of this path, called the integral invariant equator, is indicated as a function of longitude. Also shown are the set of altitudes (km) where the geomagnetic field strength is B = 0.22 Gauss. This field strength corresponds to the bottom edge of the proton belt, where the proton flux is barely detectable above cosmic ray background. The altitude shown should be correct to within ±25 km.

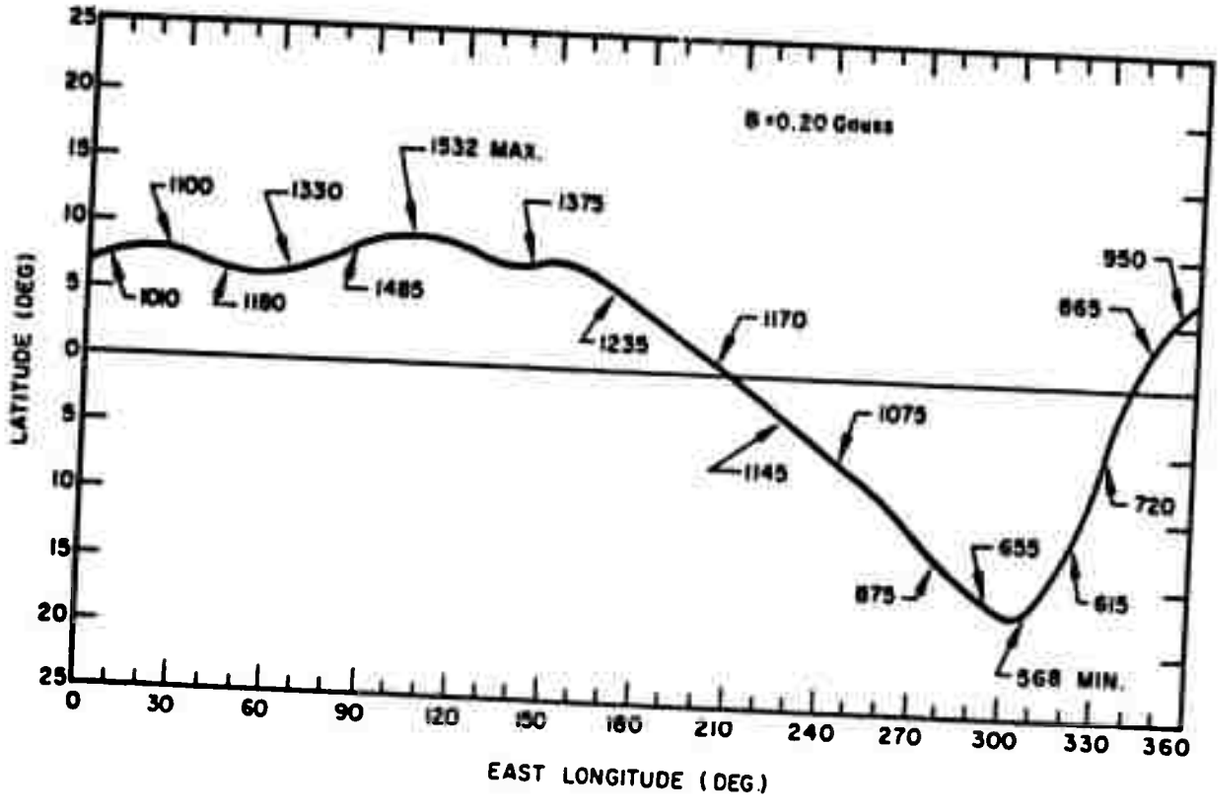

Fig. 3-5 The Integral Invariant Equator (B = 0.20 Gauss). This figure is similar to Fig. 3-4, but the altitudes shown are for a field strength B = 0.20 Gauss. At the altitudes indicated along this integral invariant, the proton flux above 40 Mev is 10^2 protons cm^{-2} sec^{-1}

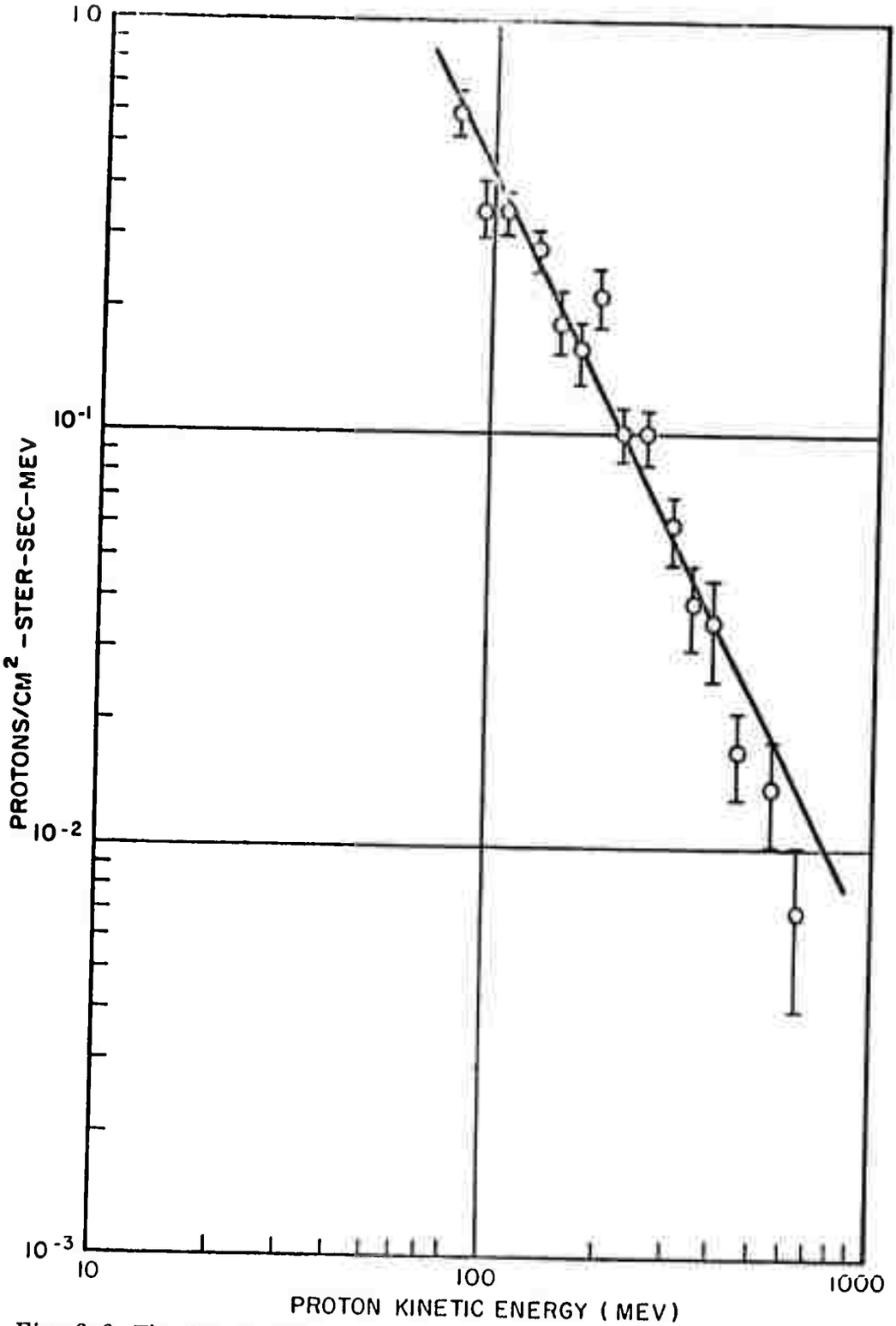

Fig. 3-6 The Energy Spectrum of Protons Above 75 Mev in the Lower Van Allen Radiation Belt at an Altitude of 1200 km. The line is a least-squares fit of the equation $N = N_1 T^{-n}$ to the data and gives $N_1 = (2.1^{+1.0}_{-0.7}) \times 10^3$ protons Mev^{-1} sterad^{-1} sec^{-1} cm^{-2} and $n = 1.84 \pm 0.08$

spectrum will have an altitude dependence, and, consequently, the Freden and White results will not necessarily hold throughout the belt.

3.2.2 Electrons

The electron belt contours are also shown in Fig. 3-3. These contours represent an estimate of the quiet-day flux of electrons with energies greater than 20 kev. There is, however, a major uncertainty in the electron flux. The flux values given in this figure are generally lower than those given by other authors. However, if more conservative values for the electron belt are desired, the given flux values should be multiplied by 10^3 for the outer zone and 10^4 for the inner zone as a reasonable upper limit for the quiet-day electron flux.

The electron spectrum has been measured by Walt et al. (Ref. 17) at the "foot" of the outer belt. Their results are shown in Fig. 3-7. As in the proton case, these results should not be expected to be valid throughout the belt.

Observations have shown that the proton belt is stable, but the electron belt undergoes changes which are associated with geomagnetic storms. After the active part of a storm is over (recovery phase – low K-index), the counting rate of instrumentation flown through the outer part of the electron belt increases; the magnitude and time of occurrence of these variations depend on the type of detector used and the characteristics of the particular geomagnetic storm. Following the active phase of the storm of 16 Aug 1959, the counters in Explorer VI showed a typical increase of about a factor of five near the middle of the electron belt. Another example of possible time variations in electron belt intensity is shown by essentially identical instruments (Anton, type-302 Geiger counters with about 1 gm/cm^2 of shielding) in the space probe Pioneer IV and the satellite Explorer VI. The difference between the counting rate at the peak of the electron belt for Pioneer IV (extrapolated) and the pre-storm, quiet-day observations for Explorer VI is about 10^3.

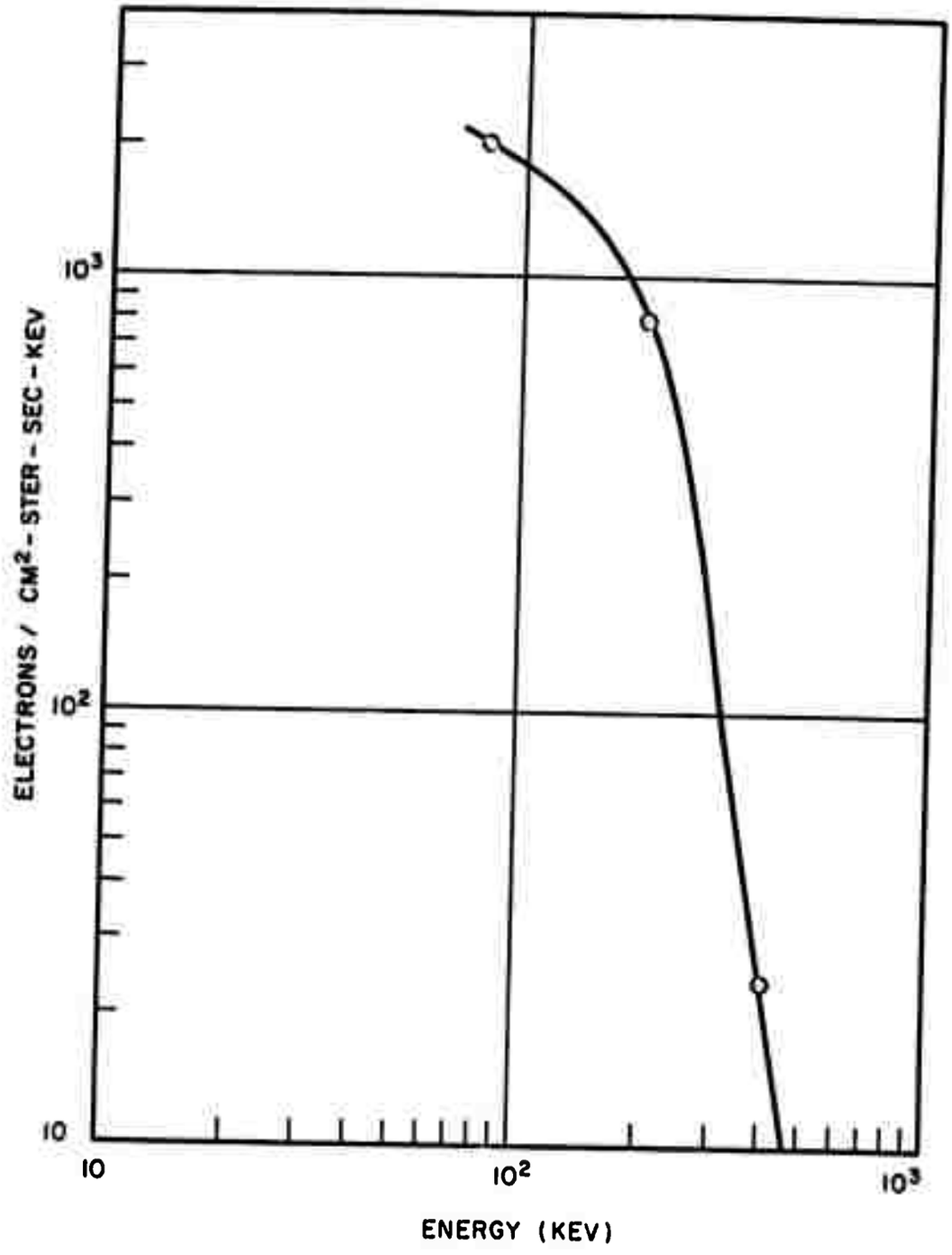

Fig. 3-7 The Differential Energy Spectrum of Electrons at the Foot of the Outer Belt

The Explorer VI results show that the time variations are very complex and do not fit into any simple pattern. For example, during the early part of the storm of 16 Aug 1959, Rosen et al. (Ref. 18) reported an increase in the outer zone in the counting rate of their plastic scintillator (which detects particles directly with high efficiency and bremsstrahlung with low efficiency) at the same time that Fan et al. (Ref. 19) and Arnoldy et al. (Ref. 20) report a decrease in two Geiger counters and one ionization chamber (which detect Van Allen electrons from their bremsstrahlung). Neither the cause for the relatively rapid changes in the observed intensity of the electron belt nor the origin of these electrons has been adequately explained.

The source of the Van Allen belt will be discussed briefly, although it does not bear directly on the matter of artificial injection. Equations of motion show that an individual charged particle cannot approach the dipole field from outside and enter a trapped orbit; further, there are no definitive experiments pointing clearly to the source of the trapped particles. There is, however, good indirect evidence on the source of Van Allen protons, namely, the beta decay of the neutron albedo caused by primary cosmic ray interactions at the top of the atmosphere. This may also be the source of the Van Allen electrons; another likely source is the solar wind plasma. Although individual particles cannot enter trapped orbits from without, the solar plasma may disrupt the geomagnetic field locally and allow injection. The energy of solar plasma electrons is thought to be small compared with the Van Allen electrons. Solar plasma injection, therefore, would have to be accompanied by the acceleration of the newly trapped electrons. This could conceivably be done by the betatron effect during magnetic storms. The source of the Van Allen electrons is one of the major unanswered questions in space physics. Experiments with artificially injected electrons, proposed in the following sections, would not result in any direct evidence on this source. However, an attempt would be made to measure the lifetime of trapped electrons. The result of the lifetime measurement would give an indication of the required strength of the source, since a rough equilibrium must exist between the number of electrons injected and the number lost.

Section 4
TECHNIQUES FOR ELECTRON INJECTION

4.1 INJECTION FROM THE EARTH'S SURFACE

It is conceivable that an electron accelerator, or a beam of neutrons from a reactor, pointed skyward, would have particle energy and flux intensity great enough to allow a detectable number of particles to emerge from the top of the atmosphere. (The neutrons would then decay and be a source of electrons.) An examination of the numbers involved, however, will quickly discourage this idea. For electrons in air, the rate of energy loss is 2 Mev/gm-cm^{-2} and the radiation length is 37 gm/cm^2. If there were no shower effects, the electrons would have to have an initial energy of 2 Bev in order to penetrate the atmosphere (the atmosphere is about 1000 gm/cm^2 thick). The shower mechanism would increase this energy by roughly a factor of 10. For neutrons in air, the mean free path for nuclear interaction is about 5 gms/cm^2. In passing through the atmosphere, the initial flux would be degraded by a factor of 10^{-70}

4.2 EXPLOSIVE INJECTION FROM A BALLISTIC ROCKET

The Argus experiment has shown that a nuclear explosion above the atmosphere will deposit a measurable number of electrons into the geomagnetic field. However, the present bomb moratorium rules out this method. A similar approach has been suggested in which a shaped-charged high explosive bomb containing an intense radioactive β-source would be detonated above the atmosphere. The explosion would atomize and partially ionize the β-source. The ionized component would be trapped by the earth's field; the source of electrons would be localized and magnetically supported so that it would not fall back into the atmosphere. A rough calculation has indicated that the fraction of a source which would be ionized by a conventional explosion is negligible. Another objection to this scheme (as well as to the Argus-type experiment) is the lack of control over the number of injected electrons and their energy.

4.3 INJECTION FROM A SATELLITE

Two methods of electron injection from a satellite have been considered. In the first method, a radioactive β-source would supply electrons; no acceleration would be required. The ejected electron beam would be defined in direction and energy by collimation and magnetic selection. This system is relatively simple, but requires a source strength of about 100 megacuries for an electron-beam current of one ma. (This number is calculated assuming that 1 percent of the decay electrons would have the appropriate direction and energy to pass through the beam selector.) The difficulties involved in handling such a source before launch, the danger of contamination from an abortive launch, and the problem of fallout when the satellite eventually reenters the atmosphere are so great that this method must be considered unfeasible.

The second method of satellite injection (and the only injection scheme in which the advantages outweigh the disadvantages) is to use an electron accelerator. For electron energies about 1 Mev, there are a number of accelerators which are either commercially available or in the design state. In the experiments we propose in the following sections, two different types of accelerator will be required. One should be a pulsed type with a high current and low duty-cycle; the other should be a d-c machine. (The pulsed accelerator cannot be used in all situations because of the satellite-charging problem.) Characteristics of two acceptable accelerators are listed in Table 4-1. Other comparable accelerators can undoubtedly be found.

In the pulsed accelerator, the instantaneous power dissipation during the pulse is 100 Mw. This energy is capacitor-stored, and the weight of the capacitors and their charging circuit is included in the listed weight of 250 lbs.

The electrostatic accelerator is made up of a number of Wimshurst-type electrostatic generators connected in series, rather than the more conventional Van de Graaff system. In designing a satellite to carry such an accelerator, allowance must be made for the gyroscopic effect of the moving parts.

Table 4-1

CHARACTERISTICS OF TWO ELECTRON ACCELERATORS

Characteristics	Varian Pulse-Transformer Electron Accelerator	High Voltage Engineering Electrostatic Accelerator
Electron Energy	1 Mev	1–2 Mev
$\frac{\Delta E}{E}$	3–4 %	1%
Beam Current	100 amps (during pulse)	10^{-3} amps
Pulse Duration	4×10^{-6} sec	d.c.
Repetition Rate	0–2.5/sec	d.c.
Beam Size	1 cm^2	1 cm^2
Power Required	1.5 kw	1.5 kw
Weight (without power supply)	250 lbs	600 lbs
Size	3 ft diam. by 5 ft length	approximately the same as the Varian accelerator
Availability	1 year	1 year

The power for these accelerators will presumably be supplied by batteries intermittently charged by banks of solar cells. To estimate the weight of the batteries and the size of the solar cell array required, it will be assumed that the accelerator operates continually, that the batteries can supply the required power for 24 hours without recharging, and that the solar cells will deliver a new 24-hour charge in a period of 12 hours. The pertinent numbers are approximately:

(1) Rechargeable batteries deliver 1 kw-hr per 15 lbs of battery weight.
(2) In the spectrum interval over which solar cells are sensitive, the sun supplies 1400 watts/m^2 above the atmosphere.
(3) The solar cell energy-conversion efficiency is 10 percent.
(4) A solar cell bank weighs 1-1/2 lbs/ft^2.

The battery weight would then be 540 lbs, the area of the solar cell array would be 230 ft^2, and the weight of the solar cells would be 350 lbs. This means that the total accelerator and power-supply weight would be 1150 lbs for the pulse transformer and 1500 lbs for the d-c machine. These numbers are conservative, and since the accelerators will actually be turned on only a small fraction of the time, these estimated weights can probably be reduced by 50 percent.

To study the feasibility of various experiments using the electron beam ejected from a satellite, we will have to assign specific characteristics to the satellite and the electron accelerator. It will be assumed that:

(1) For pulsed electron experiments, the Varian accelerator will be used: 100 amps for 4 μsec with an electron energy of 1 Mev.
For d c injection, the High Voltage Engineering electrostatic accelerator will be used: 1 ma at 1 Mev.

(2) The satellite can be put into any desired orbit, and its position as a function of time is known.

(3) The satellite is instrumented to measure and record the local direction and magnitude of the earth's magnetic field.

(4) The accelerator can be oriented by ground control or by a programmer so that the ejected electron beam will have a known but variable angle with respect to the local direction of the earth's field.

(5) In transmitting experimental data from the satellite to the ground, there is no limitation set by telemetry bandwidth on the time duration of signals.

Experiments which make use of pulsed injection could conceivably be carried out by a ballistic rocket-borne accelerator, rather than from a satellite. There would be, however, the additional requirements of a recovery capability and a great number of launching bases. Since there is no obvious advantage to a ballistic rocket system, we will restrict ourselves to satellite injection.

Section 5
DESCRIPTION OF THE EXPERIMENTS TO BE PERFORMED WITH ARTIFICIALLY INJECTED ELECTRONS

5.1 INTRODUCTION

In the following three sections, experiments to be performed with an injected electron beam are studied in detail. First, however, a general description will be given of the experiments and the types of results which might be expected.

5.2 FILLED SHELL EXPERIMENTS

An orbit is chosen such that during part of one revolution a satellite would be nearly tangent to an integral invariant surface (Section 3.1). Electrons are injected during this time of tangency with an appropriate pitch angle so that they become trapped. Because of the longitudinal drift of the electrons, a thin electron shell will spread around the earth and have a shape dictated by the integral invariant surface. After the shell has been filled, the satellite will stop injecting and on successive revolutions will pass repeatedly through the shell. Using radiation detection instruments on board the satellite, one could then measure:

- The longitudinal drift time, which would be inferred from the time elapsed between the initiation of injection and first detection
- The change of the electron-energy spectrum with time (lifetime)
- The diffusion of the well-defined edges of the shell
- A diurnal compression and expansion of the field which would shift the position of the shell
- The effect of a magnetic storm on the shape of an integral invariant surface
- The effect of a magnetic storm on the trapped electron-energy spectrum and the possible catastrophic dumping of the trapped electrons

5.3 BOUNCE-TIME MEASUREMENT

From a polar orbit satellite, a pulse of electrons would be injected perpendicular to the direction of the local magnetic field. These electrons would move along a field line to the conjugate mirror point in the other hemisphere, and then return nearly to the position of their injection. Because of the longitudinal drift of the electrons and the motion of the satellite, the electrons (after one bounce) would mirror at a point several kilometers from the satellite. This would rule out direct detection. The presence of the electrons at the mirror point, however, could be detected from their synchrotron radiation using a radio receiver on the satellite. The bounce time would be inferred from the time elapsed between injection and detection. A measurement of the bounce time will give:

- The average value of the geomagnetic field along a particular field line which could be compared to the predictions of several geomagnetic models
- The maximum latitude at which field lines close; injection at higher latitudes would lead to infinite bounce times
- The diurnal distortion of the field by the solar plasma manifesting itself as a diurnal change in bounce time at a constant latitude
- The effect on all of the above geomagnetic features due to a magnetic storm

5.4 CONJUGATE-POINT MEASUREMENT

From a polar orbit satellite, a pulse of electrons would be injected parallel to the direction of the local magnetic field. These electrons would move along a field line to the conjugate of the injection point in the other hemisphere, but would not mirror because of their injection pitch-angle. Instead, the electrons would continue moving down the field line and lose their energy by ionization in the upper atmosphere. This filament of ionization would be located by radar reflection from a ground station. From the position of the satellite at injection and the location of the point where the electrons ionize the atmosphere, the conjugate points of a particular field line can be inferred.

As in the previous experiments, repeated measurements of the position of the conjugate points could then be correlated with diurnal and magnetic storm effects. A precise location of conjugate points is not only of scientific interest, but has many potential military applications sufficiently important to justify the implementation of the experimental program.

Section 6
THE FILLING OF MAGNETIC SHELLS

6.1 INTRODUCTION

In this section, we will examine the feasibility of injecting and trapping a detectable number of electrons in a thin shell centered about an integral invariant surface. It will be assumed that the injection pitch-angle can be controlled from the satellite so that the electrons will always be trapped. Thus, the principal points to be considered are the flux intensity which can be achieved in a well-defined, isolated, thin shell and the subsequent history of intersection of the shell by the satellite. Throughout the calculation, the dipole model of the geomagnetic field will be used.

The shape of the shell to be filled will be defined arbitrarily as the volume lying between the two magnetic invariant surfaces shown in Fig. 6-1. The outer surface

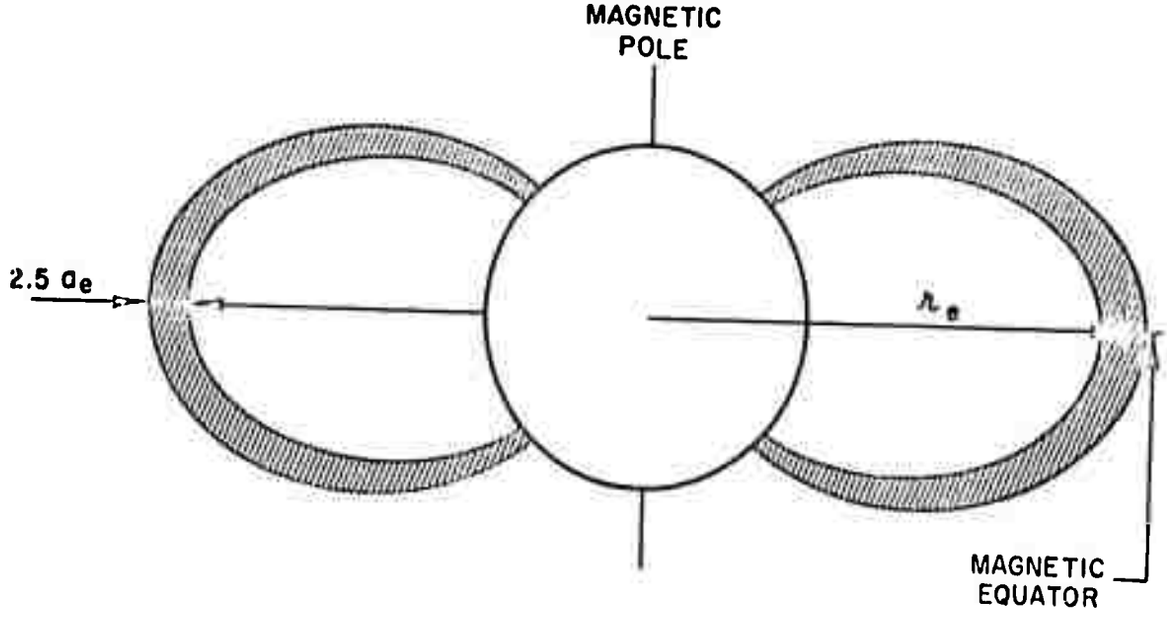

Fig. 6-1 Definition of the Magnetic Shell

crosses the magnetic equator at a distance from the center of the earth of $(r_e + 1.25\ a_e)$, and the inner surface at $(r_e - 1.25\ a_e)$. The quantity a_e is the

cyclotron radius of a 1-Mev electron at the equatorial point ($r = r_e$, $\phi = 0$) with a 90° pitch angle.

$$a_c = \frac{p}{e B_e}$$

In order that the satellite inject electrons only into this shell, the injection must be limited to the time the satellite spends in the volume defined by the two field lines which cross the magnetic equator at ($r_e + 0.25\, a_e$) and ($r_e - 0.25\, a_e$). The time the satellite spends in this volume is called injection time T_I and it is the purpose of the calculations which follow to determine T_I for various types of satellite orbits. The injection time is then used to calculate the particle flux which can be established with a given injection current, and the longitudinal extent of the shell is determined by comparison of the injection time T_I with the electron longitudinal drift time T_D. A filled shell is defined as one with no longitudinal gaps, so that electrons will be encountered on any subsequent satellite passage through the shell.

The coordinate system shown in Fig. 6-2 is used for the calculation. The orthogonal axes labelled with capital letters are fixed and centered with respect to the earth, with the Z axis coincident with the earth's spin axis and the X axis passing through the Greenwich meridian. The second set of axes labelled with lower case letters is also fixed with respect to the earth, but with origin at the displaced magnetic dipole position and with the z axis along the dipole moment. The satellite orbits are thus fixed with respect to the earth system except for rotation about the Z axis once per day at an angular velocity $\dot{\Phi}_{earth}$. The dipole field is fixed in both systems.

It is desired to describe the satellite position P in terms of the dipole radius vector, $\vec{r}$, in order to establish the satellite aximuthal range $\Delta\Phi$ during which the satellite is in the desired injection region. The injection time T_I is the time to cover this range

$$T_I = \frac{\Delta\Phi}{\dot{\Phi}_{sat.} - \dot{\Phi}_{earth}} \qquad (6.1)$$

where $\dot{\Phi}_{sat.}$ is the angular velocity of the satellite.

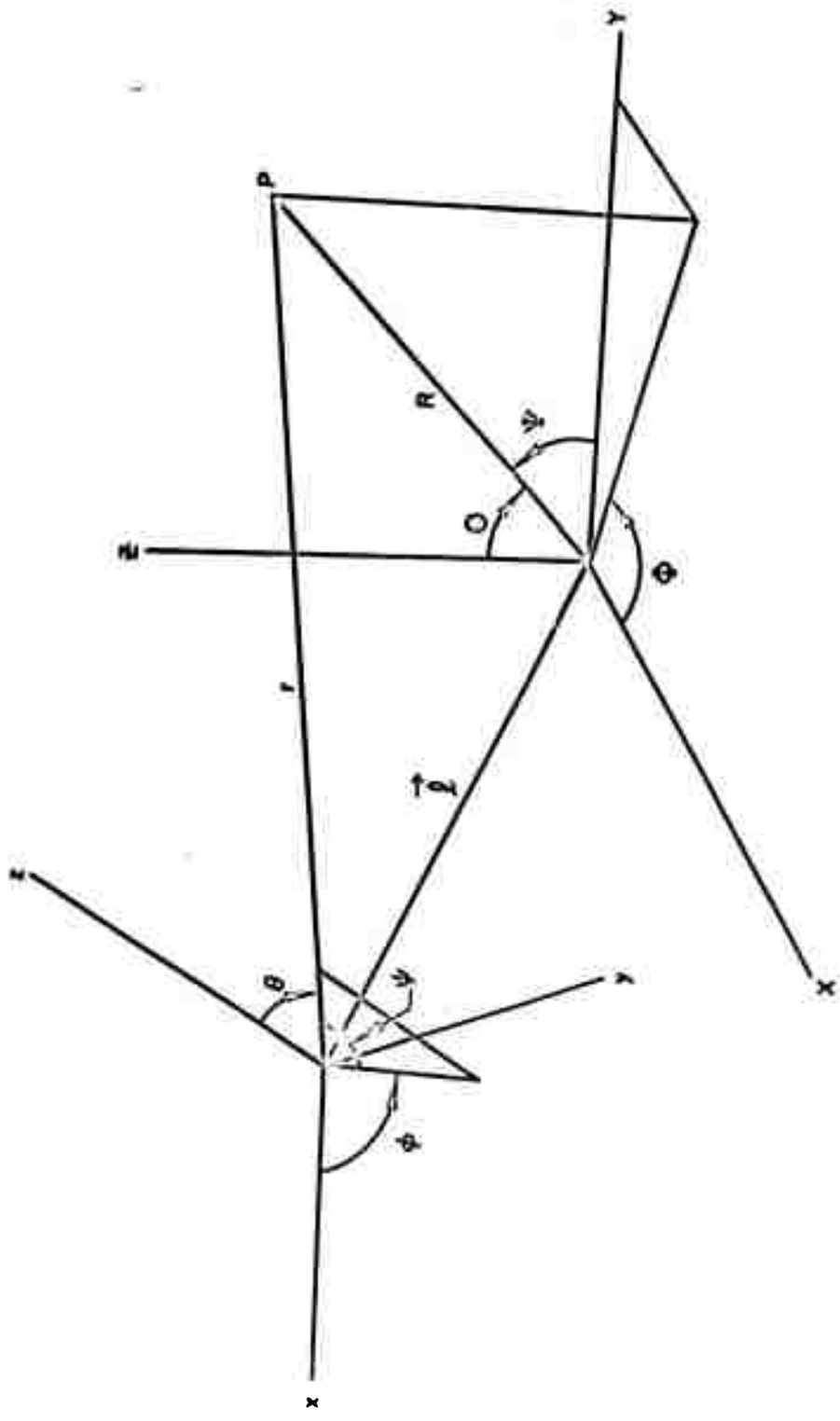

Fig. 6-2 Geographic and Geomagnetic Coordinate Systems. The Axes (X, Y, Z) Are the Geographic Coordinates. The Geomagnetic Axes (x, y, z) Are Displaced and Tilted with Respect to the Geographic System.

The expression for r in the geographic coordinate system is

$$r^2 = R^2 + \ell^2 + 2R\left[\ell_X \sin\Theta\cos\Phi + \ell_Y \sin\Theta\sin\Phi + \ell_Z \cos\Theta\right] \qquad (6.2)$$

The values of the components of ℓ in units of earth radii are

$$\bar{\ell}_X = 0.0577$$
$$\bar{\ell}_Y = -0.0324$$
$$\bar{\ell}_Z = 0.0184$$

It should be noted that barred quantities are in units of earth radii throughout this section.

6.2 EQUATORIAL ORBIT INJECTION

Simple cases are generated by assuming equatorial satellite orbits and considering the displaced dipole to be parallel to the spin axis and in the earth's equatorial plane. The problem then assumes the two dimensional geometry shown in Fig. 6-3.

The satellite orbit is given by

$$R = \frac{a\,(1 - \epsilon^2)}{1 - \epsilon\cos(\Phi - \delta)} \qquad (6.3)$$

where a and ϵ are the elliptic-orbit, semimajor axis and eccentricity, respectively, and δ is the major-axis phase angle introduced by the earth's rotation. Equation (6.2) becomes, with $\Theta = 90°$

$$r^2 = R^2 + \ell^2 + 2R\left[\ell_X \cos\Phi + \ell_Y \sin\Phi\right] \qquad (6.4)$$

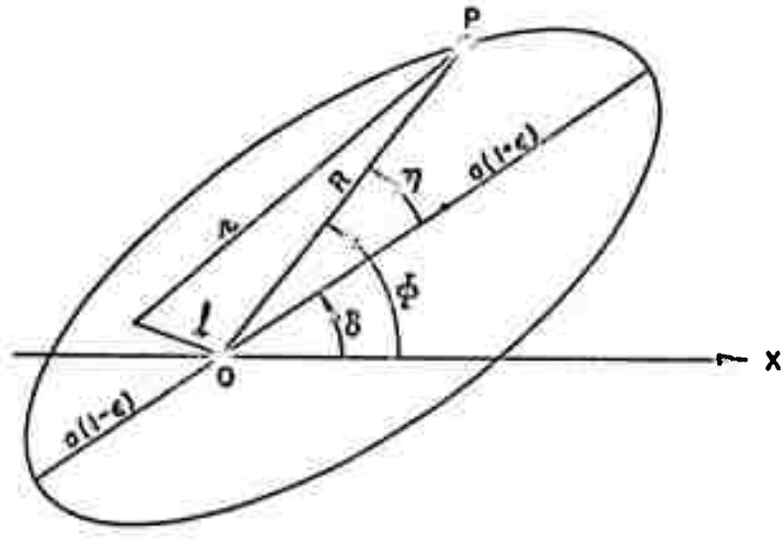

Fig. 6-3 Two-Dimensional Coordinate System for Equatorial Orbit Calculations

Differentiating Eqs. (6.3) and (6.4), and equating r and R to first order, one gets

$$\Delta r = \frac{a_e}{2} = \Delta\Phi \left\{ \left[R + \ell_X \cos\Phi + \ell_Y \sin\Phi \right] \frac{\epsilon \sin(\Phi - \delta)}{1 - \epsilon \cos(\Phi - \delta)} + \left[\ell_X \sin\Phi - \ell_Y \cos\Phi \right] \right\} \tag{6.5}$$

Several cases have been considered for equatorial orbit injection. These are obtained from Eq. (6.5) by applying special conditions which are described below.

Case 1. The tangency of orbit and invariant surface occurs at apogee when the major axis of the orbit coincides with the dipole displacement vector, which lies at 150.9° E long. Then $\Phi \approx \delta$ and $\bar{R} = \bar{a}(1 + \epsilon)$. Since $\sin \eta = \eta_1/2$ on the average,

$$\Delta\Phi_1 = 2\eta_1 \text{ and } \frac{\bar{a}_e}{2} = \epsilon\, \bar{a}\, \frac{1+\epsilon}{1-\epsilon}\, \frac{\eta_1^2}{2} \tag{6.6}$$

The numerical values of $\Delta\Phi$ for all the special cases are presented in summary in Section 6.4.

Case 2. For circular orbits, it is instructive to consider the case of the orbit intersecting the invariant surface at a point approximately at right angles to the dipole displacement vector. This can then be compared with the tangent case. From Eq. (6.5) with $\epsilon = 0$, the extreme values of $\Delta\Phi$ are obtained by finding the extremes of its coefficient.

$$\frac{d}{d\Phi}\left[-\ell_X \sin \Phi + \ell_Y \cos \Phi\right] = 0$$

The maximum coefficient is at $\Phi = 60.9°$ E, where $\eta_2 = \Phi - 60.9°$. Then

$$\Delta\Phi_2 = 2\eta_2 \text{ and } \frac{\bar{a}_e}{2} = 0.066\, \frac{\eta_2^2}{2} \tag{6.7}$$

The tangent case is again at $\Phi = 150.9°$ E in which case $\bar{a}_e/2 = 0.0348\, \eta_2^2/2$. The maximum injection time exceeds the minimum by about 40 percent.

Case 3. Injection at apogee in an elliptic orbit is shortest when the orbit major axis lies normal to the dipole displacement direction. For this case $\delta = 60.9°$ E, and $\eta_{3,4} = \Phi - 60.9°$.

Then

$$\frac{\bar{a}_e}{2} = \left[\bar{a}\epsilon\left(\frac{1+\epsilon}{1-\epsilon}\right)\left(\frac{\eta_3}{2}\right) + 0.0561\left(\frac{\eta_3}{2}\right) + 0.0665\right]\eta_3$$

$$= \left[\bar{a}\epsilon\left(\frac{1+\epsilon}{1-\epsilon}\right)\left(\frac{\eta_4}{2}\right) + 0.0561\left(\frac{\eta_4}{2}\right) - 0.0665\right]\eta_4 \qquad (6.8)$$

$$\Delta\Phi_3 = \eta_3 + \eta_4 \qquad (6.9)$$

Case 4. Injection from the satellite at a position other than apogee will, of course, reduce the length of the injection time. This reduction is obtained here for the simple case of an elliptic orbit in the equatorial plane of a geocentric dipole. For R equal to 80 percent of apogee, the shell thickness is decreased by $(0.8)^3$ because of increased magnetic field strength. The injection position Φ is obtained from the orbit equation with $R = (0.8)a(1+\epsilon)$, so that

$$0.8 = \frac{1-\epsilon}{1-\epsilon\cos\Phi}$$

and

$$\frac{\bar{a}_e}{2} = \bar{a}\epsilon\,\frac{1+\epsilon}{1-\epsilon}\,(0.8)^{-1}\sin\Phi\,\Delta\Phi_4 \qquad (6.10)$$

6.3 POLAR ORBIT INJECTION

Injection from a polar orbit satellite is another simple case. Because of the increased complexity introduced by the dipole field, the assumptions are made that the dipole is geocentric and that the rotation of the earth during injection may be neglected. The dipole coordinate system is shown in Fig. 6-4, where ψ is the magnetic latitude.

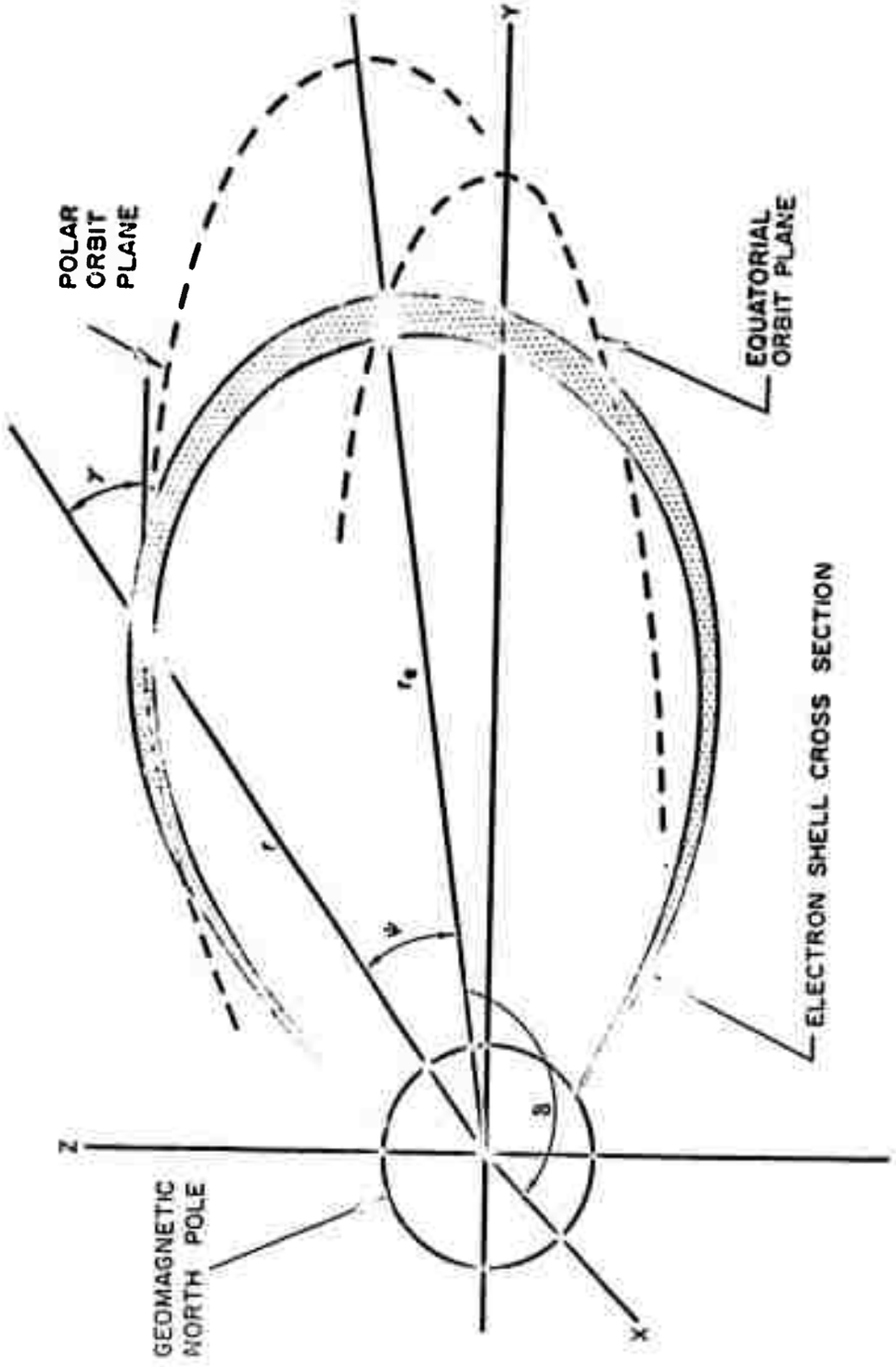

Fig. 6-4 Intersections of a Polar Orbit Satellite and an Equatorial Orbit Satellite with a Magnetic Shell

The electron shells are thinner away from the equatorial plane because of the increased magnetic field strength. Hence, the variation of shell thickness with latitude over the region of intersection must be considered in addition to the satellite position relative to the invariant surface. Furthermore, the shell thickness and satellite displacement are now measured at an angle $\pi/2 - \gamma$ to the radius vector r.

The allowable increase in shell thickness normal to the shell is given by

$$\frac{1}{\sin\gamma}\ \frac{\Delta\bar{r}_p}{4} = \frac{(1 + 3\sin^2\psi)^{1/2}}{\cos\psi}\ \frac{\Delta\bar{r}_p}{4}$$

$$= d\bar{r}_{orbit} - d\bar{r}_B$$

$$= \left[- \frac{\bar{a}(1 - \epsilon^2)\epsilon \sin\psi}{(1 - \epsilon\cos\psi)^2} + 2\bar{r}_e \sin\psi\cos\psi \right] \Delta\psi \qquad (6.11)$$

This expression can be simplified by evaluating $\Delta\bar{r}_p$ in terms of $\Delta\bar{r}_e$ which was valid at the geomagnetic equator. $B\rho$ is a constant for electrons with a given energy and pitch-angle, where ρ is the cyclotron radius. Then

$$\Delta\bar{r}_p = \Delta\bar{r}_e\ \frac{\rho_p}{\rho_e} = \Delta\bar{r}_e \left(\frac{B_{\psi=o}}{B_\psi}\right)$$

$$= \Delta\bar{r}_e \left(\frac{r}{r_e}\right)^3 \frac{1}{(1 + 3\sin^2\psi)^{1/2}}$$

$$= \Delta\bar{r}_e \frac{\cos^6\psi}{(1 + \sin^2\psi)^{1/2}} \qquad (6.12)$$

Further simplification can be made using the fact that the magnetic field line and the orbit intersect at $\bar{r}$ so that

$$\bar{r} = \frac{a(1 - \epsilon^2)}{1 - \epsilon\cos\psi} = \bar{r}_e \cos^2\psi \qquad (6.13)$$

These expressions allow Eq. (6.11) to be rewritten as

$$\frac{\Delta\bar{r}}{4} = \frac{\sin\psi}{\cos^4\psi}\left[-\frac{\epsilon\bar{r}_e^2\cos^3\psi}{a(1-\epsilon^2)} + 2\bar{r}_e\right]\Delta\psi \qquad (6.14)$$

The injection interval $\Delta\psi$ in Eq. (6.14) is to be compared with the equatorial case 4 of Section 6.2. The question is whether or not a larger angular injection interval for filling a given shell can be secured from a polar or from an equatorial satellite orbit.

Equation (6.10) may be rewritten as

$$\frac{\Delta\bar{r}}{4} = \frac{\epsilon f\bar{r}_e}{1-\epsilon}\sin\Phi\,\Delta\Phi_4 \qquad (6.15)$$

where the ratio of injection radius to apogee radius is taken as f rather than the arbitrary value of 0.8 used previously. In the case under consideration f = 1. Equation (6.14) can be simplified if the polar and equatorial orbit eccentricities are roughly equal, and if $\bar{r}_e$ is taken as comparable to, but less than, the polar orbit apogee. The result is

$$\frac{\Delta\bar{r}}{4} \approx \frac{\bar{r}_e\sin\psi\,\Delta\psi}{\cos^4\psi} \qquad (6.16)$$

Combination of the last two equations yields

$$\frac{\Delta\psi}{\Delta\Phi_4} \approx \left(\frac{\epsilon}{1-\epsilon}\right)\left(\frac{\sin\Phi}{\sin\psi}\right)\cos^4\psi \qquad (6.17)$$

6.4 SUMMARY OF THE VALUES OF $\Delta\Phi$

Table 6-1 gives some numerical values of $\Delta\dot{\Phi}$ and $\dot{\Phi}$ for the different cases discussed above. Satellite perigee was arbitrarily taken to be at $\bar{R} = 1.05$, and the equatorial pitch angle was chosen to be 30°. Several simple observations can be made about the results.

(1) For $\bar{R} > 5$, $\Delta\Phi$ for circular orbits is at least one order of magnitude larger than is obtainable at apogee from elliptic orbits.

(2) For $\bar{R} < 5$, $\Delta\Phi$ for circular orbits varies from one order of magnitude larger to one order of magnitude smaller than is obtainable at apogee from elliptic orbits.

(3) For elliptic orbits, $\Delta\Phi$ is approximately two orders of magnitude larger at apogee than at 0.8 of apogee. That is, the largest $\Delta\Phi$ occurs when

$$\sin\Phi \approx \Delta\Phi$$

(4) The comparison of polar and equatorial orbits indicates that typical $\Delta\Phi$ away from apogee are comparable for the two situations. It should be pointed out that one important assumption is made in the polar versus equatorial orbit comparison, namely, the earth's magnetic field is not being rotated out from under the satellite during injection.

Table 6-1

SATELLITE INJECTION ANGULAR INTERVALS AND ANGULAR VELOCITIES[a]

$\bar{R}$	$\Delta r \times 10^3$	$\Delta\Phi_1$	$\Delta\Phi_2$	$\Delta\Phi_3$	$\Delta\Phi_4 \times 10^3$ at 0.8R	$\dot{\Phi}_1$	$\dot{\Phi}_2$
1.5	0.0868	23.2	51.2	350.0	–	0.61	0.675
2.5	0.402	22.6	111.0	78.0	60.8	0.24	0.314
3.75	1.36	23.8	202.0	32.2	–	0.113	0.17
5.0	3.22	26.2	313.0	29.8	137.0	0.067	0.11
6.25	6.04	28.0	428.0	29.2	–	0.0425	0.081
7.5	10.9	30.8	568.0	31.5	244.0	0.030	0.060
10	25.8	34.8	862.0	34.8	356.0	0.017	0.039

[a] Distances are expressed in units of earth radii. Angles and angular velocities are expressed in milliradians and milliradians per second, respectively.

6.5 INJECTION TIME

To determine if it is possible to actually fill a given shell, the above information about $\Delta\Phi$ must be combined with the angular velocity of the satellite with respect to the local magnetic field and with the electron drift time. Table 6-2 lists some of the parameters involved as well as the ratio $\mathcal{R}$ of injection to drift time. The table is based on the orbits previously labelled as Case 3. Figure 6-5 presents in graphical form the dependence of $\mathcal{R}$ on $\overline{R}$.

Provided that injection occurs near apogee and the angular velocity vectors of the satellite and the earth are parallel, the behavior of $\mathcal{R}$ may be summarized as follows:

(1) For $\overline{R} \sim 5$, cancellation of the satellite's rotation by that of the earth is the most important factor determining the size of $\mathcal{R}$. Indeed, injection at apogee from an orbit of any allowed eccentricity will always fill a shell.

Table 6-2

RATIO OF THE INJECTION TIME TO THE DRIFT TIME

Injection at Apogee From An Equatorial Orbit Satellite in an Eccentric Dipole Field (Case 3)

$\bar{R}$	ϵ	$\dot{\Phi}_3 - \dot{\Phi}_{earth}$ (milliradians/sec)	T_D (sec)	Δt_{inj} (sec)	$\mathcal{R} = \frac{\Delta t_{inj}}{T_D}$
1.5	0.176	0.54	3,010	648	0.22
2.5	0.408	0.17	1,800	464	0.26
3.75	0.563	0.040	1,390	805	0.58
5.0	0.653	0.0059	900	5,050	5.62
6.25	0.712	0.030	722	960	1.33
7.5	0.754	0.043	600	737	1.23
10.0	0.810	0.056	450	625	1.39

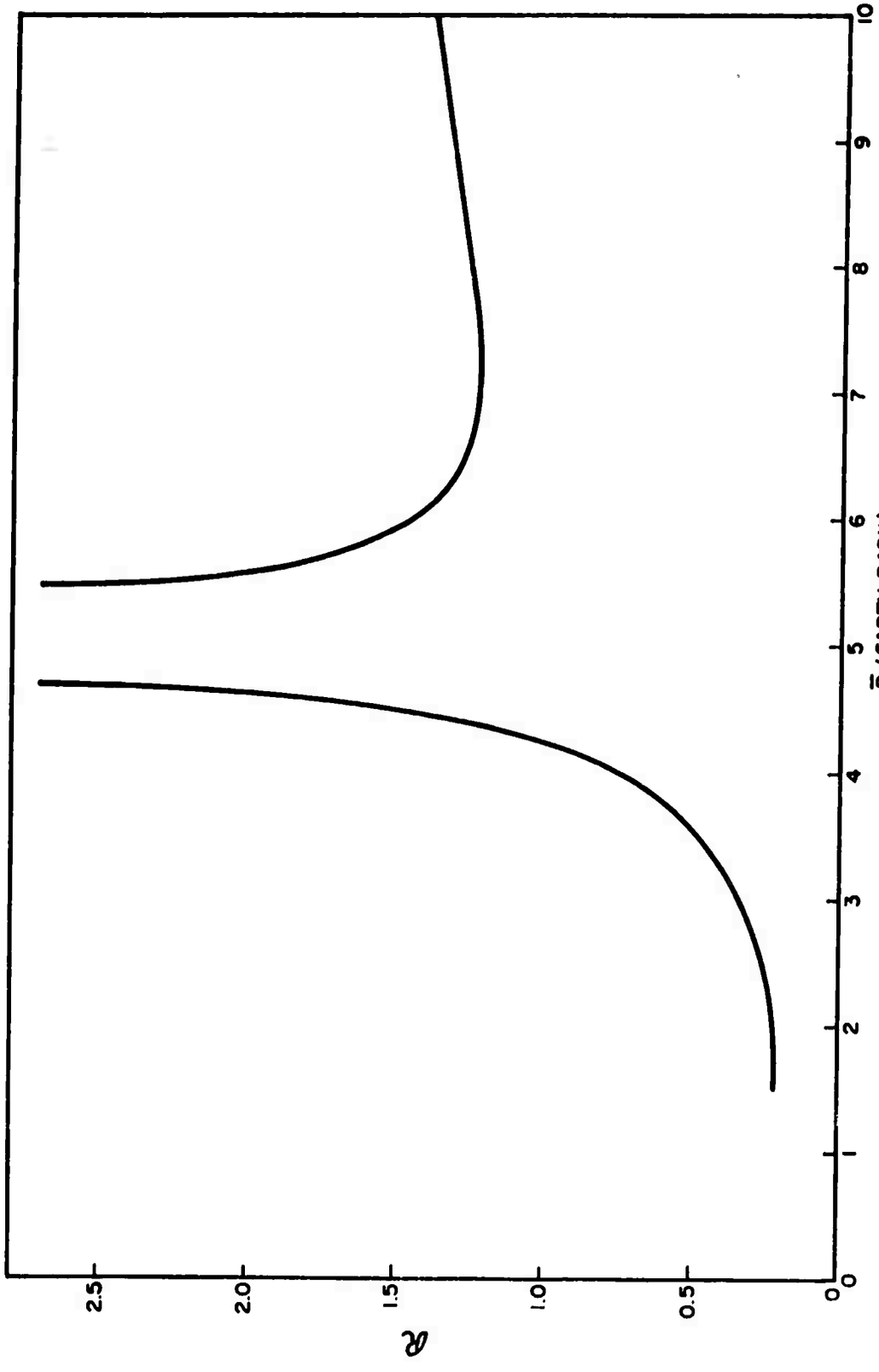

Fig. 6-5 Variation with Altitude of the Ratio of Injection Time to Electron Longitudinal Drift Time

(2) Shells having $\overline{R} \lesssim 3$ cannot be filled from the relatively high eccentricity orbits chosen, or from circular orbits. On the basis of the size of $\mathcal{R}$, elliptic orbits are about as good as circular orbits in the neighborhood of $\overline{R} \simeq 3$.

The above conclusions are probably valid for satellite orbits tilted with respect to the earth's equatorial plane by angles $\lesssim 0.5$ radians, provided the injection and magnetic lattitudes are of the same sign.

If injection occurs at some moderate distance from apogee, the values of $\mathcal{R}$ will be as much as two orders of magnitude smaller than those appearing in Table 6-2.

6.6 INFLUENCE OF ACCELERATOR BEAM FLUCTUATIONS

In addition to the radius of gyration a_e the thickness of a shell is influenced by the spread in accelerator beam energy, ΔE, and the divergence of the beam $\Delta\alpha$ along the line of injection. Consequently, the initial thickness Δr of a shell at the geometric equator may be expressed as:

$$\Delta r(a_e, E, \alpha) = 2a_e + \left(\left(\frac{\partial a_e}{\partial p} \Delta p \right)^2 + \left(\frac{\partial a_e}{\partial \alpha} \Delta\alpha \right)^2 \right)^{1/2}$$

$$= 2a_e + \left(\left(\frac{a_e}{p} \Delta p \right)^2 (a_e \cot\alpha \Delta\alpha)^2 \right)^{1/2}$$

$$= 2a_e \left[1 + \left(\left(\frac{E\Delta E}{E^2 - m^2c^4} \right)^2 + (\cot\alpha\Delta\alpha)^2 \right)^{1/2} \right] \qquad (6.18)$$

Typical numerical values for the increase in shell thickness for 1-Mev electrons injected at $\alpha = 30°$ are given in Table 6-3. These numbers indicate that ΔE and $\Delta\alpha$ probably are relatively unimportant factors in determining Δr.

Table 6-3

VALUES OF $\left(\frac{\Delta r}{2a_e} - 1\right)$

ΔE (Mev)	$\Delta \alpha$ (radians)	
	0.05	0.15
0.01	0.086	0.26
0.10	0.11	0.26

6.7 MAGNITUDE OF INJECTED FLUX

An estimate of the magnitude of the injected electron flux F is most easily obtained by considering the number of electrons crossing the equatorial plane per cm^2 per sec. The radial thickness of the shell at the equator is assumed to be $2.5a_e$; the accelerator injects a current I for a time Δt_{inj} at a geomagnetic radius r_e. Electrons are injected at the geomagnetic equator with a pitch angle α with respect to the local field, and thereafter cross the equatorial plane with the same pitch angle.

$$F_{\substack{\text{equatorial}\\ \text{plane}}} = \frac{\left(\begin{array}{c}\text{total number of}\\ \text{electrons injected}\end{array}\right)\left(\begin{array}{c}\text{number of times per sec each electron}\\ \text{crosses the equator}\end{array}\right)}{\left(\begin{array}{c}\text{cross sectional area in equatorial plane}\\ \text{as seen by the electrons}\end{array}\right)}$$

$$= \frac{6.3 \times 10^{18}\Delta t_{inj}}{2\pi r_e (2.5)a_e \cos\alpha} \quad \frac{I}{t_{bounce}}$$

$$= \frac{6.3 \times 10^{18} I}{2\pi r_e (2.5)a_e \cos\alpha} \quad \frac{\Delta\Phi}{\left(\dot{\Phi}_{satellite} - \dot{\Phi}_{earth}\right)} \quad \frac{1}{t_{bounce}} \qquad (6.19)$$

This equation assumes that no injected electrons are lost, and the electrons are spread uniformly around the shell.

Values of F and an estimate of the Van Allen electron flux above 0.9 Mev are given in Table 6-4 for the injection parameters of Case 3 found from Table 6-2.

Table 6-4

ALTITUDE DEPENDENCE OF INJECTED FLUX AND ESTIMATED VALUES OF VAN ALLEN ELECTRONS BETWEEN 0.9 AND 1.1 MEV

(Flux units are electrons per em^2 per sec)

$\bar{r}$	F	Van Allen
2.5	4600	8000
5.0	1600	200
7.5	30	2×10^{-1}
10	6	4×10^{-4}

The corrected electron spectrum of Walt, et al. (Ref. 17), was used to estimate the Van Allen flux. Extrapolation of their spectrum indicates a flux of electrons between 0.9 and 1.1 Mev of the order of 10^2 per em^2 per sec. Values of the electron flux at different geomagnetic distances can be arrived at by scaling the Walt flux of 5×10^6 electrons greater than 20 kev per em^2 per sec by the variation of quiet-day flux with distance as given by Dessler (Ref. 3). The Van Allen electron flux so obtained is uncertain by one or two orders of magnitude.

It should be noted that the initial angular distribution of injected electrons will be different from the angular distribution of Van Allen electrons. This directional feature of the injected flux may be useful in discriminating against the flux of naturally occurring electrons.

Section 7
BOUNCE-TIME MEASUREMENT

7.1 INTRODUCTION

The major obstacle to the bounce-time measurement is the detection of the injected electrons after their first bounce. We have proposed that these electrons be detected at the satellite by the radio signal from the electron's synchrotron radiation near the mirror point. To demonstrate the feasibility of this method, we will compute, in a typical case, the signal strength from the electrons and the sources of background which would interfere with the reception of the signal.

7.2 SATELLITE AND ELECTRON MOTION

We will consider that the satellite is at a low altitude (a few hundred kms) and is in a circular, polar orbit. The pulse of one-Mev electrons (100 amps for 4×10^{-6} sec) is injected nearly perpendicular to the direction of the local magnetic field. After the time for one bounce has elapsed, the electrons return and mirror at a point near the injection point, but at a lower altitude and east in longitude. During the bounce time, the satellite has also moved in latitude.

We will restrict ourselves to one special case throughout the discussion of the bounce-time measurement; namely, injection on the field line which intersects the earth at a magnetic latitude of 45° and crosses the magnetic equator at 2 earth radii from the earth's dipole center ($r_e = 2 R_E$). At this position,

$$B = 4.6 \times 10^{-5} \text{ webers/m}^2$$
$$\omega_c = 2.9 \times 10^{6} \text{ rad/sec}$$
$$\nu_c = 440 \text{ Kc/sec}$$

a_c = 100 m

T_B = 0.2 sec

Satellite velocity = 8 km/sec

Longitudinal drift velocity of the mirror point = 13.5 km/sec

After the first bounce, the relative positions of the satellite and the electrons are shown in Fig. 7-1.

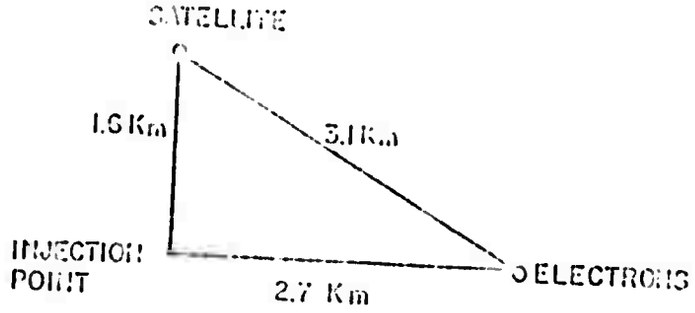

Fig. 7-1 Relative Position of the Satellite and The Electrons After One Bounce

The electrons will actually mirror at a lower altitude than the injection point for any injection pitch-angle α_i other than 90°. Of course, if α_i were exactly 90°, the injected electrons would strike the satellite after one cyclotron revolution at the time of injection. However, if $\alpha_i \leq 89°$ this will not occur, and we will assume that α_i is between 80° and 89°. An expression can be derived for the difference in altitude of the injection point and the mirror point in terms of α_i. Let the radial distance from the center of the earth to the injection point be r_i, and to the mirror point r_m. Then

$$r_i = R_E + h_i$$

$$r_m = R_E + h_m \qquad (7.1)$$

where R_E is the radius of the earth, and h_i and h_m are the altitudes of the injection point and mirror point, respectively. From the magnetic moment invariance, we have

$$B_i = B_m \sin^2 \alpha_i \tag{7.2}$$

From Eqs. (2.4) and (2.3a), we find that

$$\frac{\left(4 - 3\, r_i/r_e\right)^{1/2}}{\left(r_i/r_e\right)^3} = \frac{\left(4 - 3\, r_m/r_e\right)^{1/2}}{\left(r_m/r_e\right)^3} \sin^2 \alpha_i \tag{7.3}$$

If we take case h_i , $h_m \ll R_E$, then

$$\left(h_i - h_m\right) = \frac{R_E}{3} \epsilon_i^2 \tag{7.4}$$

where ϵ_i is defined by $\alpha_i = \frac{\pi}{2} - \epsilon_i$, $\epsilon_i < 10°$. The result does not depend on the value of r_e to the first order.

7.3 SYNCHROTRON RADIATION FROM ELECTRONS

The instantaneous power radiated by an electron with velocity $\vec{v}$ and total energy E , that is, kinetic energy plus the rest mass energy, is (Ref. 21):

$$P = (6 \times 10^9)\ e^2/c_3 \left(\frac{E}{mc^2}\right)^6 \left[\left(\frac{d\vec{v}}{dt}\right)^2 - \left(\frac{\vec{v}}{c} \times \frac{d\vec{v}}{dt}\right)^2\right] \tag{7.5}$$

In the case of an electron spiraling along a field line with pitch angle α,

$$P = (6 \times 10^9) \frac{e^2 \beta^3 \omega_c}{a_c} \sin^3 \alpha \left(\frac{E}{mc^2}\right)^4 \tag{7.6}$$

where $\beta = v/c$, and ω_c and a_c are the cyclotron angular frequency and cyclotron radius, respectively. The power radiated can then be expressed in terms of the local magnetic field strength and the pitch angle.

$$P = (6 \times 10^9) \left(\frac{e^2}{mc^2}\right)^2 \beta^2 c^3 B^2 \sin^2 \alpha \left(\frac{E}{mc^2}\right)^2 \tag{7.7}$$

If $\beta = 1$, then

$$P = (1.6 \times 10^{-14}) B^2 \sin^2 \alpha \left(\frac{E}{mc^2}\right)^2 \tag{7.8}$$

One-Mev electrons mirroring near the surface of the earth at a magnetic latitude of 45°, results in

$$P = 3 \times 10^{-22} \text{ watts}$$

In the pulse of electrons there are 2.5×10^{15} electrons, so that the power radiated by the pulse is about 10^{-6} watts at the mirror point.

This radiated power has a spectral distribution and an angular distribution which is not isotropic. Schwinger (Ref. 21) has derived the expression for the spectral distribution of an accelerating electron, and has applied the general formula to the case of a high energy electron ($\beta = 1$) moving with constant velocity in a circular path. Since the motion

is periodic, the spectrum consists of harmonics of the rotational (cyclotron) frequency $\nu_c = 440$ kc/sec. The total instantaneous power radiated into the n^{th} harmonic is P_n, and a critical harmonic number is defined by $n_c = 3/2\ (E/mc^2)^3$. In our case, $n_c = 40$. If the condition $n \ll n_c$ is satisfied, then

$$P_n = (4 \times 10^9)\ e^2/c\ \omega_c^2\ n^{1/3} \tag{7.9}$$

If the condition $n \gg 1$ is satisfied, then

$$P_n = (3.72 \times 10^9)\ e^2/c\ \omega_c^2 \left(\frac{E}{mc^2}\right)^2 \frac{n}{n_c^2} \int_{n/n_c}^{\infty} K_{5/3}(\eta)\, d\eta \tag{7.10}$$

where $K_{5/3}(\eta)$ is the Airy integral. Tomboulian and Hartman (Ref. 22) have evaluated numerically the integral in Eq. (7.10). Figure 7-2 shows the values of P_n as a function of frequency; the first seven harmonics are given explicitly, but for higher n's, only representative values of P_n are given. The most interesting feature of spectrum is the fact that due to relativistic effects the maximum power is radiated in about the 20^{th} harmonic, rather than in the first harmonic, which is the familiar case of low energy electrons.

Above 5 mc/sec, the density of the lines of the discrete spectrum becomes sufficiently large to allow a continuous approximation to be made. Defining $P(\nu)\, d\nu$ to be the power radiated at frequency ν in the interval $d\nu$, we find the continuous spectrum to be

$$P(\nu) = \frac{1}{\nu_c} P_n \tag{7.11}$$

This spectral distribution is shown in Fig. 7-3.

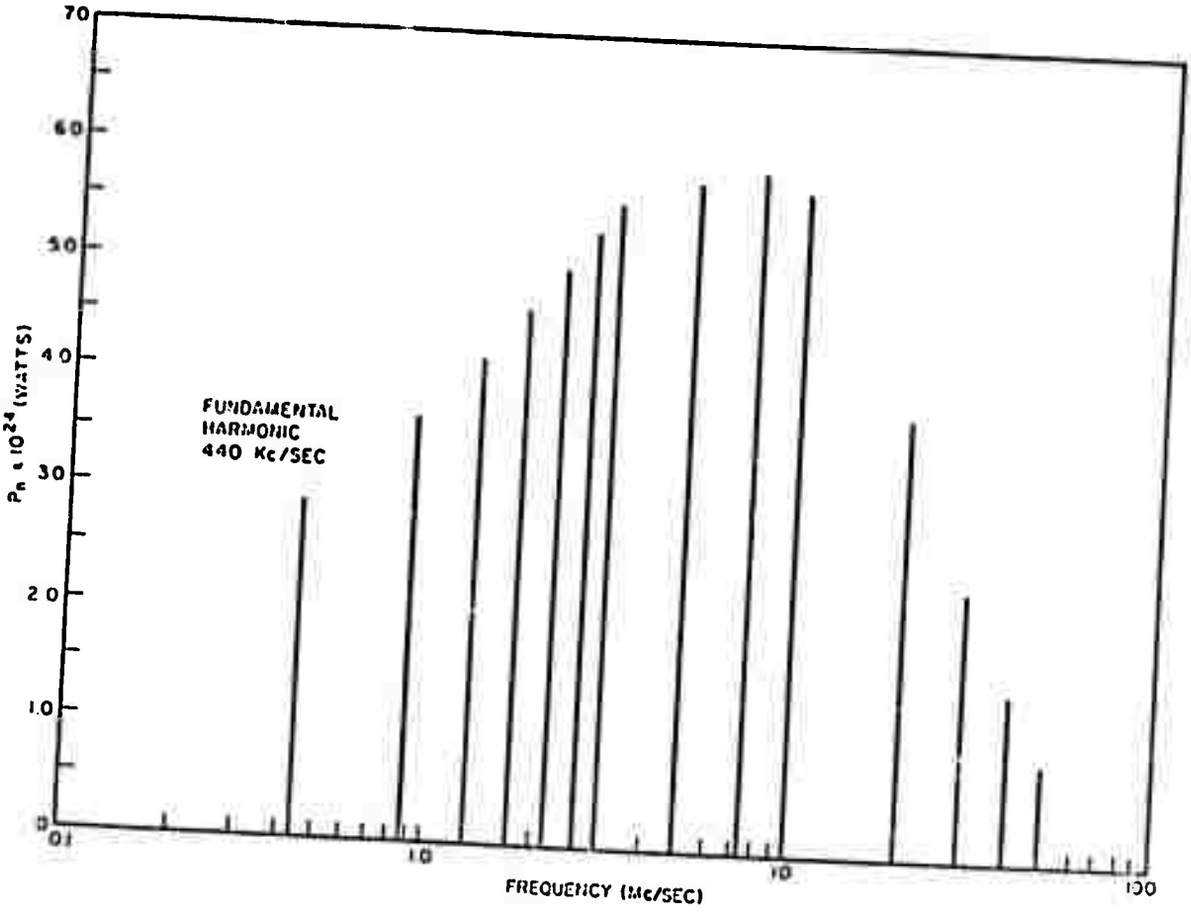

Fig. 7-2 The Line Spectrum of Synchrotron Radiation from an Electron Circulating with a Frequency of 440 Kc/sec. The first seven harmonics are shown explicity; at higher frequencies only representative lines are given

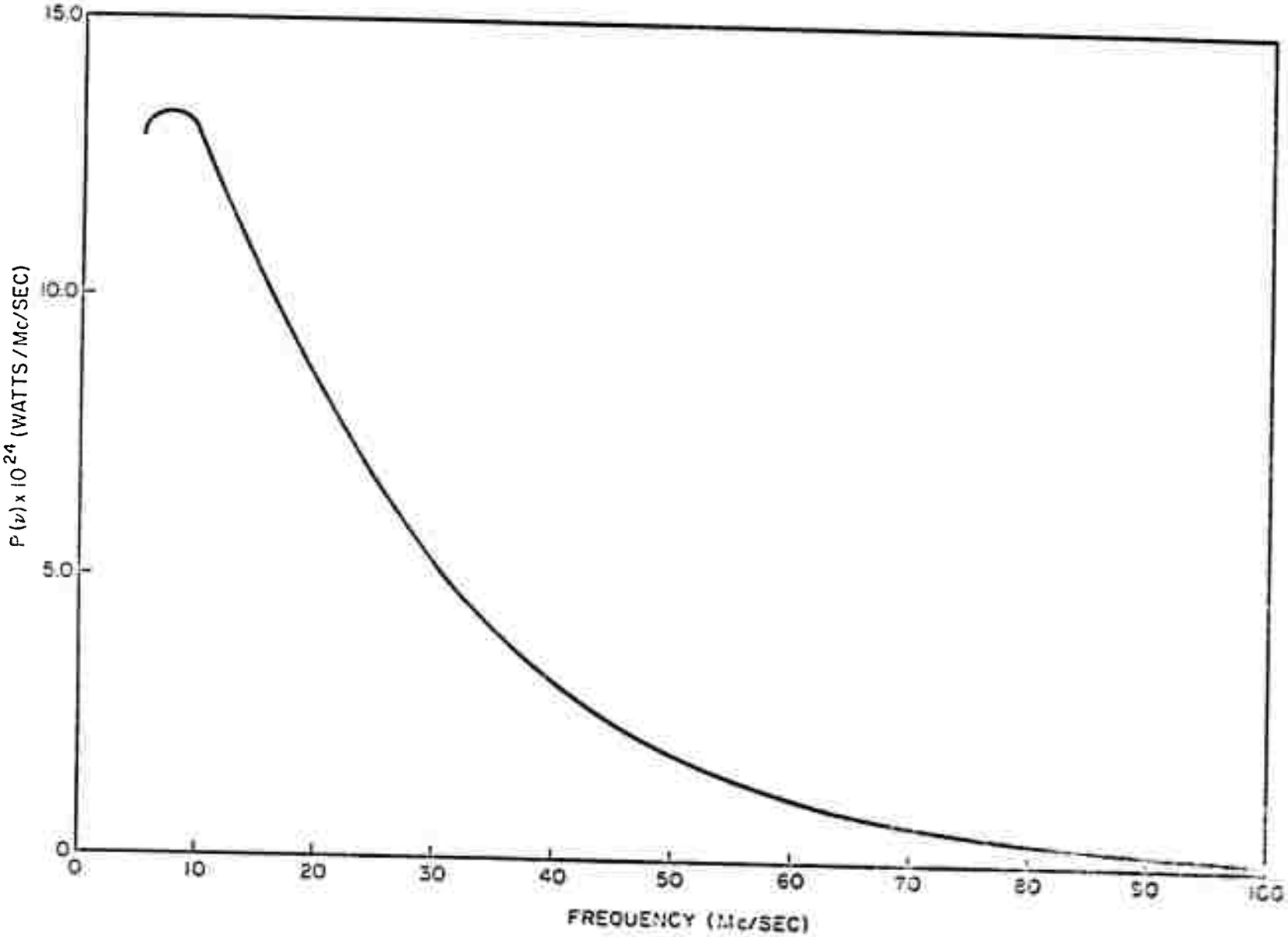

Fig. 7-3 The Continuous Approximation to the Spectrum of Synchrotron Radiation from an Electron Circulating with a Frequency of 440 Kc/sec

The angular distribution of the radiated power has also been derived by Schwinger. The expression is complicated, and for the purpose of this study, it will be sufficient to use the rough characteristics of the distribution. Namely, the power is a maximum in the orbital plane of the electrons and falls off rapidly with increasing values of the angle defined in Fig. 7-4.

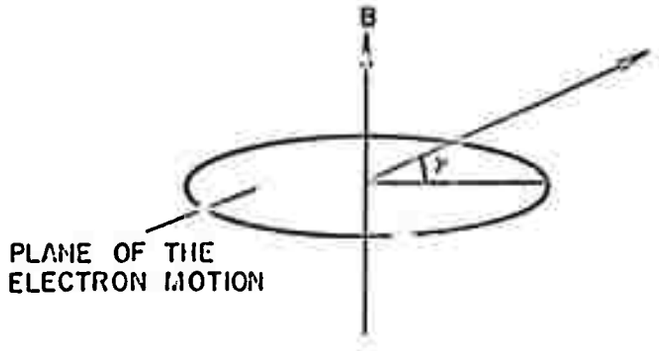

Fig. 7-4 Angular Coordinate for Synchrotron Radiation

Virtually all the radiation is emitted at angles less than $\gamma_{max} = (1/\pi\ mc^2/E)^{1/2}$. In our case, $\gamma_{max} \approx 20°$. If we assume that the angular distribution of the radiated power is constant for $0 < \gamma < \gamma_{max}$, and zero for $\gamma > \gamma_{max}$, then we can compute the power incident on an antenna at a distance L from the circulating electrons, where L is much larger than the electron's cyclotron radius.

$$S = S(\nu)\Delta\nu = \frac{NAP(\nu)\Delta\nu}{4\pi L^2 \gamma_{max}} \qquad (7.12)$$

$S(\nu)\Delta\nu$ is the signal strength at the input to a radio receiver which is tuned to a frequency ν and has a bandwith $\Delta\nu$; A is the effective area of the antenna, and N the number of circulating electrons. If we take the following parameters for the satellite experiment.

$$A = 1\ m^2$$
$$\nu = 7.5\ Mc/sec$$
$$\Delta\nu = 1\ Mc/sec$$
$$P(\nu) = 13 \times 10^{-24}\ watts/Mc/sec$$
$$N = 2.5 \times 10^{15}\ electrons$$
$$\gamma_{max} = 0.3\ radians$$
$$L = 3\ km$$

then the signal strength S is 10^{-15} watts.

7.4 SYNCHROTRON RADIATION-SIGNAL DURATION

Before examining the sources of background noise which effect the reception of the synchrotron radiation signal, an estimate will have to be made of the time duration of the signal. On one hand, we would like the signal to be as short as possible to minimize uncertainty in the measured bounce time; on the other hand, in so doing, the masking effect of the background noise becomes prohibitive. A calculation will show, however, that the duration of the signal is relatively insensitive to any practical control we might attempt to impose. If the satellite has a directional antenna, such as a parabola, the signal duration is determined by the length of time required for the electrons to pass through the acceptance angle of the antenna. The relative position of the satellite and the electrons are shown schematically in Fig. 7-5.

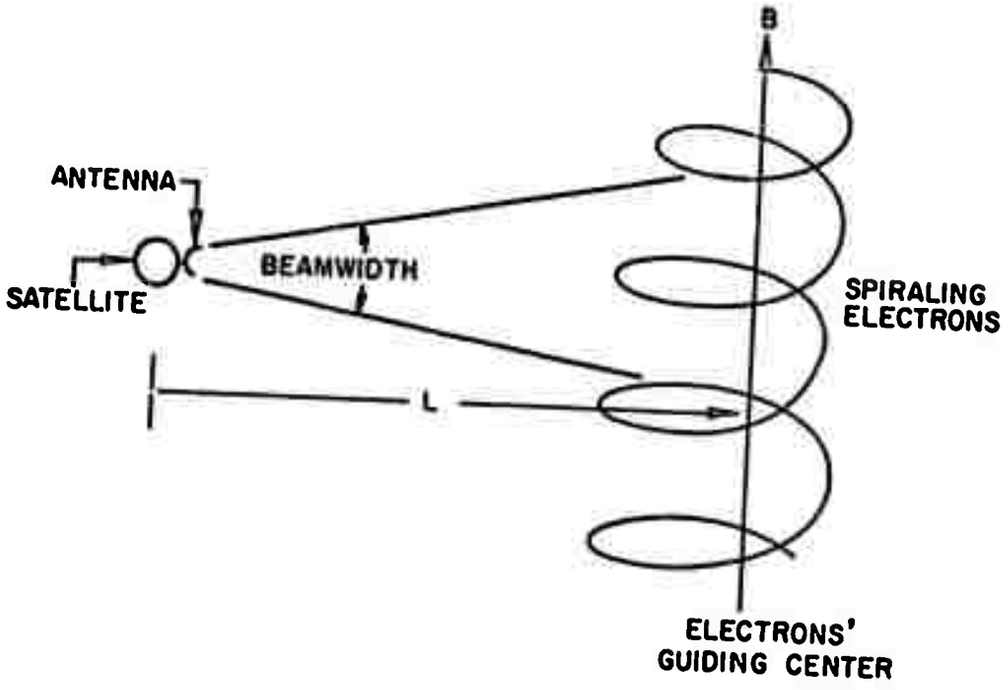

Fig. 7-5 Relative Position of the Satellite and Electrons

Since the electrons are radiating directionally, there is the question of whether the signal duration would be determined by the beamwidth of the antenna or by the maximum radiation angle γ_{max} of the electrons. For simplicity, we will take the beamwidth half-angle to be equal to γ_{max}; the signal duration will then be given by

$$T_S = \frac{4}{c}\left(\frac{R_E}{3}\right)^{1/2}\left[\left(R_E\epsilon_i^2/3 + L\gamma_{max}\right)^{1/2} - \left(R_E\epsilon_i^2/3 - L\gamma_{max}\right)^{1/2}\right] \quad (7.13)$$

where ϵ_i is defined by $\alpha_i = \pi/2 - \epsilon_i$. Equation (7.13) assumes that the electrons mirror below the region defined by the antenna beamwidth. If this is not the case, then Eq. (7.13) becomes

$$T_S = \frac{4}{c}\left(\frac{R_E}{3}\right)^{1/2}\left(R_E\epsilon_i^2/3 + L\gamma_{max}\right)^{1/2} \quad (7.14)$$

The expressions for T_S take into account the fact that electrons pass the antenna twice as they mirror and bounce. The signal duration is given in the following table for a few injection pitch-angles.

ϵ_i	T_S
0	6×10^{-4} sec
5°	1.5×10^{-4} sec
10°	8×10^{-5} sec

It is not possible to inject with ϵ_i's much greater than 10° without lowering the mirror point to such a degree that serious scattering losses occur at the first bounce in the other hemisphere before the electrons return to be monitored. There will be an intrinsic beam spread determined by the electron accelerator itself, so that it will not be possible to define the injection pitch-angle to better than a few degrees. For these reasons, the duration of the synchroton radiation signal will be about 10^{-4} sec in most cases.

The bounce time in our special case is 0.2 sec. The experimental uncertainty, therefore, associated with the bounce-time measurement would be about 0.1 percent.

7.5 BACKGROUND NOISE SOURCES

There are a number of sources of radio noise which radiate in the 10 Mc/sec region, and will be picked up by the receiver on the satellite. The ability to detect the injected electrons will be limited only by the noise background; and the signal-to-noise ratio must be estimated. We will consider the following sources of noise:

- Thermal emission from the galaxy
- Thermal emission from the sun
- Radiation from the Van Allen electrons
- Intrinsic receiver noise

Another possible source of background noise is radio transmission from the earth. This will presumably be negligible, however, since the ionosphere is opaque to radio frequencies less than about 30 Mc/sec. Most of the following information about radio noise has been taken from Pawsey and Braecwell (Ref. 23).

7.5.1 Galactic Noise

The radio emission from the galaxy can be represented as coming from a blackbody with temperature T_b. Radio astronomers scan the galaxy and present their results as a celestial mapping of T_b. From the blackbody radiation law, the power from a galactic distributed source striking an antenna which has a beamwidth half-angle of γ_{max} is represented by

$$P_{bg}(\nu)\Delta\nu = (9.67 \times 10^{-22})\nu^2 T_b A \gamma_{max}^2 \Delta\nu \qquad (7.15)$$

where A is the area of the antenna, and the satellite radio receiver is tuned to a frequency ν and has a bandwidth $\Delta\nu$ (both in Mc/sec).

When

$$\nu = 10 \text{ Mc/sec}$$
$$\Delta\nu = 1 \text{ Mc/sec}$$
$$A = 1 \text{ m}^2$$
$$\gamma_{max} = 20°$$

Then

$$P_{bg} = 1.1 \times 10^{-20} T_b \qquad (7.16)$$

Pawsey and Braecwell give the values of T_b as a function of ν for frequencies greater than 20 Mc/sec. Extrapolation of their numbers lead to galactic temperatures

at 10 Mc/sec of about 10^{6}° K in the bright center of the galaxy, and 10^{5}° K in the cold parts of the galaxy. The maximum galactic noise is, therefore,

$$P_{bg} = 10^{-14} \text{ watts}$$

7.5.2 Solar Noise

If Eq. (7.15) is multiplied by the ratio of the solid angle subtended by the sun at the point of observation, to the solid angle defined by the antenna beamwidth, and if T_b is the effective solar radio temperature, then the solar noise power is represented by

$$P_{bs} = (1.1 \times 10^{-20})\, T_b \left(\frac{\Omega_s}{\pi \gamma_{max}^2} \right) \qquad (7.17)$$

$\Omega_s = 7 \times 10^{-5}$ steradians and $T_b = 10^{6}$° K

Therefore

$$P_{bs} = 2 \times 10^{-18} \text{ watts}$$

7.5.3 Noise From Van Allen Electrons

The trapped Van Allen electrons will emit synchrotron radiation, and the spectrum of this radiation depends sensitively on the Van Allen electron spectrum, particularly in the energy interval around one Mev. Since the electron spectrum is not known well, a calculation of the synchrotron noise would not be possible. However, Kraus and Ko (Ref. 24) have scanned the region of the Van Allen belt with a ground station radio receiver. They report that the effective blackbody temperature in this region is about 10^{5}°K (extrapolated to a frequency of 10 Mc/sec). Applying Eq. (7.15) one finds a value of Van Allen electron synchrotron radiation noise to be 10^{-15} watts.

7.5.4 Receiver Noise

Due to the thermal motion of the matter making up the satellite's antenna and radio receiver, electrical noise is generated, particularly in the resistors and tubes of the first stage of the amplifier. This noise can be represented as a signal received by a noise-free receiver where the signal strength is

$$P_{br} = (1.37 \times 10^{-17}) N T_o \Delta\nu \tag{7.18}$$

The quantity N is the noise factor and depends on the type of receiver used, T_o is the temperature of the receiver, and $\Delta\nu$ is in Mc/sec. Bracewell (Ref. 25) gives a value of N = 1 for the best present-day receivers. For $T_o = 300° K$

$$P_{br} = 4 \times 10^{-15} \text{ watts}$$

7.6 SIGNAL-TO-NOISE RATIO

The description of the background noise sources indicates that the dominant source is galactic noise which gives a noise signal strength at the satellite of 10^{-14} watts, which is ten times the strength of the signal we are attempting to detect. This does not mean, however, that the signal-to-noise ratio is 1/10. A background signal can have any value without affecting the reception of the desired signal, as long as the background is constant and can be biased out. Only fluctuations in the background over a time comparable with the signal duration interfere with reception. If we assume the noise to be random, then over a time τ the noise level will have a probable rms deviation from its average value of

$$\frac{1}{(\tau\Delta\nu)^{1/2}} \tag{7.19}$$

The value of τ to be used is determined by the duration of the synchrotron radiation signal from the electrons, which in our case is 10^{-4} sec. This leads to a signal-to-noise ratio of one, which is acceptable in determining the simple yes-no situation of the electron's presence.

7.7 BOUNCE-TIME EXPERIMENTS

In most cases, the results of a bounce-time measurement cannot be estimated beforehand because of the lack of knowledge about the geomagnetic field except in very idealized models. One calculation has, however, been made of the bounce time predicted by two different geomagnetic models. The purpose of the comparison is to determine whether the experimental accuracy, which will be about 0.1 percent, is sufficient to easily differentiate between the models. The two models we have used are the dipole model and Welch's 512-term harmonic expansion (Ref. 26). The results of the comparison are shown in Table 7-1 for four different injection points. One point is near the Cape Town anomaly where the difference in predicted bounce times should be nearly a maximum. The differences are about 10 percent, and so the experimental accuracy is quite adequate.

Table 7-1

A COMPARISON OF THE BOUNCE TIMES PREDICTED BY TWO DIFFERENT GEOMAGNETIC MODELS(a)

Injection Point (Geographic Coordinates)			Bounce Time (sec)			
B Welch (Gauss)	East Longitude	South Latitude	Altitude (km)	Welch	Dipole	Difference (Welch minus Dipole)
0.25	3.75° (near Cape Town anomaly)	19.53°	532	0.107	0.097	-0.01
0.25	175.47°	18.86°	1276	0.110	0.100	-0.01
0.25	6.37°	72.64°	1631	0.754	0.746	-0.005
0.25	158.02°	54.55°	2294	0.754	0.664	-0.09

(a) The models are the dipole field and Welch's 512-term harmonic expansion.

Section 8
CONJUGATE-POINT MEASUREMENT

8.1 INTRODUCTION

The critical question in the conjugate-point measurement is the feasibility of detecting the electrons' presence in the upper atmosphere by radar reflection from the trail of ionization produced by the electrons as they spiral down a field line. In a model which will prove to be too simple to describe the real situation, the electrons are confined to a narrow pencil with a cross section of a few square centimeters defined by the accelerator at the time of injection. This narrow beam will enter the upper atmosphere normally, will ionize but not scatter, and will stop at the end of its range at an altitude of about 60 km. The atmospheric density increases exponentially as the electrons penetrate to lower altitudes; also, the energy loss per collision increases as the electrons slow down. Therefore, virtually all of the atmospheric ionization occurs near the end of the electrons' range, and we will assume that the ionized trail is confined to an altitude interval between 60 km and 70 km. Since the 1-Mev electron accelerator injects 2.5×10^{15} electrons in one puise, the energy contained in the beam is 2.5×10^{21} ev. It requires about 50 ev to produce an ion pair in a collision, which means that over the 10-km ionized trail there are 5×10^{19} ion pairs, or an ion pair linear density of 5×10^{15} ion pairs/m.

Pawsey and Braswell (Ref. 23) discuss the problem of radar reflection from the ionized trail of meteors traversing the upper atmosphere. The characteristics of the meteor trail are very similar to those of the electron trail, namely, the ionization is confined to a pencil of a few square centimeters in cross section and occurs mainly at altitudes around 80 km. A bright visual meteor will produce about 10^{14} ion pairs per meter of path, and is easily detected by radar reflection. The electron beam produces a trail with an ion density an order of magnitude larger, and should therefore give a substantial radar reflection. Because of the effects which arise in ionized columns containing very great ion pair densities, this conclusion is not necessarily valid. The reader is referred to the chapter on meteor detection in Pawsey and Braewell.

In this study we have restricted ourselves to the detection of the electron trail by radar reflection methods. However, additional calculations may show that the trail is optically visible as well. It is not possible to conclude immediately that since a meteor trail is visible, the electron trail with a comparable ion pair density will be visible. In the case of a meteor, the amount of its energy which goes into light is thought to be determined by a different mechanism than in the electron case.

The above model of the electron ionized trail is inadequate because the electrons are not confined to a narrow pencil, and the effect of scattering as the electrons slow down in the atmosphere is appreciable. In the following sections we will:

(1) Compute the shape of the electron beam as it strikes the top of the atmosphere
(2) Determine the effect of scattering
(3) Compute the radar reflection from an extended region of ionization

8.2 THE SHAPE OF THE ELECTRON BEAM AT THE CONJUGATE TO THE INJECTION POINT

The shape of the electron beam after one traversal from the injection point to the conjugate point will be determined by several effects.

8.2.1 Magnetic Moment Nonconservation

Electrons which are injected at very small pitch angles in a curved magnetic field do not satisfy the conditions for adiabatic invariance of the magnetic moment so that their pitch angle at the point conjugate to the injection point is not equal to the injection pitch angle. This is because at small pitch angles appreciable change in the field can occur within the distance covered by the guiding center during one cyclotron revolution. The effect of the field curvature is such that electrons which are injected parallel to a field line will arrive at the conjugate point with a finite pitch angle. The following is a correct description of the motion. An electron would move parallel to the field line until the field's curvature causes $\vec{v}$ and $\vec{B}$ to diverge, which creates a non-zero pitch angle. The electron would then have a component of velocity perpendicular to the field and would start to spiral, keeping the center of gyration

on the original injection field line. The pitch angle would continue to increase until the point is reached where the magnetic moment invariance is obeyed, and, thereafter, the motion will be properly described by that law. Alfvén (Ref. 9) discusses this situation, and sets the following criterion for the magnetic moment conservation. The perpendicular component of the electron's velocity must be much greater than the electron's longitudinal drift velocity.

$$v \sin \alpha >> v_D \tag{8.1}$$

This condition on α imposes the greatest restriction at the equator. If we arbitrarily set $v_D = (0.01)\ v \sin \alpha_e$, and if $\alpha_e << 1$, then

$$\alpha_e = \frac{3p}{eB_e r_e} \times 10^2 \tag{8.2}$$

For the field line which crosses the magnetic equator at 2 earth radii, $\alpha_e = 1.5°$. An electron with a pitch angle α_e at the equator will follow a field line to the top of the atmosphere where its pitch angle will be α_o.

$$\frac{\alpha_o^2}{B_o} = \frac{\alpha_e^2}{B_e} \tag{8.3}$$

For the field line r_e = 2 earth radii and $\alpha_e = 1.5°$, then

$$\alpha_o = 5°$$

The cyclotron radius at the top of the atmosphere will, therefore, be about 10m.

8.2.2 Accelerator Beam Spread

Although the beam is well collimated by the electron accelerator, there will be some finite beam divergence. Presumably, this beam spread will be less than 5°. The conclusion which can be drawn from the arguments in the above paragraph is that an electron injected with any pitch angle less than 5° will arrive at the conjugate point with a pitch angle of about 5°. Therefore, the effect of the beam spread at injection is completely masked by the magnetic moment non-conservation.

8.2.3 Energy Dependence of the Longitudinal Drift Velocity.

The injected electrons will have a finite energy spread determined by the accelerator (3 percent to 4 percent for the Varian Pulse Transformer). The longitudinal drift velocity of the electrons is energy dependent. Consequently, the electrons will arrive at the conjugate point with a longitudinal spread. Equations (3.13a) and (3.14) give the rate of change of the electron's longitude averaged over one bounce.

$$\overline{\frac{d\phi}{dt}} = \frac{3}{2} \frac{pv}{er_e^2 B_e} \tag{8.4}$$

An electron with momentum p and velocity v shifts in longitude an amount $\Delta\Phi$ over the time required to move from the injection point to the conjugate point.

$$\Delta\phi = 6 \frac{p}{er_e B_e} \tag{8.5}$$

At the conjugate point, this shift in longitude would correspond to a linear displacement given by

$$D_L = \Delta\phi \frac{R_E^{3/2}}{r_e^{1/2}}$$

$$D_L = 6 \frac{p}{e B_e} \left(\bar{r}_e\right)^{-3/2} \tag{8.6}$$

where $\bar{r}_e$ is in units of earth radii. We want to compute the change in D_L resulting from a change in the electron's kinetic energy T.

$$\frac{d D_L}{dT} = \frac{6}{e B_e} \left(\bar{r}_e\right)^{-3/2} \frac{1}{v} \tag{8.7}$$

For a 1-Mev electron moving along the field line, $r_e = 2$ earth radii, and for $dT = (0.03)\ T = 3 \times 10^4$ ev,

$$dD_L = 50\text{m}.$$

8.2.4. Beam Blow-up Due to Coulomb Repulsion

Consider a beam of electrons of length L with cross-sectional radius b moving with velocity v and containing N electrons distributed uniformly through the beam.

If $b \ll L$, then at the surface of the beam, in a region not too close to the ends, there is an outward directed electric field given by

$$E = \frac{e}{2\pi\epsilon_o} \frac{N}{bL} \tag{8.8}$$

Due to the magnetic field associated with the motion of the electrons, there is also an inward directed force at the surface given by

$$F_B = \frac{\mu_o}{2\pi} \frac{v^2 e^2 N}{bL} \tag{8.9}$$

The ratio of these opposing forces is

$$\frac{F_E}{F_B} = \frac{1}{\epsilon_o \mu_o v^2} \tag{8.10}$$

or

$$\frac{F_E}{F_B} = \frac{c^2}{v^2} \tag{8.11}$$

Since v can never be identically equal to c, the net force is outward, and without constraints the beam would blow up. In our case, however, there is a mechanism which limits the blow-up. The beam is actually moving in the atmospheric plasma which can be thought of as a highly polarizable medium. The beam would blow up until a point is reached where enough polarized plasma occupies the space between individual electrons in the beam to neutralize their Coulomb repulsion. An argument can be made as to the distance which must exist between electrons before they essentially lose communication. The following sketch (Fig. 8-1) represents the situation where two of the beam electrons are separated and neutralized by the polarized, fully-ionized plasma between them.

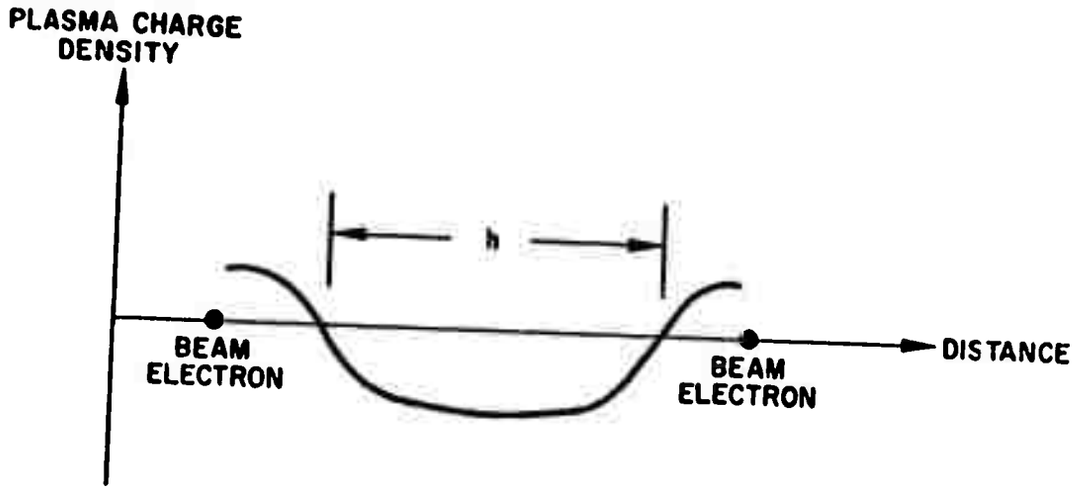

Fig. 8-1 Separation and Neutralization of Two Beam Electrons by Polarized, Fully Ionized Plasma

In the interval h there is a net negative charge density n_e, and for simplicity, it will be assumed that n_e is uniform. In this region, Poisson's equation for the potential is

$$\frac{d^2V}{dx^2} = \frac{e\, n_e}{\epsilon_o} \tag{8.12}$$

Integrating twice, we have

$$V = \frac{1}{2}\,\frac{e\, n_e}{\epsilon_o}\, h^2 \tag{8.13}$$

In order for the plasma to have polarized to the extent shown in the sketch, the electric forces must have overcome the thermal motion of the plasma. If this is true, then the potential in Eq. (8.13) must correspond to a change in energy of at least 1/2 kT, where T is the temperature of the plasma. Equating the electrical potential energy to the thermal energy we find that

$$\frac{1}{2}\,kT = \frac{1}{2}\,\frac{e^2 n_e}{\epsilon_o}\,h^2 \tag{8.14}$$

Solving for h results in

$$h = \left(\frac{\epsilon_o\, kT}{e^2\, n_e}\right)^{\frac{1}{2}} \tag{8.15}$$

The quantity h defined by Eq. (8.15) is called the Debye shielding distanee. At an altitude of a few hundred kilometers, the atmospherie temperature is about 10^3 °K and the free electron density is about 10^{12} eleetrons/m^3. If we assume that n_e in the above equation has the full value of the total free eleetron density, then $h = 2 \times 10^{-3}$ m.

If the beam has a length L and a radius b, the average distance between electrons is approximately

$$\eta = 2\left(\frac{b^2 L}{N}\right)^{1/3} \tag{8.16}$$

At injection $b \approx 1$ cm, $N = 2.5 \times 10^{15}$ electrons, and $L = 1.2 \times 10^3$ m, (taking the electron's velocity equal to that of light, and a pulse duration of 4×10^{-6} sec)

$$\eta_{inj} = 7 \times 10^{-6}\text{m}.$$

The beam will blow up, both in cross section and length, until the average distance between electrons is roughly the Debye distance which is 300 times η_{inj}. This means that b will increase to about 3 m and L to about 4×10^5 m.

8.3 BEAM SPREAD DUE TO MULTIPLE SCATTERING IN THE ATMOSPHERE

Because of the cumulative effects of small angle scattering, the electron beam will spread appreciably during its passage through the atmosphere. The importance of this spread can be seen from the values of $\left(\theta^{\overline{2}}\right)^{1/2}$ as a function of altitude h. The angle θ is the angle between the electron velocity vector and the vertical.

h (km)	$\left(\theta^{\overline{2}}\right)^{1/2}$
75	0.34
70	0.58
65	0.85
60	≈ 1.0

The small-angle approximations used in computing these values are not valid for $\theta^{\overline{2}} \approx 1$, but the indication is clear that by the time the beam gets to 70 km its direction is no longer well defined.

The rapid spread of particles is prevented by the earth's magnetic field which for this calculation will be assumed vertical. This field will constrain the particles so that they move in spirals, thereby limiting their horizontal motion between collisions to the diameter of the spiral.

An approximate calculation will be carried out to get an idea of how important the effect is. Numerical calculations indicate that during most of the passage through the atmosphere, the change in pitch angle per cyclotron revolution is smaller than the instantaneous

pitch angle. Hence, the spread of particles will be treated as a diffusion of the guiding centers. At each altitude, the energy will be assumed monoenergetic and equal to the average energy at that altitude. The gyration radius will be computed at each altitude assuming this average energy, and assuming $\theta = \left(\overline{\theta^2}\right)^{1/2}$ until θ becomes equal to 60°, below which altitude θ will be assumed to remain at 60°. The time a particle takes in traversing Δh is equal to $\Delta t = \left(\frac{\Delta h}{v \cos \theta}\right)$, and the spread in the beam during that time will be equal to

$$\Delta r = \Delta t \langle \Delta r(\theta, n) \rangle = \Delta t \langle \Delta r(h) \rangle \tag{8.17}$$

where n is the number of atoms cm^{-3} and is a single-valued function of h, as is θ Thus, the problem involves finding an expression for $\langle \Delta r(h) \rangle$ which is the average change per unit time of the distance between the guiding center of a particle and the centroid of the electron beam.

With the geometry shown in Fig. 8-2,

- r = distance from centroid to guiding center before collision
- r' = distance from centroid to guiding center after collision
- ψ = projection of scattering angle on horizontal plane
- ξ = orbit phase angle
- a = cyclotron radius

$$h^2 = a^2 + a^2 - 2a^2 \cos \psi = 2a^2 (1 - \cos \psi) = a^2 \psi^2 \tag{8.18}$$

$$r'^2 = r^2 + h^2 - 2rh \cos \left[\pi - \xi - \frac{(\pi - \psi)}{2}\right] \tag{8.19}$$

$$\Delta(r^2) = a^2 \psi^2 - 2ra \psi \sin \left(\xi - \frac{\psi}{2}\right) \tag{8.20}$$

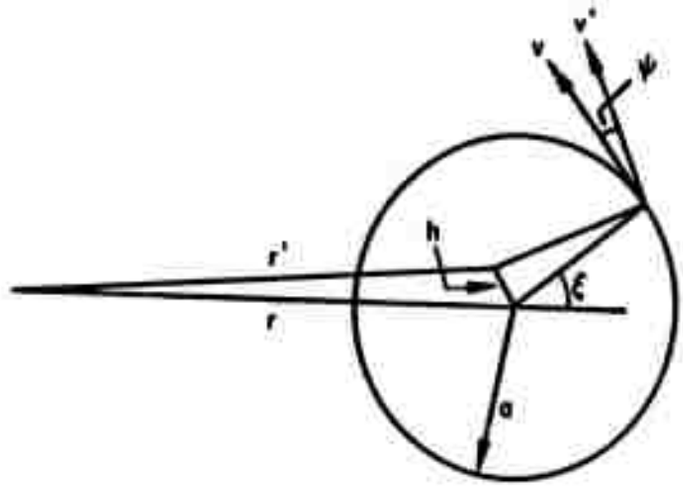

Fig. 8-2 Projection of Scattering Angles on the Plane of Electron Motion

When the right hand side of Eq. (8.20) is expanded,

$$\Delta(r^2) = -2ra\,\psi \sin\xi + \psi^2 (a^2 + ra\cos\xi) \tag{8.21}$$

Then

$$\Delta r \approx \frac{\Delta(r^2)}{2r} = -a\psi \sin\xi + \frac{\psi^2}{2r}(a^2 + ra\cos\xi) \tag{8.22}$$

To find averages, we must get ψ in terms of scattering angle η and azimuthal scattering angle ϕ (Fig. 8-3).

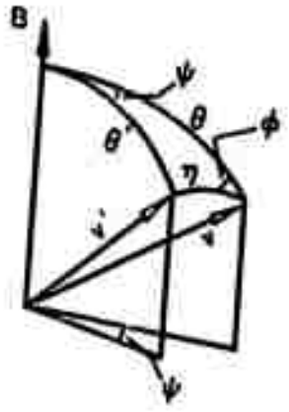

Fig. 8-3 Definition of Scattering Angles

$$\frac{\sin \psi}{\sin \eta} = \frac{\sin \phi}{\sin \theta'}$$

$$\sin \psi \approx \psi = \sin \eta \frac{\sin \phi}{\sin \theta'} \tag{8.23}$$

$$\cos \theta' = \cos \eta \cos \theta + \sin \eta \sin \theta \cos \phi$$

$$\sin \theta' = \left(1 - (\cos \eta \cos \theta + \sin \eta \sin \theta \cos \phi)^2\right)^{1/2}$$

$$\sin \theta' \approx \sin \theta \tag{8.24}$$

Therefore,

$$\psi \approx \eta \frac{\sin \phi}{\sin \theta} \tag{8.25}$$

And then,

$$\Delta r = - a \sin\xi \left(\eta \frac{\sin\phi}{\sin\theta}\right) + \eta^2 \frac{\sin^2\phi}{\sin^2\theta} \frac{1}{2r} (a^2 + ra\cos\xi)$$

$$\Delta r = - a\eta \frac{\sin\phi \sin\xi}{\sin\theta} + \eta^2 \frac{\sin^2\phi}{2r\sin^2\theta} (a^2 + ra\cos\xi) \qquad (8.26)$$

The scattering cross section for electrons in air will be taken to be

$$\sigma(\eta) = \frac{Z^2 e^4}{4m^2 c^4} \frac{1-\beta^2}{\beta^4} \frac{1}{\sin^4\frac{\eta}{2}} = A \frac{1}{\sin^4\frac{\eta}{2}} \qquad (8.27)$$

The average change in r per collision is given by

$$\left|\Delta r\right| = \int_0^{\pi}\int_0^{2\pi} \Delta r(\phi,\eta)\, \sigma(\phi,\eta)\, d\phi\, d\eta \sin\eta \qquad (8.28)$$

Substituting and integrating we get

$$\left|\Delta r\right| = 4A \cdot \frac{2\pi}{r} \frac{1}{\sin^2\theta} (a^2 + ar\cos\xi) \int_{\eta_{min}}^{\pi} \frac{d\frac{\eta}{2}}{\frac{\eta}{2}} \qquad (8.29)$$

$$\left|\Delta r\right| = \frac{8\pi A}{r\sin^2\theta} (a^2 + ar\cos\xi)\, \ell n\left(\frac{2}{\eta_{min}}\right) \qquad (8.30)$$

Performing the average over orbital phase angle ξ ,

$$\{\Delta r\}_{orbit} = \int_0^{2\pi} \frac{\{\Delta r\}\, d\xi}{2\pi}$$

$$\{\Delta r\}_{orbit} = \frac{8\pi A}{r \sin^2 \theta}\, a^2\, \ell n \left(\frac{2}{\eta_{min}}\right) \tag{8.31}$$

The change in r per unit time is then

$$\langle \Delta r \rangle = \{\Delta r\}\, n\, v$$

$$\langle \Delta r \rangle = \frac{8\pi\, Anv}{r \sin^2 \theta}\, a^2\, \ell n \left(\frac{2}{\eta_{min}}\right) \tag{8.32}$$

$$\Delta(r^2) = 2r\, \Delta r$$

$$\Delta(r^2) \cong \frac{d(r^2)}{dt} = \frac{16\pi\, Anv}{\sin^2 \theta}\, a^2\, \ell n \left(\frac{2}{\eta_{air}}\right) \tag{8.33}$$

If the right hand side is expressed as a function of t by noting that $h = h(t)$, the equation can then be integrated numerically.

$$\frac{d(r^2)}{dt} = f(t)$$

$$r^2 = \int_0^t f(t')\, dt' = r^2(t) = r^2(h) \tag{8.34}$$

The numerical results are summarized in the curve of Fig. 8-4.

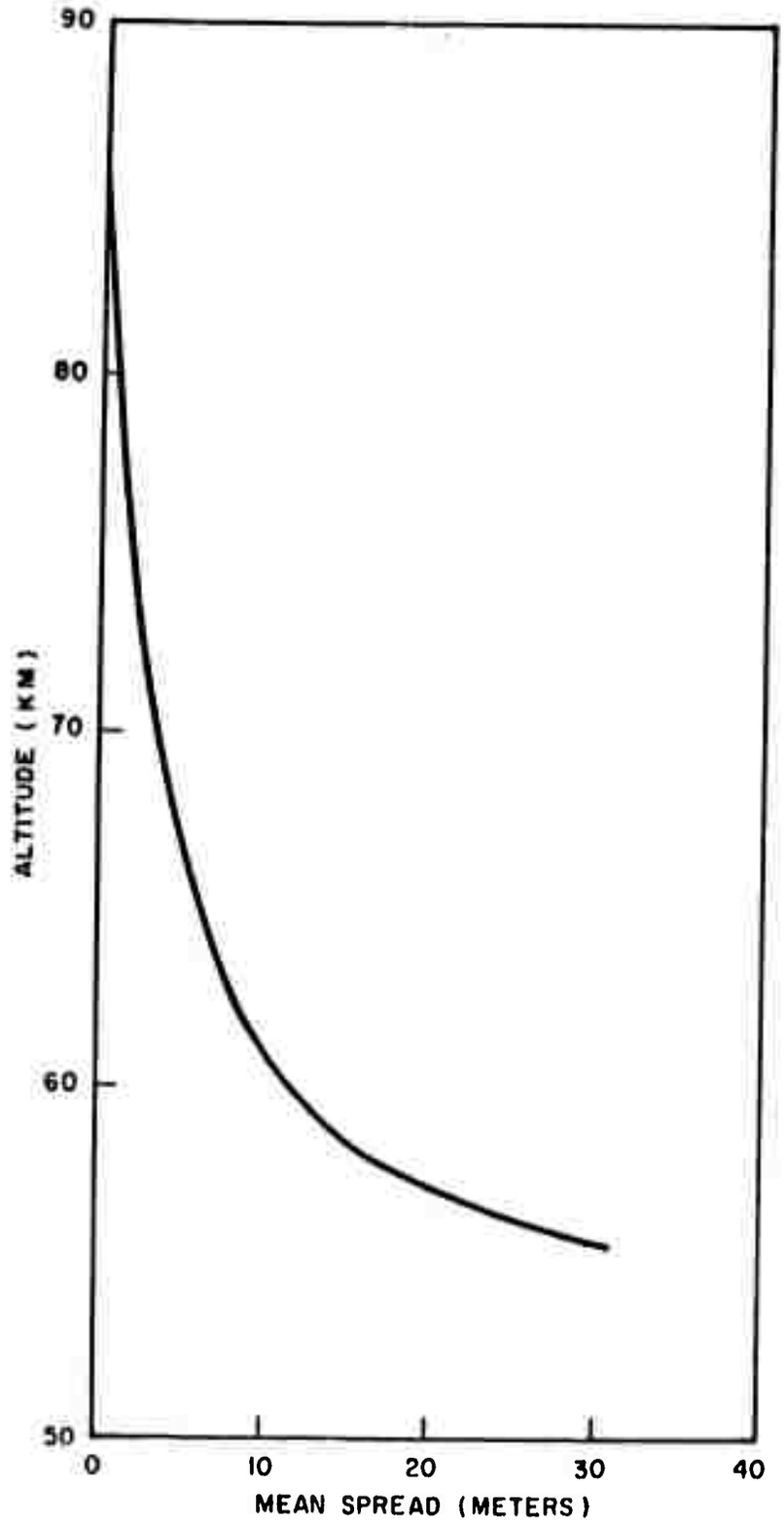

Fig. 8-4 The Mean Spread Due to Multiple Scattering of a Narrow Beam of 1 Mev Electrons Striking the Top of the Atmosphere

8.4 RADAR REFLECTION FROM AN EXTENDED REGION OF IONIZATION

Combining the results of the calculations in Sections 8.2 and 8.3, the region of ionization is found to have the following dimensions. In altitude, it will begin about 70 km and end at about 60 km; in longitude, it will have a width of about 100 m; in latitude, it will have a thickness of about 50 m. As computed in Section 8.1, there will be about 5×10^{19} ion pairs distributed throughout this volume. If we assume that the distribution is uniform, then there will be an ion pair density of 10^{12} electrons/m^3.

We will assume that a radar station can direct its beam onto this "curtain" of ionization, and the question is whether or not there will be a detectable echo. (Fig. 8-5).

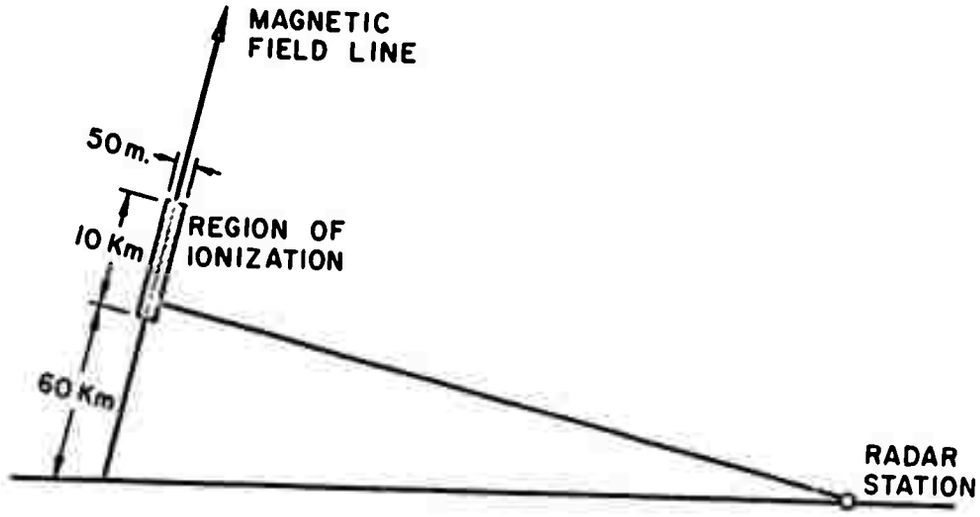

Fig. 8-5 Relative Position of Radar Station and the Region of Ionization

The amount of reflected power is determined by the radar transmitter's frequency and the plasma frequency associated with the ionized region. If the radar frequency is less than the plasma frequency there is almost total reflection, and if it is greater, there is almost no reflection. The maximum frequency of the radar transmitter is related to the ion pair density in a highly reflective ionized region by

$$\nu_r^2 \approx 81N \tag{8.35}$$

where ν_r is in cps and N in ion pairs per m^3. In our case, $N = 10^{12}$ ion pairs/m^3 and $\nu_r = 10$ Mc/sec. The conclusion is that a 10 Mc/sec radar transmitter would easily detect the presence of the electron beam in the upper atmosphere.

8.5 CONJUGATE-POINT MEASUREMENT

The problem of radar reflection has more facets than is indicated by the simple calculation above. These additional complications do not affect the basic feasibility of the method, but must be examined nonetheless.

(1) Due to the interference phenomenon, the strength of the reflected signal may depend sensitively on the angle at which the radar beam strikes the ionized region. Normal incidence will produce the maximum reflection.

(2) The persistence of the ionization is determined by the rate of recombination. The ionization may last for the order of a few seconds which should be long enough to allow the radar to scan and lock on.

(3) The accuracy with which the position of the ionized region can be located will be determined by the angular resolution of the radar transmitter and the distance between the transmitter and the reflector. Because of the line-of-sight requirement, a particular radar station will have a maximum range of about 1,000 km for conjugate-point detection. If the beamwidth of the 10 Mc/sec radar is about 10°, then at the maximum range, the uncertainty in the conjugate-point position would be about 200 km. This poor accuracy is unacceptable. The accuracy can be improved by the use of aircraft-borne

radar so that the transmitter can be close to the region of ionization. If the aircraft is within 10 km of the position of the ionization, the uncertainty in the measurement would be about 2 km.

(4) Dyce (Ref. 27) has studied the problem of radar reflection from auroral displays. He has indicated that it would be possible to locate the position of the ionized region with ground-based radar with greater accuracy by (1) using higher frequency radar reflections from those parts of the ionized region having a statistically higher ion-pair concentration, and (2) making use of pairs of transmitters and receivers as a radar interferometer.

(5) Because of the longitudinal drift of the electron beam, the position of the ionized region will be slightly east of the magnetic conjugate to the injection point. A correction can be made to the data to take account of this fact. In the case of injection at a magnetic latitude of 45°, the eastward displacement would be about 3 km.

(6) For a given set of injection positions, Table 8-1 gives the position of the conjugate points predicted by a dipole field and predicted by Welch's 512-term harmonic expansion of the geomagnetic field. It is the purpose of this comparison to indicate the magnitude of the uncertainty in the position of conjugate points as determined by two different geomagnetic models.

Table 8-1

A COMPARISON OF THE GEOGRAPHIC POSITIONS OF CONJUGATE POINTS PREDICTED BY TWO DIFFERENT GEOMAGNETIC MODELS[a]

Injection Point (Geographic Coordinates)				Conjugate Points (Geographic Coordinates)		
B (Gauss)	East Longitude	South Latitude	Altitude (km)	East Longitude Difference (Welch minus Dipole)	North Latitude Difference (deg.)	Altitude Difference (km)
0.25	3.78° (near Cape Town anomaly)	19.53°	532	-0.23°	+9.59°	+428
0.25	175.47°	18.86°	1,278	-2.42°	+11.28°	-239
0.25	6.37°	72.64°	1,631	+9.82°	-14.83°	+325
0.25	158.02°	54.55°	2,294	-5.54°	+11.16°	-173

(a) The models are the dipole field and Welch's 512-term harmonic expansion.

Section 9
SATELLITE CHARGING

9.1 INTRODUCTION

The most fundamental problem which must be examined in order to demonstrate the feasibility of artificial injection, even in principle, is the problem of satellite charging. If the satellite were moving in a perfect vacuum, electrons could be ejected only when the potential of the satellite (due to the residual positive charge) rose to a value equal to the electrons' kinetic energy. At this point, electrons could no longer leave and the useful life of the satellite would have ended. In the case of pulsed injection, the time for a satellite to rise to one million volts would be 1 μsec, for d-c injection, it would be 1/10 sec. Researchers in the field of ionic rocket propulsion have studied this problem, and have found the only suitable solution for their application to be the simultaneous expulsion of positive and negative charge in the thrust beam. This solution is, however, impractical in our case for the following reason: If the electrons are not to be decelerated, there must be not only satellite neutrality, but, also, no charge separation in the ejected ionized beam. This means that the electrons and positive ions in the beam must have the same velocity. If the positive ions are protons with the velocity of a one-Mev electron, then the proton kinetic energy is 2 Bev, which is obviously impractical. The fact is, of course, the satellite is not moving in a vacuum, but in a rather complicated environment made up of the earth's magnetic field and a thermally agitated, tenuous atmosphere, partially neutral and partially ionized. Figures 9-1, 9-2, and 9-3 show the orders of magnitude associated with the atmosphere in the satellite region. The ionized component of the atmosphere is a source of free electrons which would tend to neutralize a charging satellite.

The effect of the ambient plasma on a passive satellite has been studied (Ref. 28), and it has been shown that a satellite would pick up more electrons than positive ions (owing to

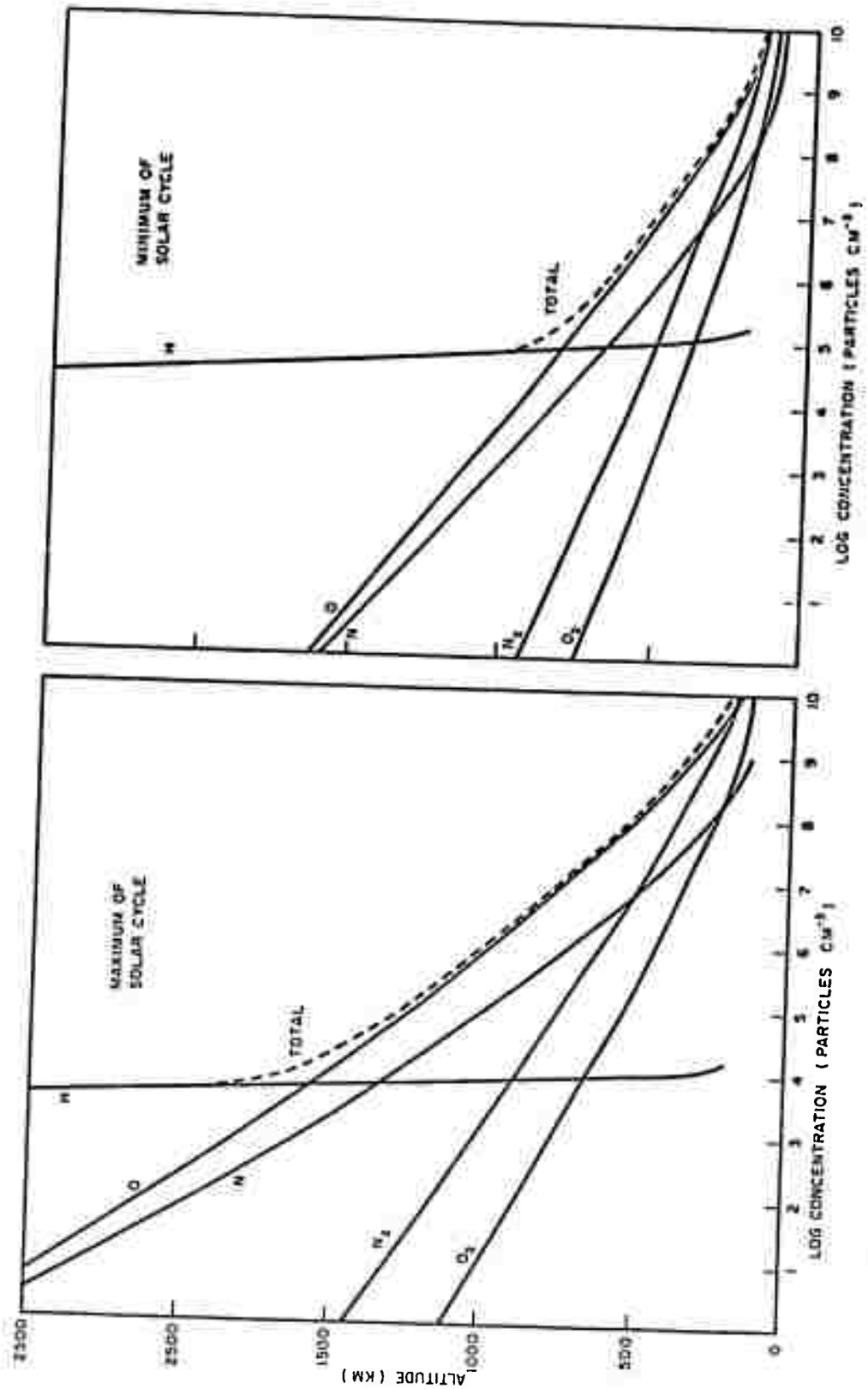

Fig. 9-1 The Logarithm of the Concentration of the Various Atmospheric Constituents at Two Extremes of the Solar Cycle

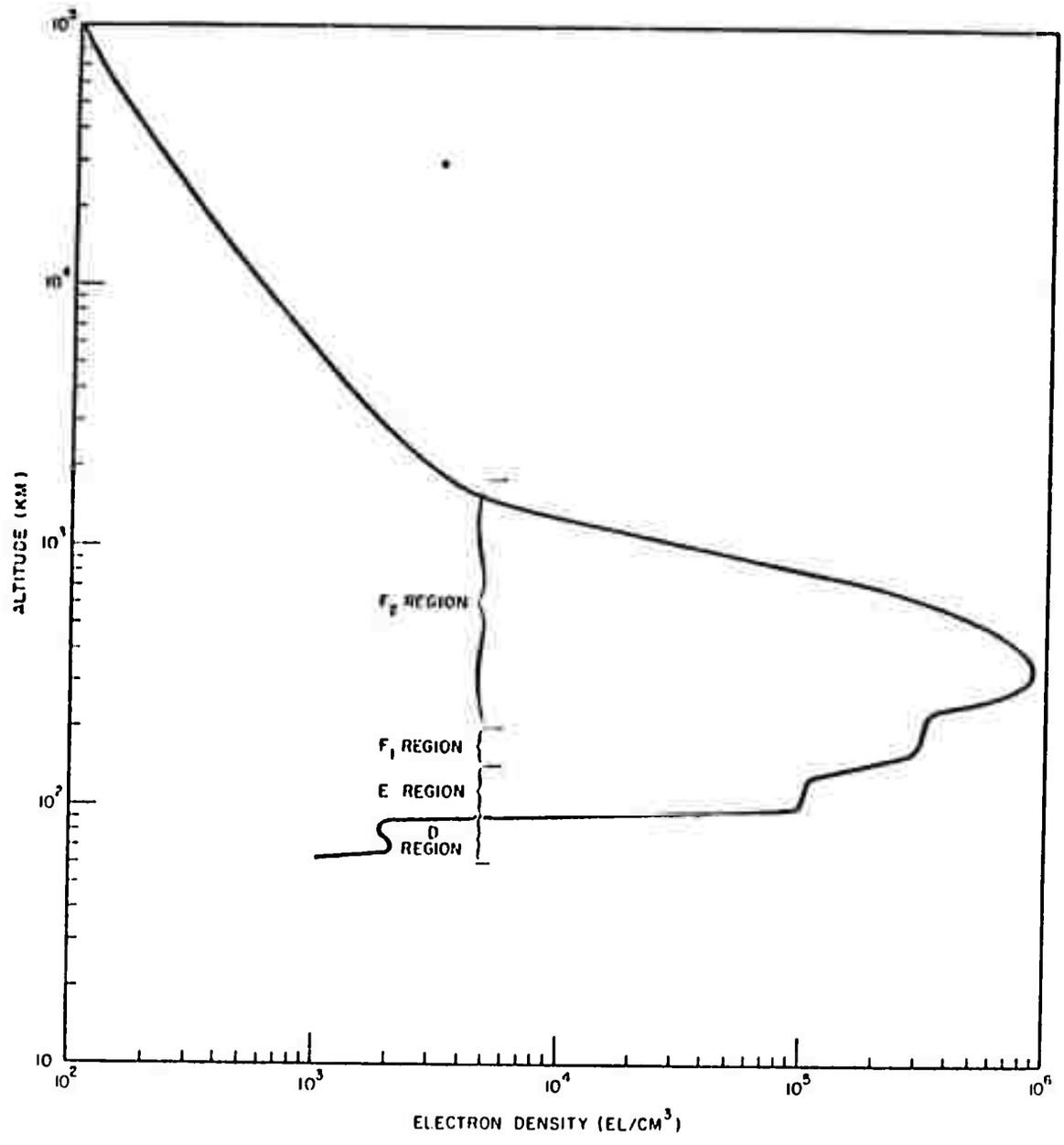

Fig. 9-2 A Normal, Daytime, Free-Electron Distribution During Sunspot Maximum

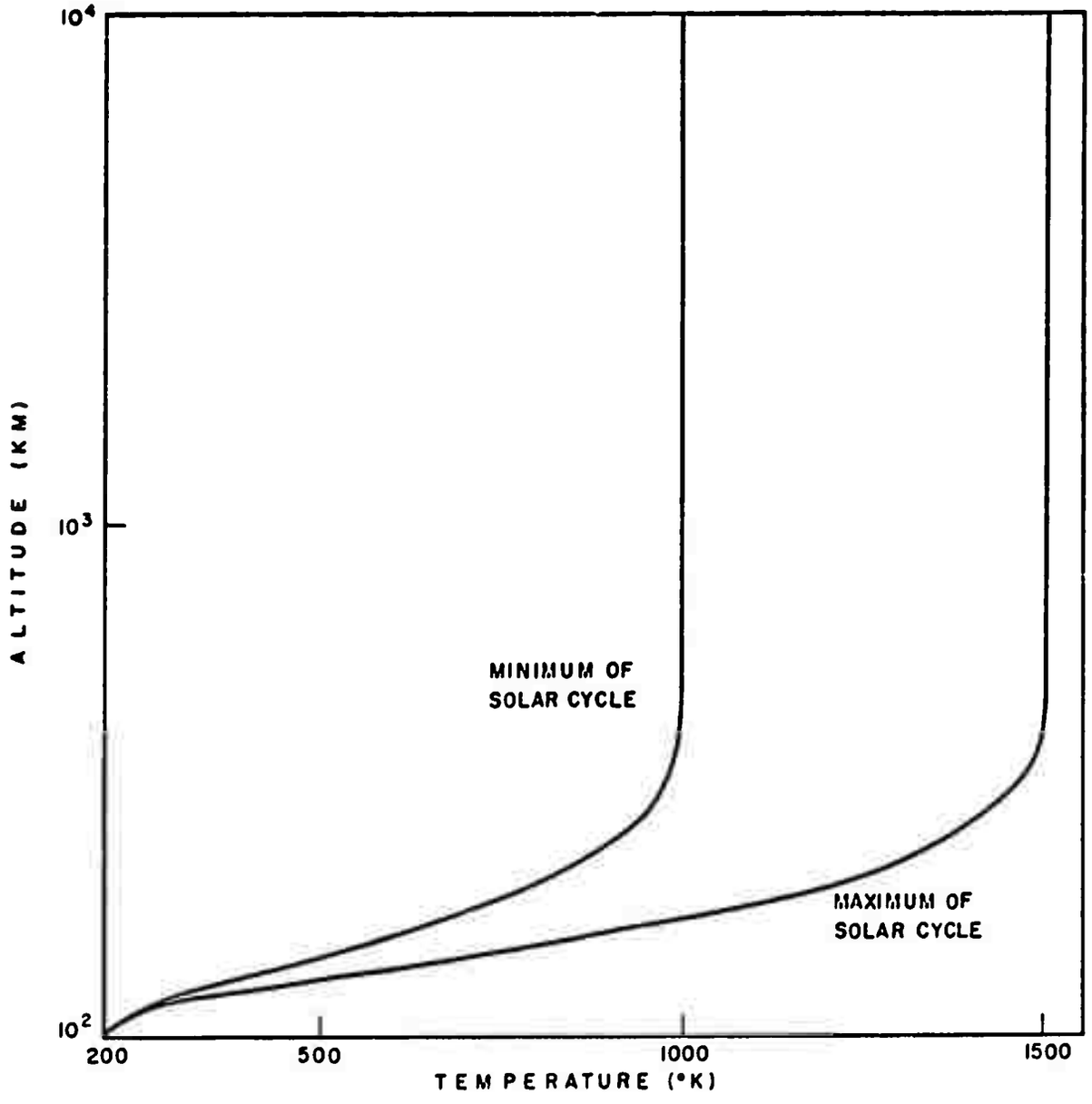

Fig. 9-3 Vertical Temperature Distribution at the Two Extremes of the Solar Cycle

the difference between the thermal velocities of electrons and ions at the same temperature) and would rise to a potential between 10 and 100 volts. For a reasonable-size satellite ejecting a large electron current and charging positively, this thermal effect would not be sufficient to maintain neutrality. However, the electric field of the charged satellite would draw the electrons out of the plasma at a much greater rate. The question, then, is: To what potential will a satellite rise before the current being drawn out of the ambient plasma is sufficient to offset the ejected current and limit the potential?

9.2 NEUTRALIZATION BY A THERMAL PLASMA

It would be possible to maintain satellite neutrality by the electron "thermal excess". The size of the satellite, however, would have to be very large. The average velocity of particles at temperature T is

$$v = \left(\frac{2\,k\,T}{m}\right)^{1/2} \tag{9.1}$$

where k is Boltzmann's constant, and T is in degrees Kelvin. For electrons at 1,000° K (0.1 ev)

$$v = 200 \text{ km/sec}$$

A nitrogen ion at the same temperature has a thermal velocity of 1 km/sec. Consequently, the motion of the plasma ions can be neglected. Note that a typical satellite velocity is about 8 km/sec; ions do not strike the satellite but are swept up by it.

The thermal electron current incident on the surface of a spherical satellite is

$$I_{Th} = 4\pi a^2 n_e ev \tag{9.2}$$

where a is the satellite's radius and n_e is the plasma electron density. For the two cases of pulsed and d-c injection, if current equilibrium is achieved, the following satellite

radii are required. (Throughout the study of satellite charging, it will be assumed that pulsed injection occurs at low altitudes ($n_e \sim 10^6$ electrons/cm^3) and d-c injection at high altitudes ($n_e \sim 10^2$ electrons/cm^3).)

$I_{injected} = I_{Th}$ (amps)	n_e (elect/cm^3)	a (m)
100 (pulsed)	10^6	16
10^{-3} (d.c.)	10^2	5

The charging problem can therefore be solved in the last resort by using an Echo-type satellite shell.

In the case of pulsed injection with a pulse repetition rate of about one per second, a normal-size satellite charged as high as a million volts would be neutralized completely by the thermal electrons in the time between pulses.

9.3 THE EFFECT OF A PLASMA ON A CHARGED SATELLITE

9.3.1 Description of the Model to be Studied

Let us take a simple model in which the the following assumptions are made:

- The satellite is a spherical conductor with a radius a, and is ejecting a constant electron current I_β.
- The effect of the earth's magnetic field is neglected, as well as any magnetic effects due to the ejected current or the flow of plasma electrons.
- Initially, the plasma is neutral and has a constant electron number density n_e
- The satellite and the ambient ions are at rest, and the thermal motion of the plasma electrons is neglected.
- In describing the effect of an electric field on the plasma electrons, it will be assumed that it is possible to assign a transient conductivity σ_t to the medium; that is, a conductivity which is a function of time but which approaches asymptotically a constant value σ_o characteristic of a steady-state current flow in the plasma.

Spitzer (Ref. 12) has described the problems involved in defining a plasma conductivity and gives the steady-state values for various models.

9.3.2 Transient Conductivity

The equation of motion of an electron in the plasma is

$$m \frac{d\vec{v}}{dt} = e\vec{E} - \alpha\vec{v} \tag{9.3}$$

where the effect of collisions within the plasma has been represented by a retarding force proportional to the electron's velocity. The constant α can be evaluated by noting that in the steady state

$$e\vec{E} = \alpha\vec{v} \tag{9.4}$$

The current density is given by

$$\vec{j} = e n_e \vec{v} \tag{9.5}$$

Combining Eqs. (9.4) and (9.5) we obtain

$$\vec{j} = \frac{n_e e^2}{\alpha}\vec{E} = \sigma_o \vec{E} \tag{9.6}$$

Therefore,

$$\alpha = \frac{n_e e^2}{\sigma_o} \tag{9.7}$$

if the electric field does not vary appreciably over the distance between collision centers or in times comparable with the collision period, then Eq. (9.3) may be integrated

$$\vec{v} = \frac{\sigma_o}{n_e c}\left[1 - \exp -\left(\frac{n_e e^2}{m \sigma_o}\right)t\right] \vec{E} \qquad (9.8)$$

where it has been assumed that the initial velocity is zero. Applying Eq. (9.5)

$$\vec{j} = \sigma_o\left[1 - \exp -\left(\frac{n_e e^2}{m \sigma_o}\right)t\right] \vec{E} \qquad (9.9)$$

The transient conductivity is then

$$\sigma_t = \sigma_o\left[1 - \exp -\left(\frac{n_e e^2}{m \sigma_o}\right)t\right] \qquad (9.10)$$

For the simple plasma we have assumed, σ_o is given by (Ref. 12)

$$\sigma_o = \frac{\gamma_E T^{3/2}}{(38) Z \ln \Lambda} \quad \text{mho/m} \qquad (9.11)$$

where T is the plasma temperature, Z is the ionic charge, and the values of $\ln \Lambda$ and γ_E are given in Table 9-1. The conductivity is shown in Fig. 9-4, assuming the plasma is singly ionized ($Z = 1$). The remarkable feature is the constancy of the conductivity over the large range of altitudes.

The values of the quantity $(n_e e^2 / m \sigma_o)$ appearing in the exponent in Eq. (9.10) are given in the table below.

Table 9-1

VALUES OF $\mathcal{L}n\Lambda$

Temp (°K)	Electron Density n_e (elect/cm^3)								
	1	10^3	10^6	10^9	10^{12}	10^{15}	10^{18}	10^{21}	10^{24}
10^2	16.3	12.8	9.43	5.97	---	---	---	---	---
10^3	19.7	16.3	12.8	9.43	5.97	---	---	---	---
10^4	23.2	19.7	16.3	12.8	9.43	5.97	---	---	---
10^5	26.7	23.2	19.7	16.3	12.8	9.43	5.97	---	---
10^6	29.7	26.3	22.8	19.3	15.9	12.4	8.96	5.54	---
10^7	32.0	28.5	25.1	21.6	18.1	14.7	11.2	7.85	4.39
10^8	34.3	30.9	27.4	24.0	20.5	17.0	13.6	10.1	6.69

Values of γ_E

Ionic Charge Z	1	2	4	16	∞
	0.582	0.683	0.785	0.923	1.000

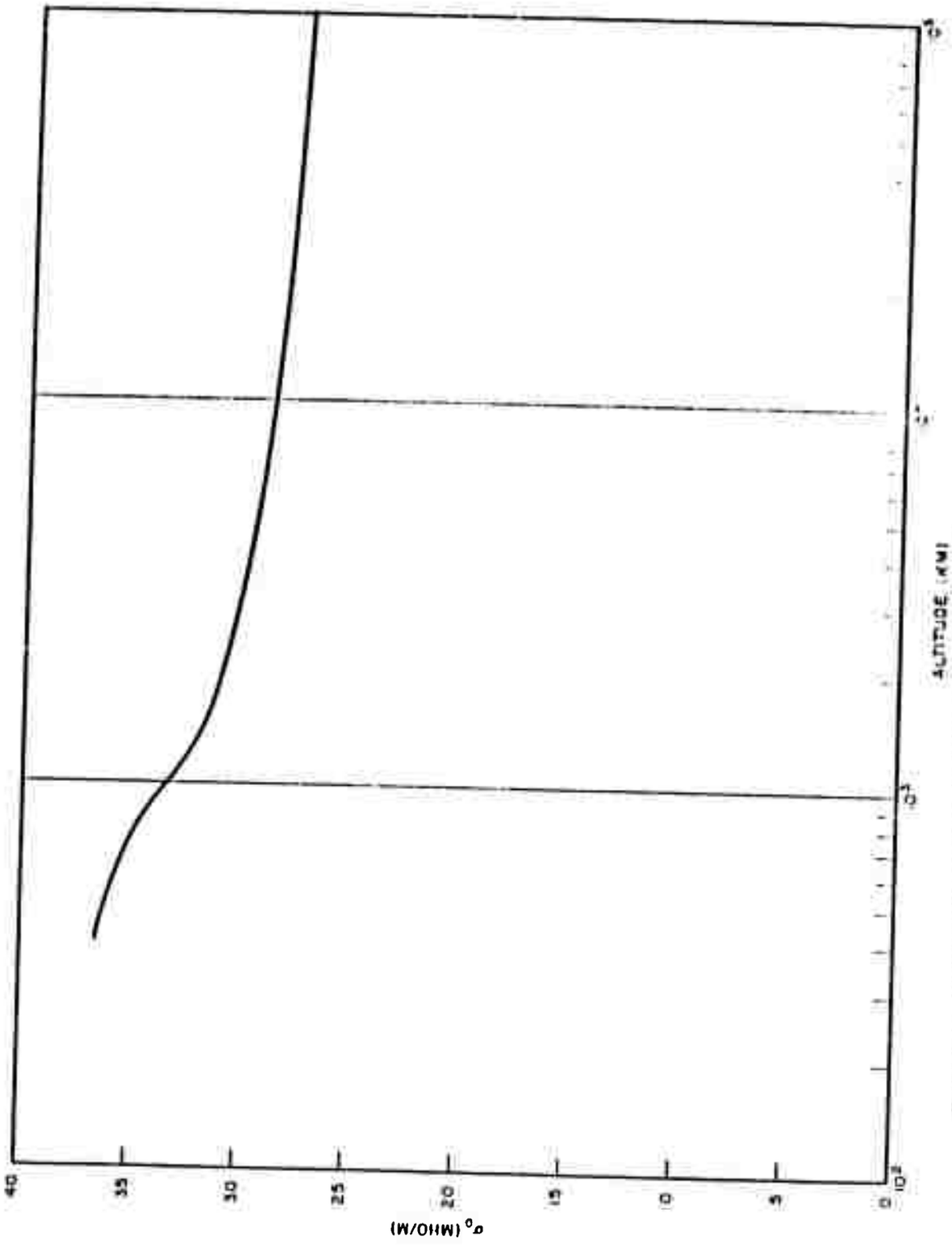

Fig. 9-4 Atmospheric DC Conductivity in the Absence of a Magnetic Field

Injection	$n_e \left(\text{elect}/\text{cm}^3\right)$	$\left(\frac{n_e e^2}{m\sigma_o}\right) \text{sec}^{-1}$	λ(m.)
pulsed	10^6	10^3	10^2
d.c.	10^2	10^{-1}	10^6

In the pulsed injection, the pulse duration is 4×10^{-6} sec; the exponential in Eq. (9.10) can therefore be replaced by

$$\left(1 - \frac{n_e e^2}{m\sigma_o} t\right) \tag{9.12}$$

giving

$$\sigma_t = \frac{n_e e^2}{m} t \tag{9.13}$$

This equation shows that the plasma current is limited by the electron's inertia rather than by collisions. In the d-c case, the value of the exponent indicates that the time for the steady state to be achieved is about 10 sec.

The quantity $\left(\frac{n_e e^2}{m\sigma_o}\right)$ is equal to the plasma collision frequency which leads to the values of the mean free path for electrons λ appearing in the table above.

9.3.3 The Satellite Potential

We are now in a position to write an equation for the potential on the satellite as a function of time.

$$V_s = q_s/C_s \tag{9.14}$$

The capacity of the satellite is

$$C_s = 4\pi\epsilon_o a \tag{9.15}$$

(There is some arbitrariness in the permittivity assigned to a plasma, but with the conductivity we have used, the permittivity will have its vacuum value ϵ_o).

The satellite charge is

$$q_s = I_\beta t - 4\pi a^2 \int_o^t j(a, t')\, dt' \tag{9.16}$$

From the definition of the transient conductivity

$$\begin{aligned} j(a, t) &= \sigma_t E(a, t) \\ &= \sigma_t \frac{q_s}{4\pi\epsilon_o a^2} \end{aligned} \tag{9.17}$$

Therefore,

$$q_s = I_\beta t - \frac{1}{\epsilon_o} \int_o^t \sigma_{t'} q_s\, dt' \tag{9.18}$$

Differentiating both sides we have

$$\frac{dq_s}{dt} + \frac{\sigma_t}{\epsilon_o} q_s = I_\beta \tag{9.19}$$

The solution of this equation which satisfies the initial condition $q_s(0) = 0$ is

$$q_s = \left[\exp - \int_o^t \sigma_{t'}/\epsilon_o \; dt'\right] \int_o^t dt'\, I_\beta \exp \int_o^{t'} \sigma_{t''}/\epsilon_o \; dt'' \tag{9.20}$$

For the case of pulsed injection σ_t is given by Eq. (9.13).

$$q_s = I_\beta \left[\exp - \left(\frac{n_e e^2}{m\epsilon_o} \right) \frac{t^2}{2} \right] \int_o^t dt' \exp \frac{n_e e^2}{m\epsilon_o} \frac{t'^2}{2} \qquad (9.21)$$

The quantity $\left(\frac{n_e e^2}{\epsilon_o m} \right)$ is the square of the plasma frequency ω_p. For an electron density of 10^6 electrons per cm^3, $\omega_p = 5.65 \times 10^7$ rad/sec. Equation (9.21) can be integrated approximately to give

$$q_s = I_\beta t \left[(0.3) \exp \left(- \frac{\omega_p^2}{2} t^2 \right) + \frac{(1.2)}{\omega_p^2 t^2} \left(1 - \exp \left(- 0.6 \omega_p^2 t^2 \right) \right) \right] \qquad (9.22)$$

In two limiting cases, q_s becomes

$$\begin{aligned} q_s &= I_\beta t \left(1 - 0.35 \omega_p^2 t^2 \right) && \omega_p^2 t^2 \ll 1. \\ q_s &= \frac{(1.2)}{\omega_p^2 t} I_\beta && \omega_p^2 t^2 \gg 1. \end{aligned} \qquad (9.23)$$

From Eqs. (9.14) and (9.22), the satellite potential can be computed and is shown in Fig. 9-5. The potential initially rises as if there were no plasma present. It is during this time that the electron's inertia is being overcome. Then, after about 10^{-8} seconds have elapsed, a significant number of electrons start pouring in and the potential flattens off and then falls. At the end of the pulse, q_s decays at a much greater rate

$$q_s = q_s(T) \exp - \frac{\omega_p^2}{2} \left(t^2 - T^2 \right) \qquad t > T \qquad (9.24)$$

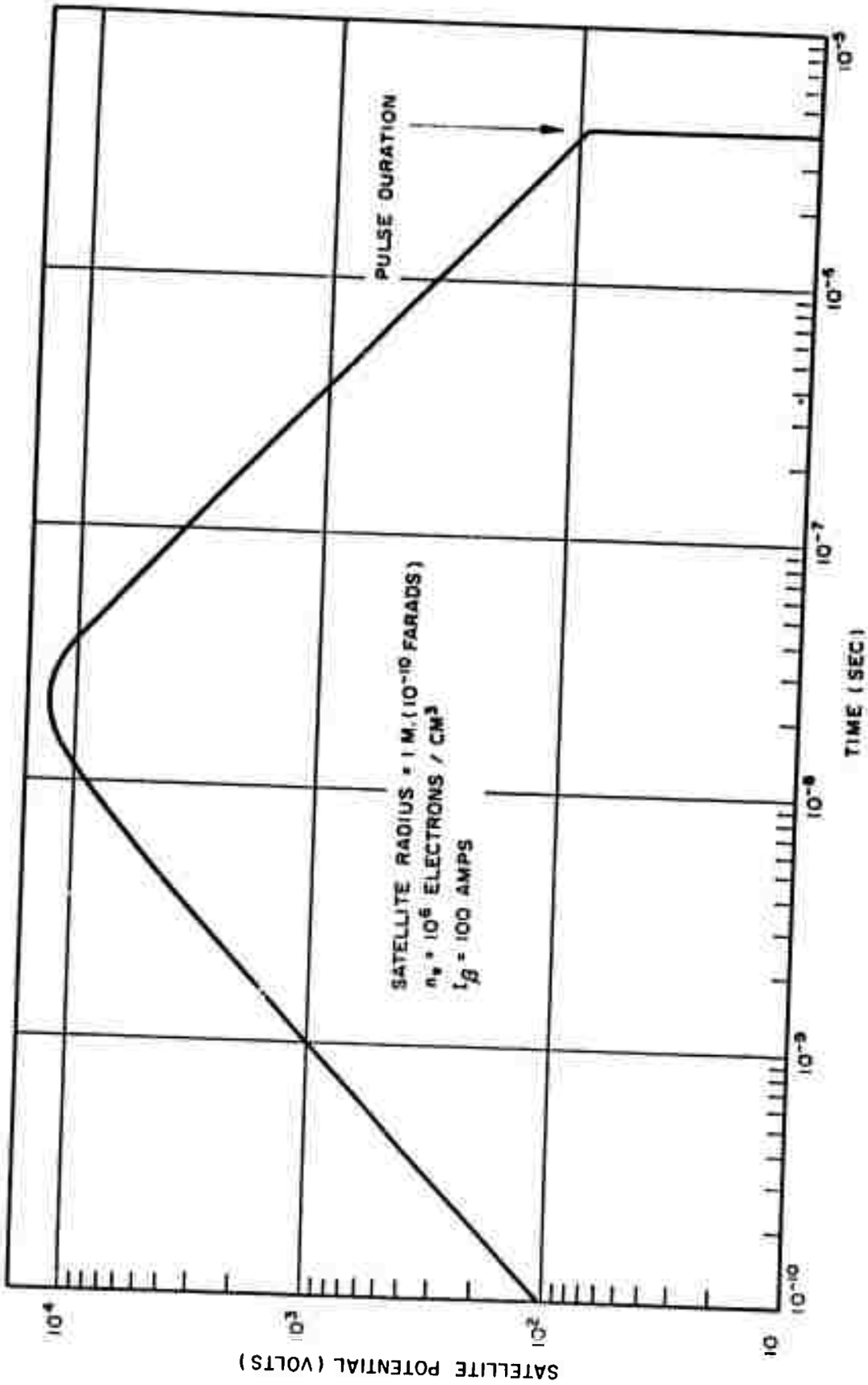

Fig. 9-5 Satellite Potential During the Electron Injection Pulse

where T is the pulse duration. The pulsed accelerator described in Section 4.3 has an intrinsic energy spread of about 4 percent of the injection energy or 4×10^4 volts. This means that the effect of the satellite charging would be essentially negligible.

In the case of d-c injection,

$$\omega_p = 5.65 \times 10^5 \text{ rad/sec}^{-1} \qquad (n_e = 10^2 \text{ electrons/cm}^3)$$

Using Eq. (9.22) to compute the transient charging of the satellite at the time of the initiation of injection, it is found that the satellite potential rises to a maximum of 10 volts. After about 10 seconds have elapses, σ_t can be replaced by σ_o, and the potential achieves its steady-state value of a fraction of a volt.

9.3.4 Validity of the Model

For the model we have taken, it is clear that satellite charging is not a serious problem. However, the question of the validity of the assumptions involved in making the calculations must be examined. It will not be possible to rigorously justify the model, but a number of arguments can be made which indicate that the maximum satellite potential will not be vastly different from that computed.

Geomagnetic field makes conductivity anisotropic. The presence of the earth's magnetic field has the effect of making the conductivity no longer isotropic. In the direction parallel to the magnetic field, the conductivity will be equal to the value we have used. Perpendicular to the magnetic field, however, the conductivity will be many orders of magnitude smaller. Our model can be applied to this situation if we allow current to flow onto the satellite only along the magnetic field lines, setting the conductivity in other directions equal to zero. In this case, Eq. (9.16) must be replaced by

$$q_s = I_\beta t - 4\pi a^2 \int_0^{\frac{\pi}{2}} d\theta \cos^2\theta \sin\theta \int_0^t dt' \, j(a, t'). \qquad (9.25)$$

Then,

$$q_s = I_\beta t - 4/3\pi a^2 \int_0^t j\,(a,t')\,dt' \qquad (9.26)$$

where j(a, t) remains the current density at the satellite surface with no magnetic field present. The solution of Eq. (9.26) is the same as Eq. (9.22) with ω_p^2 replaced by $1/3\ \omega_p^2$. This will increase the maximum satellite potential by a factor of $3^{1/2}$

Plasma density remains nearly constant. In relating $\vec{j}$, $\vec{v}$, and $\vec{E}$, it was assumed that the plasma electron density remains constant. To make this assumption reasonable, it can be shown that if at some time the plasma charge density ρ in the vicinity of the satellite differs from zero, the plasma will return to neutrality in a time which is short compared with the time for any significant change of the satellite potential to occur. From Maxwell's equations and the condition of charge conservation:

$$\nabla \cdot \vec{E} = \rho/\epsilon_o \qquad (9.27)$$

$$\nabla \cdot \vec{j} = -\frac{\partial \rho}{\partial t} \qquad (9.28)$$

$\vec{j}$ and $\vec{E}$ are related by

$$\vec{j} = \sigma_t \vec{E} \qquad (9.29)$$

Solving for ρ from these three equations

$$\frac{\partial \rho}{\partial t} = -\frac{\sigma_t}{\epsilon_o}\rho \qquad (9.30)$$

and integrating we get

$$\rho = \rho_o \exp -\int_0^t \sigma_{t'}/\epsilon_o\, dt' \qquad (9.31)$$

If we take the value of σ_t from Eq. (9.13), then

$$\rho = \rho_o \exp -\frac{\omega_p^2}{2} t^2 \quad \text{results} \tag{9.32}$$

The time interval for ρ to fall to e^{-1} of its initial value is

$$t_{e^{-1}} = \frac{2^{1/2}}{\omega_p} = 2.5 \times 10^{-8} \text{ sec} \tag{9.33}$$

If we look at Fig. 9-5, we see that the time for the satellite potential to fall to e^{-1} of its maximum value is about 10^{-7} sec, or four times the plasma neutralization time constant. This argument does not hold in the time interval in which the satellite is rising to its maximum. However, in this interval, the rate of satellite charging is essentially that with no plasma present, and the assumption of a constant n_e (and a constant $\vec{E}$, as discussed in the next paragraph) is not required.

The effect of a varying electric field. In order to be able to integrate the equation of motion of a plasma electron (Eq. (9.3)), the electric field had to be constant to the degree that the energy gained between collisions was nearly constant. From the computed values of the mean free paths and collision frequencies, it is clear that this assumption is invalid. Let us calculate the satellite charge again without this restriction on the electric field, but taking n_e constant and neglecting collisions altogether.

$$m \frac{d\vec{v}}{dt} = e \vec{E} \tag{9.34}$$

$$q_s = I_\beta t - 4\pi a^2 \int_0^t j(a, t')\, dt' \tag{9.35}$$

$$\vec{j} = e n_e \vec{v} \tag{9.36}$$

$$E(a, t) = \frac{q_s(t)}{4\pi\epsilon_o a^2} \tag{9.37}$$

Differentiating Eq. (9.35) twice and combining the above equations we find that

$$\frac{d^2 q_s}{dt^2} = -\frac{e^2 n_e}{n_i \epsilon_o} q_s = -\omega_p^2 q_s \qquad \text{results} \tag{9.38}$$

The solution of this equation is

$$q_s = \frac{I_\beta}{\omega_p} \sin \omega_p t \tag{9.39}$$

With the modified assumptions, then, q_s oscillates. The important thing, however, is that the maximum value of q_s leads to a maximum satellite potential of 2×10^4 volts for pulsed injection, and 20 volts for d-c injection. These values are approximately equal to those computed before.

In conclusion, the results of this analysis indicate that the maximum potential to which the satellite will rise is about 3×10^4 volts in the pulsed case, and about 30 volts in the d-c case. Therefore, satellite charging will not seriously affect the monoenergetic property of the electron beam for the accelerators considered in this study.

Section 10
DIAMAGNETIC EFFECT OF THE INJECTED ELECTRONS

10.1 INTRODUCTION

It will be necessary to compute the magnetic field associated with the injected electron current to show that it is small compared with the earth's field in the region in which the electrons are moving. If this were not the case, the electrons would see a modified field, and it would be much more difficult to correlate the results of the various experiments with similar phenomena occurring in the unperturbed field. In the worst case, the earth's field could be reduced (the electron current produces a diamagnetic field) to the point where the electrons would no longer be magnetically contained.

10.2 PULSED INJECTION

The cyclotron period of a high-energy electron in a magnetic field is

$$T_c = \frac{2\pi}{c} \frac{p}{Be} \tag{10.1}$$

where p is the electron's momentum. For a 1-Mev electron circulating near the surface of the earth, the cyclotron period is nearly equal to the duration of the injection pulse (4×10^{-6} sec), and becomes much longer far from the earth. Therefore, the pulse of electrons can be represented by a single current loop carrying 100 amps. From Smythe (Ref. 1), the components of the magnetic field of a current loop are given by the following equations, where the coordinate system is defined in Fig. 10-1.

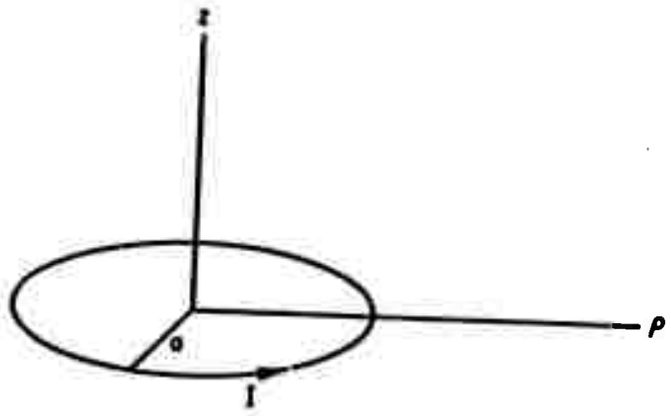

Fig. 10-1 Coordinate System of a Current Loop

$$B_z = \frac{\mu_o I}{2\pi} \frac{1}{\left[(a+\rho)^2 + z^2\right]^{1/2}} \left[K + \frac{a^2 - \rho^2 - z^2}{(a-\rho)^2 + z^2} E \right] \tag{10.2}$$

$$B_\rho = \frac{\mu_o I}{2\pi} \frac{z}{\rho\left[(a+\rho)^2 + z^2\right]^{1/2}} \left[-K + \frac{a^2 + \rho^2 + z^2}{(a-\rho)^2 + z^2} E \right] \tag{10.3}$$

$$K = \int_o^{\pi/2} \frac{d\theta}{\left(1 - k^2 \sin^2 \theta\right)^{1/2}} \tag{10.4}$$

$$E = \int_o^{\pi/2} d\theta \left(1 - k^2 \sin^2 \theta\right)^{1/2} \tag{10.5}$$

$$k^2 = \frac{4a\rho}{(a+\rho)^2 + z^2} \tag{10.6}$$

To compute the field in the vicinity of the current filament itself, we set

$$\begin{aligned} \rho &= a - \epsilon \\ \epsilon/a &\ll 1 \\ z &\ll a,\ \rho \\ z &\approx \epsilon \end{aligned} \tag{10.7}$$

Then,

$$k^2 \approx 1 - \frac{1}{4a^2}(\epsilon^2 + z^2) \tag{10.8}$$

$$K \approx \ell n \frac{8a}{\left(\epsilon^2 + z^2\right)^{1/2}} \tag{10.9}$$

$$E \approx 1 \tag{10.10}$$

Keeping only the dominant terms, we find that B_z becomes

$$B_z = \frac{\mu_o I}{2\pi}\left[\frac{\epsilon}{r^2} + \frac{1}{2a}\,\ell n \frac{8a}{r}\right] \tag{10.11}$$

where $r = \left(\epsilon^2 + z^2\right)^{1/2}$, which is the radial distance from the center of the current filament (see Fig. 10-2).

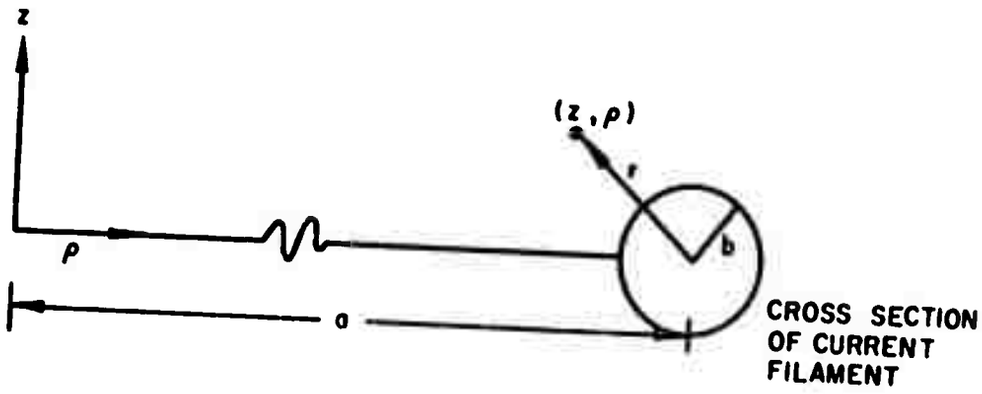

Fig. 10-2 Cross Section of a Current Loop

The first term in Eq. (10.11) is simply the "straight wire" magnetic field, and the second term is the effect of the curvature of the "wire." We will neglect the first term because it produces a magnetic "pinch," but does not result in a diamagnetic field; the second term does.

$$B_{dia} = \frac{\mu_o I}{4\pi a} \ell n \frac{8a}{r} \qquad (10.12)$$

As $r \to 0$, B_{dia} diverges. However, the current filament must not be taken as infinitely thin, but as having some finite spatial distribution. We will define a current density $j(r)$ constant for $r<b$ and zero for $r>b$, where b is the cross sectional radius of the current filament.

$$j = \frac{I}{\pi b^2} \qquad (10.13)$$

The diamagnetic field is then

$$B_{dia} = \lim_{\delta \to 0} - \frac{\mu_o}{4\pi a} \frac{I}{\pi b^2} \left[\int_o^{r-\delta} \rho \, d\rho \int_o^{\pi} d\varphi \, \ell n \frac{(r^2 + \rho^2 - 2r\rho \cos \varphi)}{64a^2} \right.$$

$$\left. + \int_{r+\delta}^{b} \rho \, d\rho \int_o^{\pi} d\varphi \, \ell n \frac{(r^2 + \rho^2 - 2r\rho \cos \varphi)}{64a^2} \right] \qquad (10.14)$$

Integrating and keeping only the dominant term we get

$$B_{dia} = \frac{\mu_o I}{4\pi a} \ell n \frac{8a}{b} \qquad (10.15)$$

The diamagnetic field , then, is essentially constant in the vicinity of the current filament. The radius of curvature a is related to the magnetic field by

$$a = \frac{p}{Be} \qquad (10.16)$$

Therefore,

$$\frac{B_{dia}}{B} = \frac{\mu_o I}{4\pi} \frac{ce}{cp} \ell n \frac{8a}{b} \qquad (10.17)$$

In the case of a 1-Mev electron circulating near the surface of the earth, the parameters in Eq. (10-17) have the following values at a magnetic latitude of 30°.

$I = 100$ amps

$B = 0.34$ gauss $= 3.4 \times 10^{-5}$ webers/m^2

$a = 140$ m

$cp = 1.4$ Mev $= 2.24 \times 10^{-13}$ joules

And if b = 1 cm, then

$$\frac{B_{dia}}{B} = 1.6 \times 10^{-2}$$

The effect of the diamagnetic field is, therefore, negligible.

10.3 DC INJECTION

In the case of d-c injection, the argument of the last section does not apply because the electron current is distributed over a large volume of space and cannot be represented by some simple configuration such as a loop or a solenoid. We will, instead, assume that the density of injected electrons is high enough so that we can assign a volume magnetization to the region occupied by the electrons. Associated with each electron is a magnetic moment

$$M = \pi e \nu_c a^2 \text{ amps-m}^2 \qquad (10.18)$$

where ν_c is the cyclotron frequency and a is the cyclotron radius. Taking the electron's velocity to be equal to c , we find that

$$\nu_c = \frac{\omega_c}{2\pi} = \frac{c}{2\pi a}$$

$$a = \frac{p}{Be} \qquad (10.19)$$

Therefore,

$$M = \frac{cp}{2B} \qquad (10.20)$$

The electron number density is n_e, and the magnetic moment per unit volume is

$$\mathcal{M} = n_e \frac{cp}{2B} \qquad \text{amp/m} \tag{10.21}$$

The quantity $\mathcal{M}$ is called the magnetization, and is the source of a diamagnetic field

$$B_{dia} = \mu_o n_e \frac{cp}{2B} \tag{10.22}$$

We must now digress in order to compute the value of n_e. In the experiment described in Section 6.1, it is proposed to inject electrons into a volume, the cross section of which is shown in Fig. 6-1.

The shaded region in this figure is defined approximately by the two field lines which cross the magnetic equator at $(r_e - a_e)$ and $(r_e + a_e)$, where a_e is

$$a_e = \frac{p}{cB(r = r_e,\ \psi = 0)} = \frac{p}{eB_e} \tag{10.23}$$

For a dipole field, the equation of a field line is given by

$$r = r_e \cos^2 \psi \tag{10.24}$$

The volume of the "magnetic shell" is represented by

$$V = 4\pi \int_0^{\cos^{-1}\left(R_E/r_e\right)^{1/2}} \cos\psi \, d\psi \int_{(r_e - a_e)\cos^2\psi}^{(r_e + a_e)\cos^2\psi} r^2 \, dr \tag{10.25}$$

where R_E is the radius of the earth.

$$V \approx 3.5\pi\, a_e\, r_e^2 \qquad a_e \ll r_e \tag{10.26}$$

The electron number density is approximately

$$n_e = \frac{I_\beta}{e}\,\frac{T_D}{V} \tag{10.27}$$

where I_β is the current injected from the satellite while the shell is being filled, and T_D is the time for the electrons to drift longitudinally once around the earth which is approximately the length of the injection time. From Eq. 3.14,

$$T_D = \frac{4\pi}{3}\,\frac{r_e^2}{a_e c} \tag{10.28}$$

Going back to the expression for the diamagnetic field [Eq. (10.22)], and substituting from Eqs. (10.26), (10.27), and (10.28)

$$\frac{B_{dia}}{B} = \mu_o\, n_e\, \frac{cp}{2B^2} = (0.2)\,\mu_o\, I_\beta\, \frac{e}{p}\left(\frac{B_e}{B}\right)^2 \tag{10.29}$$

This ratio has its maximum value at the equator ($B = B_e$).

$$\frac{B_{dia}}{B} = (0.2)\,\mu_o\, I_\beta\, \frac{e}{p} \tag{10.30}$$

For one Mev electrons and $I_\beta = 10^{-3}$ amps

$$\frac{B_{dia}}{B} = 5 \times 10^{-8}$$

The diamagnetic effect is completely negligible.

Using the above formulas, it might be interesting if we compute an approximate value of the achievable electron density in a filled magnetic shell.

$$n_e = (0.4)\ I_\beta \frac{cB_e^2}{cp^2} \qquad (10.31)$$

For a dipole field,

$$B_e = (9.1 \times 10^{15})\ r_e^{-3} \quad \text{webers/}_{m^2}$$

Taking the case where $r_e = 2$ earth radii,

$$n_e = 7 \text{ electrons/}_{m^3}$$

which gives a flux of 2×10^5 electrons per cm^2 per sec.

Section 11
CONCLUSIONS AND RECOMMENDATIONS

11.1 CONCLUSIONS

Three types of experiments in which electrons are injected artificially into the earth's magnetic field by satellite-borne accelerators have been considered and appear to be feasible. Each of these experiments has considerable scientific merit and military usefulness. The experiments are:

(1) Integral invariant surfaces can be covered by fast electrons which have been injected by a d-c accelerator operating during the passage of the satellite through the surface. The longitudinal drift of the electrons serves to close the shell and so can provide a measure of the longitudinal drift time. In addition to this, the electron life-times, the mechanisms determining the life-times, and diurnal and magnetic storm effects on the shape of the surface can be observed. It appears that inclined elliptical orbits with electrons injected near apogee are probably most suitable for both injection and subsequent observation of the electrons.

(2) The bounce time of the electrons injected by a pulsed accelerator can be measured by detection of the synchroton radiation with a radio receiver carried in the injecting satellite. Injection would be made at magnetic pitch angles of 90 deg with a pulse duration of four μsec. After one or more bounces, the electrons will be mirrored in the vicinity of the satellite and the time between injection and subsequent mirroring can be measured. This experiment will measure the average value of the magnetic field along the field line on which injection is made and will permit comparison of this average with that given by various geomagnetic field models. The variation of the magnetic field produced by diurnal effects and by magnetic storms can

be observed as can the maximum latitude at which closed lines occur. A polar orbit satellite should be used for this experiment.

(3) Geomagnetic conjugate points can be measured by injecting electrons along a magnetic field line and observing the points at which the electrons penetrate the atmosphere in opposite magnetic hemispheres. The electrons would be injected from a pulsed accelerator, carried by a polar orbit satellite. The establishment of conjugate points is particularly important to military applications.

11.2 RECOMMENDATIONS

Since these experiments appear to be feasible and desirable, it is recommended that further effort be put into optimizing the physic's design of the experiments and into the development of an engineering program plan. The physic's design of the experiments should receive further attention in the following areas:

(1) In order to optimize the injection and subsequent detection of electrons by a satellite carrying a d-e accelerator, the motion of the satellite in the magnetic field of the earth should be considered in detail. This consideration should include the inclination, eccentricity, precession, and decay of the satellite orbit, and the rotation of the earth and its magnetic field. The study will require machine calculation.

(2) Measurements of the natural electron flux which will contribute a background for electron detectors should be pursued. These measurements are currently in progress at a number of agencies, but some additional measurement are required. In particular, the flux of electrons having energies near one mev should be established at different earth radii.

(3) The technique of detecting the synchroton radiation from a vehicle-borne radio receiver should be explored further. It may be possible to observe the natural synchroton radiation from Van Allen electrons or from auroral electron fluxes with receivers carried in sounding rockets or satellites.

(4) The detection of atmospheric ionization in the conjugate point experiment should be further investigated. Fruitful areas for investigation include looking at auroras with radar and measuring the electron flux which produces visible auroras. It may be possible to do the conjugate point experiment by optical means rather than by radar.

(5) An engineering program plan and cost estimate should be developed at the completion of the additional physic's study. The program plan should be developed after careful consideration of special equipment which will be required both in the satellite and on the ground. Development of special equipment such as accelerators, low-noise radio receivers, and vehicle memory systems will probably be required.

Section 12
REFERENCES

1. W. R. Smythe, Static and Dynamic Electricity, New York, McGraw-Hill, 1950, pp. 270–271

2. W. D. Parkinson and J. Cleary, "The Eccentric Geomagnetic Dipole," Geophys. J., Vol. 1, 1958, p. 346

3. Satellite Environment Handbook, ed. F. S. Johnson, Stanford, Calif., Stanford University Press, 1961

4. E. H. Vestine and W. L. Sibley, "The Geomagnetic Field in Space, Ring Currents, and Auroral Isochasms," J. Geophys. Res., Vol. 65, 1960, pp. 1957–1979

5. E. N. Parker, "Interactions of the Solar Wind with the Geomagnetic Field," Physics of Fluids, Vol. 1, 1958, pp. 171–187

6. L. Bierman, "Physical Processes in Comet Tails and Their Relation to Solar Activity," Société Royale des Sciences de Liège, Vol. 13, 1953, pp. 291–302

7. F. S. Johnson, "Composition of Outer Space," Astronautics, Vol. 54, 1960, pp. 30–31

8. For a summary of Störmers work, see, C. Chapman and J. Bartels, Geomagnetism, Vol. 2, 1940, p. 834

9. H. Alfvén, Cosmical Electrodynamics, London, Oxford University Press, 1950

10. T. G. Northrup and E. Teller, "Stability of the Adiabatic Motion of Charged Particles in the Earth's Magnetic Field," Phys. Rev., Vol. 117, 1960, pp. 215–225

11. D. C. Jensen, R. W. Murray, and J. A. Welch, Jr., "Tables of Adiabatic Invariants for the Geomagnetic Field 1955.0," AFSWC-TN-60-8, Kirtland Air Force Base, New Mexico, 1960, p. 109

12. L. Spitzer, Jr., Physics of Fully Ionized Gases, Interscience Publishers, New York, 1956

13. J. A. Welch and W. A Whitaker, "Theory of Geomagnetically Trapped Elecrons from an Artificial Source," J. Geophys. Res., Vol. 64, 1959, p. 909

14. M. Walt and W. M. Mac Donald, Annals of Phys. (to be published) 1961

15. A. J. Dragt, Program Abstracts, Meeting of Amer. Geophys. Union, Washington, D.C., 1960, pp. 29–30

16. S. C. Freden and R. S. White, "Particle Fluxes in the Inner Radiation Belt," J. Geophys. Res., Vol. 65, 1960, pp. 1377–1383

17. M. Walt, L. F. Chase, Jr., J. Cladis, W. L. Imhof, and D. J. Knecht, "Energy Spectra and Altitude Dependence of Electrons Trapped in the Earth's Magnetic Field," Space Research, ed. H. Kallman, Bijl, North Holland, Amsterdam, 1960, pp. 910–920

18. A. Rosen, T. A. Farley, and C. P. Sonett, "Soft Radiation Measurements on Explorer VI Earth Satellite," Space Research, ed. H. Kallman, Bijl, North Holland, Amsterdam, 1960

19. C. Y. Fan, P. Meyer, and J. A. Simpson, "Trapped and Cosmic Radiation Measurements from Explorer VI," Space Research, ed. H. Kallman, Bijl, North Holland, Amsterdam, 1960, pp. 951–966

20. R. L. Arnoldy, R. A. Hoffman, and J. R. Winckler, "Observations of the Van Allen Radiation Regions During August and September, 1959, Part I," J. Geophys. Res., Vol. 65, 1960, pp. 1361–1376

21. J. Schwinger, "On the Classical Radiation of Accclerated Electrons," Phys. Rev., Vol. 75, 1949, pp. 1912–1925

22. D. H. Tomboulian and P. L. Hartman, "Spectral and Angular Distribution of Ultraviolet Radiation from the 300-Mev Cornell Synchrotron," Phys. Rev., Vol. 102, 1956, pp. 1425–1426

23. J. L. Pawsey and R. N. Bracewell, Radio Astronomy, London, Oxford University Press, Chap. 2 and 10, 1955

24. J. D. Kraus and H. C. Ko, "Celestial Radio Radiation," Ohio State University Rep't 73, 1958

25. R. N. Bracewell, private communication

26. J. A. Welch, private communication For a description of the 512-term geomagnetic model, see Ref. 11

27. R. B. Dyce, private communication

28. D. B. Beard and F. S. Johnson, "Charge and Magnetic Field Interaction With Satellites," J. Geophys. Res., 65, 1960, p. 1

29. D. A. Hamlin, R. Karplus, R. C. Vik, and K. M. Watson, "Mirrow and Azimuthal Drift Frequencies for Geomagnetically Trapped Particles," J. Geophys. Res. Vol. 66, 1961, p. 1

DISTRIBUTION

No. of Cys.

HEADQUARTERS USAF

1 Hq USAF (AFDAP), Wash 25, DC
1 Hq USAF (AFORQ), Wash 25, DC
1 Hq USAF (AFDRT-GW/1), Wash 25, DC
1 Hq USAF (AFCIN), Wash 25, DC
1 Hq USAF (AFTAC), Wash 25, DC

ATIC, Wright-Patterson AFB, Ohio
1 (AFCIN 4F2A, Maj Pearce)
1 (AFCIN 4B1A, Library)

1 AFOAR (RRN, Maj Munyon), Bldg T-D, Wash 25, DC

MAJOR AIR COMMANDS

AFSC, Andrews AFB, Wash 25, DC
1 (SCR)
1 (SCR-2, Capt Ray Berrier)

1 Office of Aerospace Research, AFOSR, (SREC), Wash 25, DC

AFSC ORGANIZATIONS

Office of Aerospace Research, Hq AFCRL, L.G. Hanscom Fld, Bedford, Mass
1 (Tech Library for: Mr. Horowitz)
1 (CRZCT, H.P. Gavin)

1 BSD (Tech Library), AF Unit Post Office, Los Angeles 45, Calif
1 SSD (TDC 61-372-2), AF Unit Post Office, Los Angeles 45, Calif
1 ASD (WWAD), Wright-Patterson AFB, Ohio
1 ESD (Tech Library), Hanscom Fld, Bedford, Mass
1 AFMTC (MTASI), Patrick AFB, Fla
1 Aeronautical Research Lab (RRLO, Mr. Cady), Wright-Patterson AFB, Ohio
1 AEDC (AEOI), Arnold AFS, Tenn
1 APGC (PGTRI), Eglin AFB, Fla
1 RADC (RCOIL-2), Griffiss AFB, NY

AFSWC, Kirtland AFB, NMex
1 (SWNH)
60 (SWOI)
1 (SWRPA)
1 (SWRPS, Maj Nadler)

DISTRIBUTION (Cont'd)

No. of Cys.	
1	(SWRPT, Capt Welch)
1	(SWRPL, Capt O'Brien)
1	(SWRJ)

OTHER AIR FORCE AGENCIES

1	Director, USAF Project RAND, via: Air Force Liaison Office, The RAND Corporation (RAND Library for: Dr. A. Latter), 1700 Main Street, Santa Monica, Calif

ARMY ACTIVITIES

1	Chief of Research and Development, Department of the Army, (Special Weapons and Air Defense Division), Wash 25, DC
1	ARGMA (Tech Library), Huntsville, Ala
1	Director, Ballistic Research Laboratories (Library for: Mr. E.O. Baicy), Aberdeen Proving Ground, Md
1	Director, Evans Signal Laboratory (Weapons Effects Section), Belmar, NJ
1	Commanding Officer, US Army Signal Research and Development Laboratory (Tech Library for: Dr. W. McAfee), Ft Monmouth, NJ

NAVY ACTIVITIES

1	Chief of Naval Operations, Department of the Navy (OP-36), Wash 25, DC
1	Commanding Officer, Naval Research Laboratory (Tech Library), Wash 25, DC
1	Commanding Officer, Naval Radiological Defense Laboratory, (Technical Information Division), San Francisco 24, Calif
1	Office of Naval Research (Dr. W.J. Thaler), Wash 25, DC

OTHER DOD ACTIVITIES

1	Director, Weapon Systems Evaluation Group, Room 2E1006, The Pentagon, (Dr. Gerald Rosen), Wash 25, DC
1	Chief, Defense Atomic Support Agency (Document Library Branch for: Maj Ralph Pennington), Wash 25, DC
1	Commander, Field Command, Defense Atomic Support Agency, (FCAG3), Sandia Base, NMex
10	ASTIA (TIPDR), Arlington Hall Sta, Arlington 12, Va
1	Director, Advanced Research Projects Agency, Department of Defense, The Pentagon (Lt Col Roy Weidler), Wash 25, DC

AEC ACTIVITIES

1	US Atomic Energy Commission (Technical Reports Library, Mrs. J. O'Leary for DMA), Wash 25, DC

DISTRIBUTION (Cont'd)

No. of Cys.	
1	President, Sandia Corporation (Document Control Division for: Dr. Tom Cook), Sandia Base, NMex
1	Chief, Technical Information Service Extension, US Atomic Energy Commission, Box 62, Oak Ridge, Tenn
1	Director, University of California Lawrence Radiation Laboratory, (Technical Information Division, Mr. Clovis Craig for: Mr. N.C. Christofilos), P.O. Box 808, Livermore, Calif
1	Director, Los Alamos Scientific Laboratory (Helen Redman, Report Library), P.O. Box 1663, Los Alamos, NMex

OTHER

1	Institute for Defense Analysis, Room 2B257, The Pentagon, (Dr. W. Bradley), Wash 25, DC
1	General Electric TEMPO (Dr. R.W. Hendrick), 735 State Street, Santa Barbara, Calif Contract AF 29(601)-4194
1	Lockheed Missile & Space Division (Dr. Roland E. Meyerott), 3251 Hanover St., Palo Alto, Calif Contract AF 29(601)-4136
1	E.H. Plesset Associates (Dr. Harris Mayer), 1281 S. Westwood Blvd, Los Angeles 24, Calif Contract AF 29(601)-1897
1	Republic Aviation Corporation, MSD (Mr. Jeff Meeker), 223 Jericho Turnpike, Mineola, Long Island, NY Contract AF 29(601)-2792
1	Convair, Division of General Dynamics (Dr. Daniel Hamlin), 3165 Pacific Highway, San Diego 12, Calif Contract AF 29(601)-2567
1	University of Chicago, Institute of Air Weapons Research, Museum of Science and Industry, Chicago 37, Ill, THRU: ASD (WWRP), (Mr. Gard), Wright-Patterson AFB, Ohio Contract AF33(616)-6824
1	Armour Research Foundation (Mr. C. Haaland), 10 W. 35th St., Chicago 16, Ill
1	Lincoln Laboratories (Dr. J. Pannell), Massachusetts Institute of Technology, P.O. Box 73, Lexington, Mass
1	Edgerton, Germeshausen & Grier, Inc., (Dr. M. Shuler), 1100 Brookline Ave., Boston 15, Mass
1	Official Record Copy (SWRPA, Lt Schiff)